OL

NASA CR-135127
PSI TR-53

SLL 80-352/OL

LASER-HEATED ROCKET STUDIES

by

N. H. Kemp, R. G. Root, P.K.S. Wu, G. E. Caledonia
and A. N. Pirri

PHYSICAL SCIENCES INC.

prepared for

NATIONAL AERONAUTICS AND SPACE ADMINISTRATION
NASA Lewis Research Center

Contract NAS 3-19695

May 1976

Accession Number: 3939

Publication Date: May 01, 1976

Title: Laser-Heated Rocket Studies

Personal Author: Kemp, N.H.; Root, R.G.; Wu, P.K.S.; Caledonia, G.E.

Corporate Author Or Publisher: Physical Sciences Inc., 30 Commerce Way, Woburn, MA 01801 Report Number: PSI TR-53

Report Prepared for: National Aeronautics and Space Administration, Lewis Research Center, Cleveland, OH 44135 Report Number Assigned by Contract Monitor: SLL 80 352; NASA CR-135127

Comments on Document: Archive, RRI, DEW.

Descriptors, Keywords: Laser Heat Rocket Propulsion Hydrogen Plasma Radiation Nozzle Flow Boundary Layer Flow Core Stationary Continuous Wave Impulse Thermal Efficiency LSC Support Combustion Breakdown Molecule Particulate Loss

Pages: 00131

Cataloged Date: Nov 30, 1990

Contract Number: NAS3-19695

Document Type: HC

Number of Copies In Library: 000001

Record ID: 25316

Source of Document: DEW

1. Report No.	2. Government Accession No.	3. Recipient's Catalog No.
NASA CR-135127		

4. Title and Subtitle	5. Report Date
LASER-HEATED ROCKET STUDIES	May 1976
	6. Performing Organization Code 6K561

7. Author(s)	8. Performing Organization Report No.
N. H. Kemp, R. G. Root, P. K. S. Wu, G. E. Caledonia and A. N. Pirri	PSI TR-53
	10. Work Unit No. Y0R 6858

9. Performing Organization Name and Address	11. Contract or Grant No.
Physical Sciences Inc. 30 Commerce Way Woburn, MA 01801	NAS3-19695
	13. Type of Report and Period Covered Final Report April 28, 1975-April 28, 1976

12. Sponsoring Agency Name and Address	14. Sponsoring Agency Code
National Aeronautics and Space Administration Lewis Research Center Cleveland, OH 44135	5323 500-318

15. Supplementary Notes

Project Monitor, Stephen M. Cohen, Laser and Energy Systems Branch, NASA Lewis Research Center, Cleveland, Ohio

16. Abstract

This report describes studies of CW laser-heated rocket propulsion, in both the flowing-core and stationary-core configurations, with most attention focused on the former. (It is the second such study performed by PSI following the work described in Ref. 1). In the present work, the laser radiation considered was 10.6 μm, and the working gas was unseeded hydrogen. The areas investigated included initiation of a hydrogen plasma capable of absorbing laser radiation, the radiation emission properties of hot, ionized hydrogen, the flow of hot hydrogen while absorbing and radiating, the heat losses from the gas and the rocket performance. The stationary-core configuration was investigated qualitatively and semi-quantitatively.

It was found that the flowing-core rockets can have specific impulses (I_{sp}) between 1500 and 3300 sec. They are small devices, whose heating zone is only a millimeters to a few centimeters long, and millimeters to centimeters in radius, for laser power levels varying from 10 to 5000 kW, and pressure levels of 3 to 10 atm. Heat protection of the walls is a vital necessity, though the fraction of laser power lost to the walls can be as low as 10% for larger powers, making the rockets thermally efficient.

A number of major areas of uncertainty have been identified for further exploration. Chief among these is the properties of laser supported combustion (LSC) waves in hydrogen. Others are an efficient method of heat protection, the effect of radial temperature profiles on radiation loss, and the effect of wider variation of operating parameters. For the stationary-core concept, absorption lengths of hot hydrogen radiation in cold hydrogen are needed, and a study of entrainment of the core gas by the flowing propellant gas should be made.

17. Key Words (Suggested by Author(s))	18. Distribution Statement
Laser Propulsion Hydrogen Plasma Radiation Hydrogen Nozzle Flow Hydrogen Boundary Layers	Unlimited

19. Security Classif. (of this report)	20. Security Classif. (of this page)	21. No. of Pages	22. Price*
Unclassified	Unclassified	131	

* For sale by the National Technical Information Service, Springfield, Virginia 22161

NASA CR-135127
PSI TR-53

LASER-HEATED ROCKET STUDIES

by

N. H. Kemp, R. G. Root, P. K. S. Wu, G. E. Caledonia
and A. N. Pirri

PHYSICAL SCIENCES INC.
30 Commerce Way
Woburn, MA 01801

prepared for

NATIONAL AERONAUTICS AND SPACE ADMINISTRATION
LEWIS RESEARCH CENTER

Contract NAS 3-19695

May 1976

FORWARD

The research described in this report was performed for the Laser and Energy Systems Branch at the NASA/Lewis Research Center under Contract NAS3-19695. The NASA Project Manager was Mr. Stephen M. Cohen. Some of the work was also partially supported by the Rocketdyne Division of Rockwell International under Purchase Order R54PAK651434 as a subcontract to NASA Contract NAS3-19728.

Dr. Peter Nebolsine contributed helpful discussions to Section 3, Dr. Girard Simons to Sec. 10, and Dr. Kurt Wray to many aspects of the work. The authors would like to express their appreciation to Ms. Irene Scanzillo, Ms. Anne McGee, Ms. Karen Rawlinson and Ms. Janice Ragucci for their help in preparing this report, and to Ms. Reeva Golub for computational assistance.

SUMMARY

This report describes studies of CW laser-heated rocket propulsion, in both the flowing-core and stationary-core configurations, with most attention focused on the former. (It is the second such study performed by PSI following the work described in Ref. 1). In the present work, the laser radiation considered was 10.6 μm, and the working gas was unseeded hydrogen. The areas investigated included initiation of a hydrogen plasma capable of absorbing laser radiation, the radiation emission properties of hot, ionized hydrogen, the flow of hot hydrogen while absorbing and radiating, the heat losses from the gas and the rocket performance. The stationary-core configuration was investigated qualitatively and semi-quantitatively.

It was found that the flowing-core rockets can have specific impulses (I_{sp}) between 1500 and 3300 sec. They are small devices, whose heating zone is only a millimeters to a few centimeters long, and millimeters to centimeters in radius, for laser power levels varying from 10 to 5000 kW, and pressure levels of 3 to 10 atm. Heat protection of the walls is a vital necessity, though the fraction of laser power lost to the walls can be as low as 10% for larger powers, making the rockets thermally efficient.

A number of major areas of uncertainty have been identified for further exploration. Chief among these is the properties of laser supported combustion (LSC) waves in hydrogen. Others are an efficient method of heat protection, the effect of radial temperature profiles on radiation loss, and the effect of wider variation of operating parameters. For the stationary-core concept, absorption lengths of hot hydrogen radiation in cold hydrogen are needed, and a study of entrainment of the core gas by the flowing propellant gas should be made.

TABLE OF CONTENTS

LIST OF ILLUSTRATIONS

1. INTRODUCTION

This is the final report on the second contract issued by NASA/ Lewis Research Center to Physical Sciences Inc. for a study of a laser-heated rocket. The results of the first contract were reported in Ref. 1.

The present study dealt with the details of a number of aspects of a laser-powered rocket engine absorbing CO_2 laser radiation (10.6 μm) by inverse Bremsstrahlung, and using hydrogen as the working gas. There were two general areas of study. The first was the initiation of a high temperature plasma capable of absorbing the laser radiation. The second was the analysis of a steady coaxial-flow, laser-powered rocket engine in two different configurations. One configuration was a flowing core of plasma, absorbing the laser energy, being heated, and expanding to generate thrust. This core is surrounded by a cooling buffer gas flowing the annulus between the core and the engine walls. The other configuration was a stationary stable plasma absorbing the laser energy, and transmitting it to a propellant gas flowing around it, which in turn expands to generate thrust.

The general geometries of these two configurations are shown in Fig. 1.1. In the flowing-core concept, cold hydrogen flows into the engine, parallel to the laser beam, and flows into a standing laser supported combustion (LSC) wave. This wave heats the hydrogen up to a temperature at which it can absorb laser energy by inverse Bremsstrahlung. The hydrogen is further heated by this process while flowing in a variable area streamtube, until all the laser energy is absorbed. The temperature of the hydrogen is sufficiently high that it is a dissociated and ionized plasma behind the LSC wave, and radiates energy. When all the laser energy is absorbed, the heated plasma expands through a nozzle to generate thrust. This plasma core streamtube will transmit energy through its side walls by both convection and radiation, and to protect the rocket walls a co-flowing buffer gas stream not heated by the laser may be necessary. The amount of buffer gas flow necessary is determined by the amount of energy lost radially by the plasma core.

In the stationary-core concept, a hot core of stationary hydrogen continually absorbs laser radiation and re-radiates it to a surrounding annular streamtube of flowing hydrogen propellant gas. The propellant gas absorbs the core radiation and becomes heated. After passing the core, it is expanded to generate thrust. The propellant gas also acts as a buffer to protect the walls from the hot core.

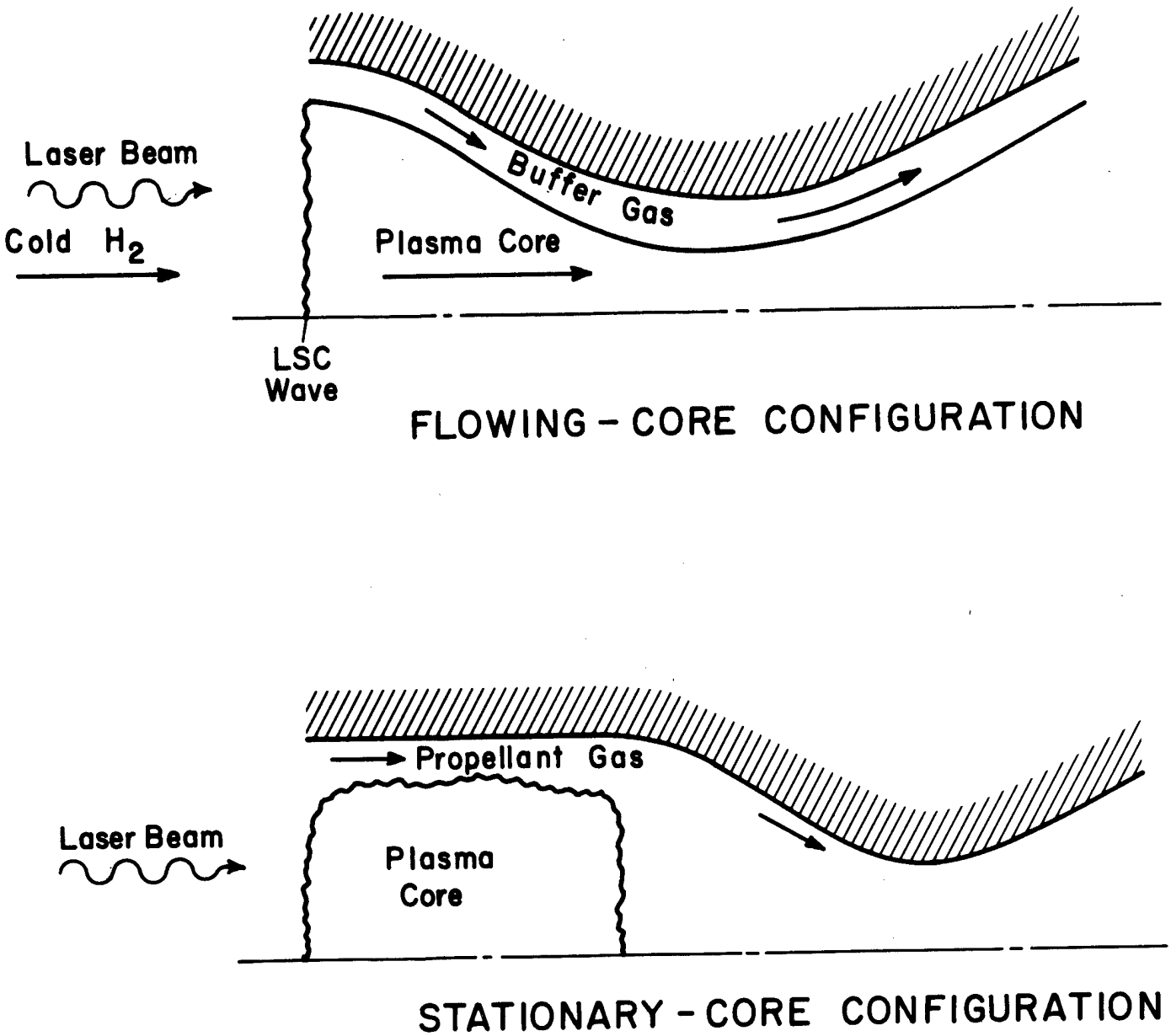

Fig. 1.1 Geometry of Laser-Heated Rockets

Clearly, these kinds of engines depend on a large number of physical processes. There is laser radiation absorption, for which the inverse Bremsstrahlung mechanism has already been defined as the desirable mechanism in Ref. 1. There is the radiation emission by the hydrogen plasma, which is a loss in the flowing-core concept and the main energy transfer mechanism in the stationary-core concept. There is the absorption of plasma radiation by colder hydrogen, which heats the propellant gas in the stationary-core concept, and the on-coming gas in the LSC wave. This absorption also can protect the walls. There is convective heat transfer from the hydrogen plasma core to the surrounding environment. There is the flow of heated hydrogen in a variable area streamtube while dissociating and ionizing. There is the LSC wave mechanism by which a laser can convert room-temperature hydrogen to a plasma which can absorb the laser energy. There is the interfacial mixing as the propellant gas flows past the core in the stationary-core concept.

In addition to these processes important to the steady state operation of the rocket, other physical phenomena are pertinent to the initiation of the absorbing plasma. These include the possible mechanisms of gas breakdown by electric discharge, by a focussed laser, or by absorption of laser energy by molecules or particles.

Although all these processes are involved in the operation of a laser-heated rocket, not all of them are studied in detail in this report. Here, the emphasis is on the flowing-core concept, and the processes important to its operation are the ones to which most attention is given. The work can be viewed as an extension of the studies presented in Ref. 1.

Information is presented on the three mechanisms of plasma initiation by electric arc discharge, by laser-induced breakdown, and by molecular and particulate abosrption, in Secs. 2, 3 and 4. A detailed study of the radiative emission from hydrogen is given in Sec. 5, leading to expressions useful for coupling the emission to the fluid mechanics of flowing hydrogen. Section 6 presents an estimate of the intensity vs wave speed for LSC waves in hydrogen by a rough extension of one of the theories for air. In Sec. 7 is a detiled description of a hydrogen plasma in chemical equilibrium, absorbing laser radiation by inverse Bremsstrahlung, radiating, and flowing through a variable area channel. Section 8 presents calculations on the heat loss by both radiation and convection of the flowing plasma core, and an estimate of the radiation which can be absorbed by particles in a buffer gas. In Sec. 9, the performance of the flowing plasma core as a rocket is given, based on the description of the core in Sec. 7. The stationary-core rocket is discussed in Sec. 10 in a qualitative and semi-quantitative way, based on estimates of the physical phenomena involved. The conclusions obtained so far in the study of laser-heated rockets are presented in Sec. 11.

The cases calculated for the flowing-core streamtube were laser powers of 10, 100 and 5000 kW, each at 3 and 10 atm initial pressure. These choices were made to provide information on sizes of engines in which NASA/Lewis has expressed interest. An experimental engine designed to operate at 10 kW, 3 atm is being designed and built by Rocketdyne Division of Rockwell International, under contract to NASA/Lewis, and the same organization is doing a study of a 5000 kW engine. PSI has aided Rocketdyne with the fluid mechanics and radiation aspects of their program, under a subcontract. The choice of a 100 kW laser was made to provide an intermediate size between 10 and 5000 kW, which might some day be tested. The calculations at the higher pressure of 10 atm were made to show the effect of pressure level on the core flow.

In addition to the laser power, and pressure level, there are a number of other parameters which could be varied in the calculations. One is the laser intensity which determines the mass flow rate per unit area into the core. In the present work this was held fixed at 3.67E9 W/m^2 (3.67E5 W/cm^2), which seems a value at which the LSC wave could be supported. When better knowledge of LSC waves in hydrogen is available, other values may be of interest. (The cross-sectional area of the rocket is inversely proportional to this intensity for a fixed laser power.) A second parameter which could be varied is the streamtube velocity distribution, which was also held fixed in the present calculations. Such parametric calculations could be performed by a slight improvement of the core flow program used here, and would aide in mapping out the regions of interest for laser-heated rockets.

2. PLASMA INITIATION BY ELECTRIC DISCHARGE

One possible technique for initiating laser supported combustion (LSC) waves in hydrogen gas is through use of an electric discharge. The purpose of the discharge is to supply an initial density of electrons in the gas so that the degree of absorption of laser energy by inverse Bremsstrahlung is sufficient to drive the gas to the required temperature for formation of a stable LSC wave. Electric discharges have previously been successfully used to initiated LSC waves in air[2]. No such studies are available for hydrogen. Thus the first question to be answered is what type of discharge is best suited for LSC ignition.

Electrical discharges can be broken into two basic groups, depending on whether they are or are not self-sustaining. In the latter group, designated as Townsend discharges, electrons are formed at the cathode by a technique such as thermionic emission; these are then accelerated by the electric field and, depending upon the field strength, these initial electrons can further ionize the gas within the discharge gap. The characteristic electron densities in such discharges are $\sim 10^{12}$/cc and the electron temperatures can be several electron volts, well out of equilibrium with the gas translational temperature.

As the voltage is increased across the electrodes a point is reached where a spark is created across the gap. This spark is a result of gas breakdown and will occur even if the cathode does not emit electrons, thus the term self-sustaining. The voltage at which a spark will occur, V_s, is a function of the product of gas pressure and gap distance, pD. The functional dependence of V_s on pD is described by a Paschen curve which is peculiar to the discharged gas. The Paschen curve for hydrogen is shown in Fig. 2.1 and, as an example, it can be seen at 1 atm and a gap length of 1 cm an applied field over 10,000 volts is required for sparking.

There are a variety of types of self-sustained (spark) discharges[3]; however, only two characteristic forms will be considered in the present discussion. The first of these is a glow discharge, characterized by electron densities of $\sim 10^{15}$/cc and electron temperatures of several eV, and the second is a thermalized arc discharge characterized by electron densities of $\sim 10^{17}$/cc and an electron temperature of order one eV, in equilibrium with the gas translational temperature.

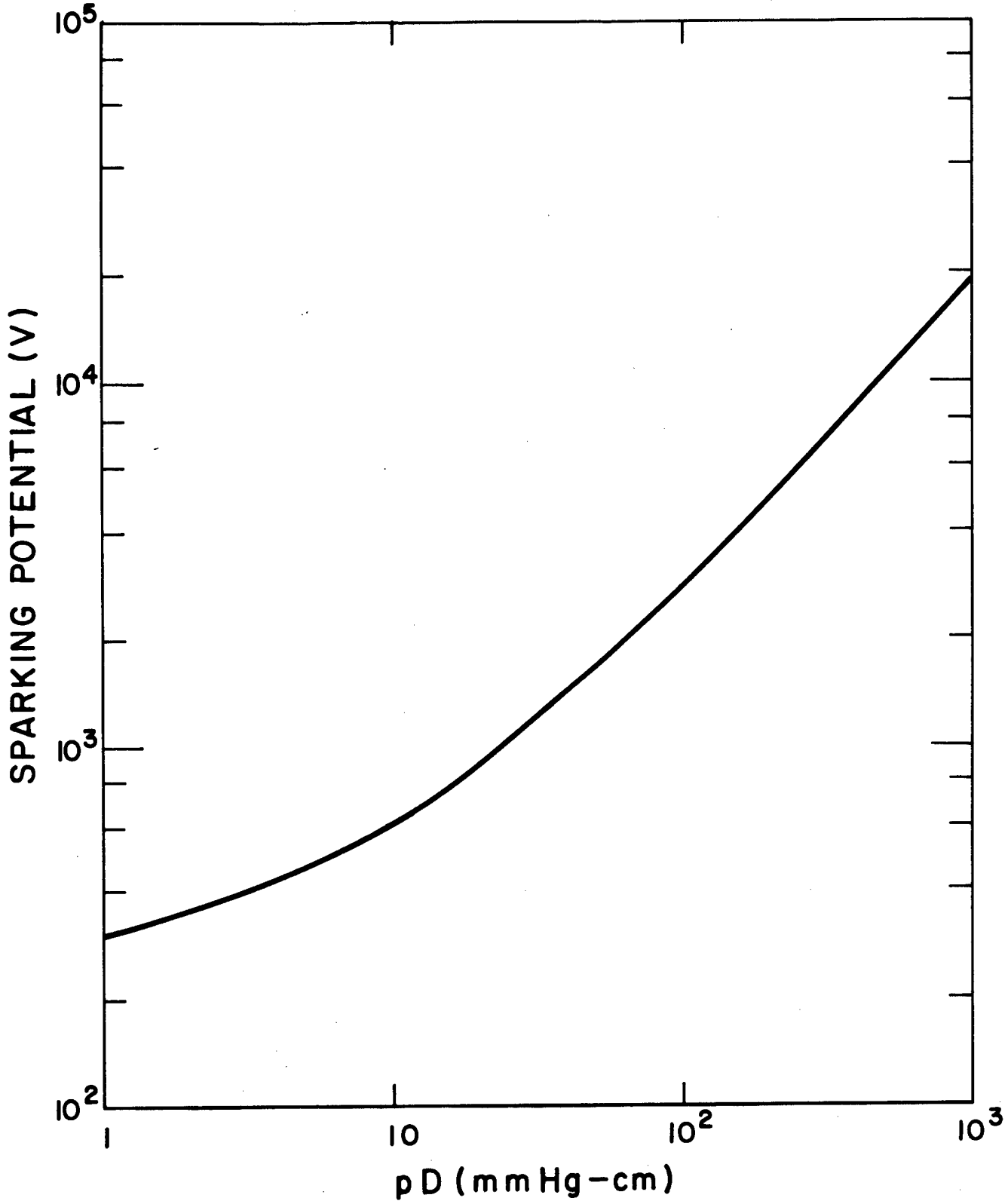

Fig. 2.1 Paschen Curve for Hydrogen

These three types of discharges, Townsend, glow and thermalized arc, have been examined under generic conditions for discharge initiation in order to determine which type is best suited for LSC ignition. This is not meant to imply that all three types of discharge may be attainable in a specific environment. Indeed Townsend and glow discharges are more favorably produced at sub-atmospheric pressures; however, the properties of a discharge are determined not only by pressure but also by numerous other factors such as voltage, gap size, electrode configuration, and the energy content of the relevant electronics.

The scenario considered is that of a discharge operating perpendicular to the gas flow, the latter being co-axial with the laser beam. The distance between anode and cathode is not specified but must be larger than the laser spot size since laser irradiation of the electrode elements is not desirable. The discharge length and gas velocity have arbitrarily been chosen to be 1 cm and 10^3 cm/sec respectively, so the gas flow time τ_F in the discharge region is 1 msec. Note this assumption does not imply that the discharge occurs simultaneously along the 1 cm length. In the case of a spark discharge the streamers would be considerably smaller than this. However, once a spark is initiated, it will attempt to travel along the path of least resistance and thus follow the flowing gas for some distance.

Once the discharge is initiated the gas in the discharge region will begin to absorb the laser energy via neutral-electron inverse Bremsstrahlung (or if the electron density is high enough by ion-electron inverse Bremsstrahlung). The total energy absorbed per unit volume of ionized gas is given by

$$\Delta E = \int_0^{\tau_F} k_L I \, dt \qquad (2.1)$$

where I is laser intensity and k_L is the inverse neutral Bremsstrahlung absorption coefficient at the laser frequency, defined by

$$k_L = \alpha_L (T) \, n n_E \, cm^{-1} \qquad (2.2)$$

where n is total gas number density, n_E is the electron number density and α_L (T) is a function of temperature (or, more appropriately, electron temperature in non-equilibrium situations) and frequency which is specific to the absorbing gas.

As the gas absorbs energy it will heat, causing an initial pressure rise and subsequent expansion which complicates the evaluation of relationship (2.1). In the present analysis a firm upper bound on the energy absorbed by the gas has been determined by assuming that the number density of the gas remains constant as the temperature increases. In this case, since the electron density of the discharge is specified, k will be determined by the form of α_L (T). In the cold gas the dominant neutral species will be H_2; however, as the gas is heated, dissociation will occur and hydrogen atoms will become the dominant neutral partner for the absorption process. The reduced absorption coefficients k_L' for H and H_2 are shown in Fig. 2.2 as a function of temperature, for a wavelength of 10.6 μm. These predictions have been developed from sources described in Reference 1. It is to be noted that the reduced absorption coefficients for the two gases are quite similar and that they scale approximately inversely with the temperature. The reduced absorption coefficient may be related to α_L (T) of Eq. (2.2) by the relationship

$$k_L' = \alpha_L (T)\, kT \quad , \tag{2.3}$$

where k is the Boltzmann constant, and thus for these gases α_L(T) is approximately a constant for λ = 10.6 μm. Therefore, from Fig. 2.2, k_L may be approximated by

$$k_L \approx 3.5 \times 10^{-37}\, n n_E, \ cm^{-1} \tag{2.4}$$

Taking $n = 2.5 \times 10^{19}$ part/cc, corresponding to p = 1 atm and T = 300°K, Eq. (2.1) then reduces to

$$\Delta E = 10^{-20}\, n_E I, \ Joules/cc \tag{2.5}$$

Equation (2.5) provides an approximate estimate of the amount of energy absorbed in one msec by a constant density, constant electron density plasma. The increase in temperature of the gas which is a result of this absorption may be deduced by consideration of the thermodynamic properties of heated hydrogen. The variation with temperature of the enthalpy/unit mass of constant pressure hydrogen plasmas is shown in Fig. 2.3 for pressures between 1 - 1000 atm. These predictions were taken from the analysis of Patch[4]. The enthalpy variation of a constant density hydrogen plasma may be deduced from a cross interpolation of the constant pressure data. Thus for a given amount of absorbed energy, as predicted by Eq. (2.5), a unique plasma temperature may be determined.

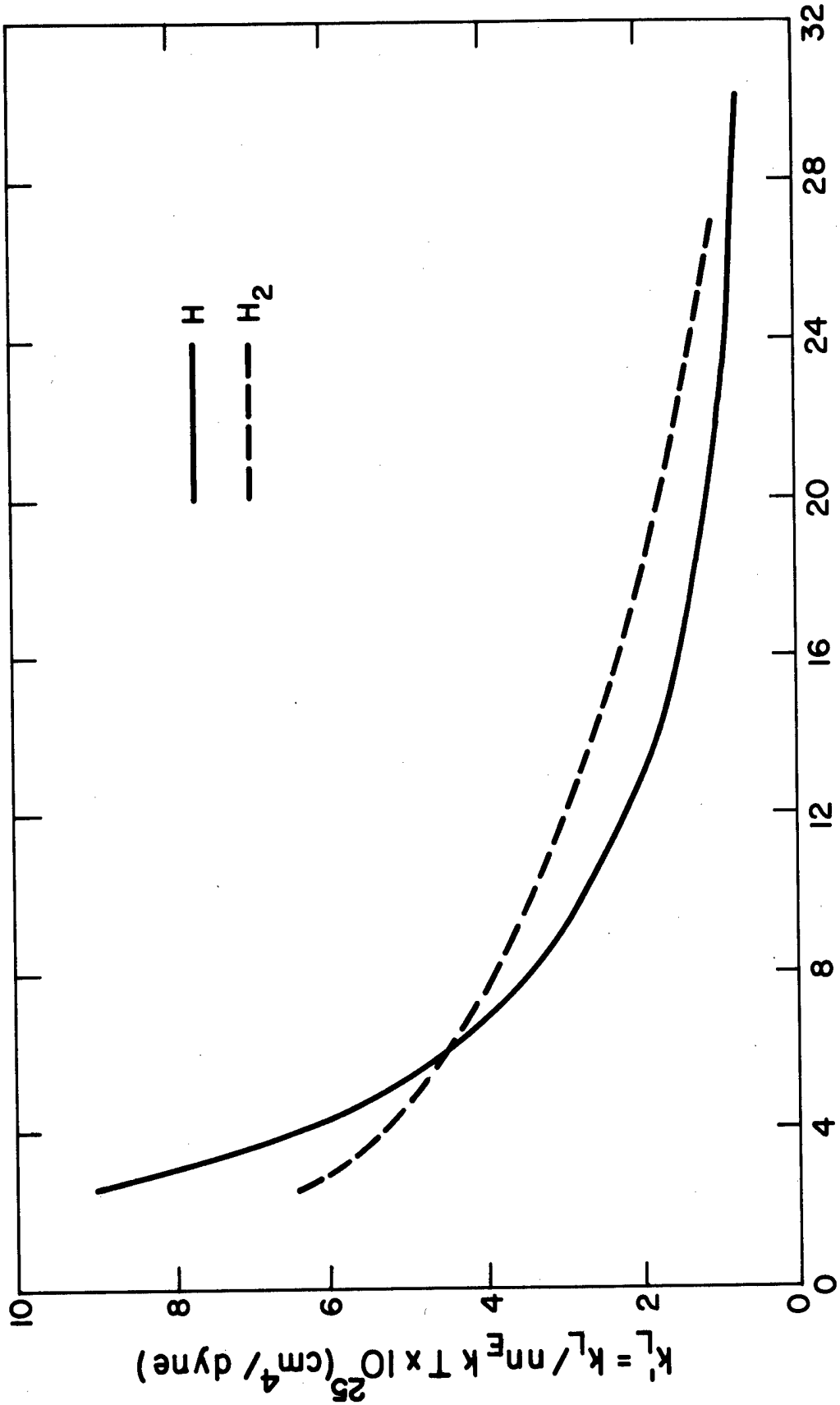

Fig. 2.2 Neutral Inverse Bremsstrahlung Reduced Absorption Coefficient for 10.6 μm

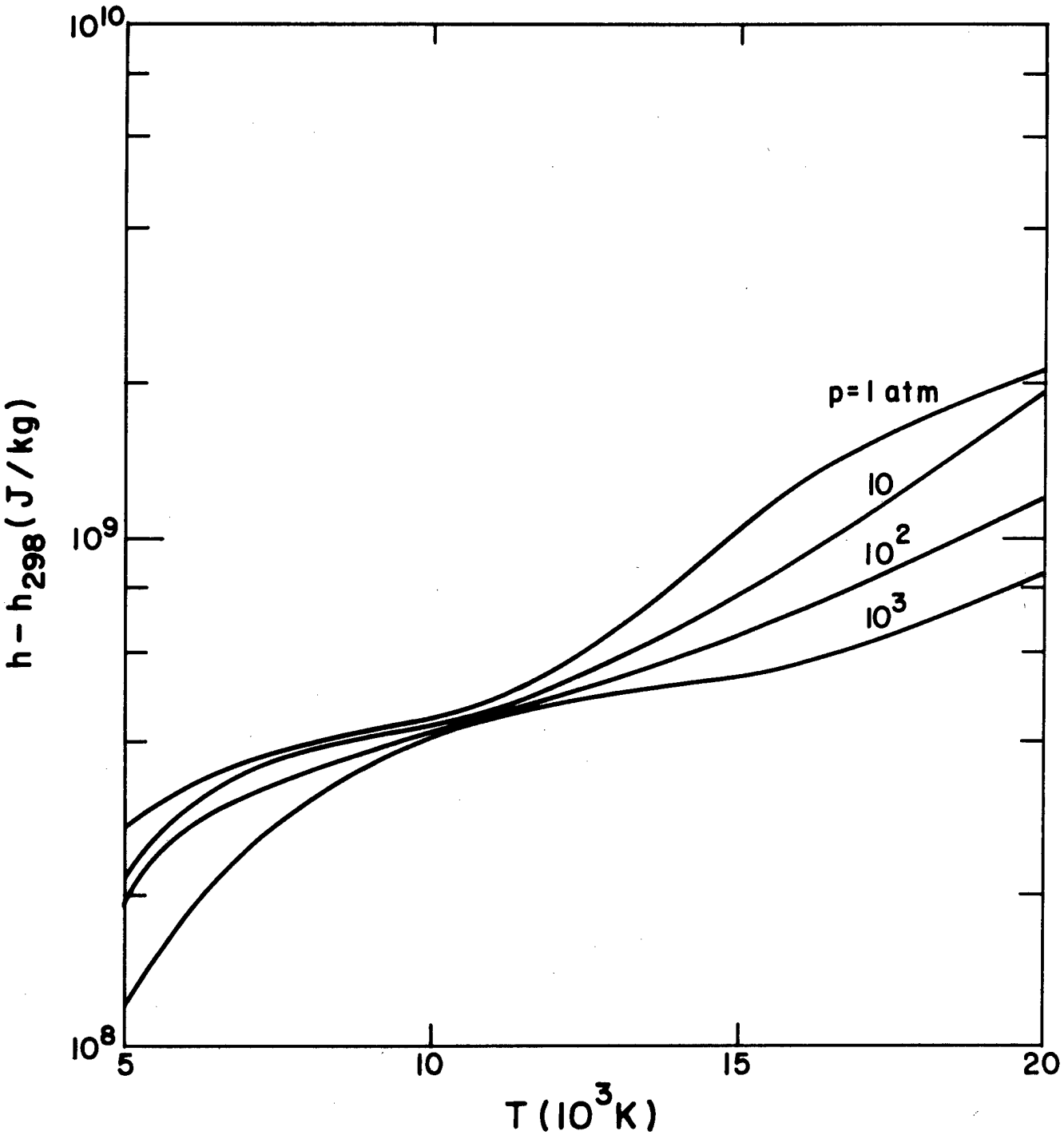

Fig. 2.3 Enthalpy of Hydrogen

Equation (2.5) has been evaluated as a function of laser intensity for the three generic discharges discussed earlier. The results are shown in Fig. 2.4. The final hydrogen plasma temperature which would be attained for a given amount of absorbed energy is shown on the right hand scale. Also shown as tick marks on the curves is the temperature at which the level of thermal ionization exceeds the ionization level created in the discharge. This latter temperature is a useful criterion for ignition inasmuch as a stable LSC wave would exhibit ionization levels higher than that created in the discharge (at the specified total densities). It can be seen from Fig. 2.4 that a Townsend discharge will not produce ignition and that a glow discharge would be effective at best only for intensities $> 10^6$ W/cm^2. Recalling that the results of Fig. 2.4 represent a strong upper bound on the absorbed energy, it would appear that the thermalized arc discharge is best suited for the successful electric discharge initiation of LSC waves in hydrogen.

From a systems viewpoint it is desirous to define the minimum discharge requirements for successful ignition, in terms of electrical energy content, device size and sophistication. Unfortunately, it is difficult to provide such a definition by theoretical means. The production of stable thermalized arcs is still more of an art than a science. One standard technique for their generation is through use of an over-voltaged capacitor. The evidence[5] suggests that a plasma with electron densities of $\sim 10^{15}$/cc is forced from the cathode end by high velocity ionizing waves into a spark channel. This streamer provides a finite resistance path for discharge of the capacitor. As the capacitor discharges, the gas in the streamer region will be heated by ohmic power dissipation. Presently, this behavior cannot be predicted a priori inasmuch as the plasma resistivity is a function of plasma electron density and streamer size, and the electron density in turn is connected to the rate of ohmic heating. This analysis is further complicated by the hydrodynamic behavior of the gas[6]. The initial spark can lead to formation of a cylindrical shock wave which can produce further ionization.

In any event, such discharges are readily produced in hydrogen and thermal equilibration times have been observed to be tens of nanoseconds[5, 7]. The discharged gas is low density (relative to ρ_∞) but highly ionized. Indeed measurements[7] performed in hydrogen in near atmospheric discharges exhibit electron concentrations near the anode as high as 10^{18}/cc and final temperatures as high as 50 - 60,000°K. It is concluded that LSC wave ignition may be achieved through use of a thermalized arc discharge; however, it is felt that optimum discharge conditions should be determined by laboratory experiments rather than through theoretical analysis.

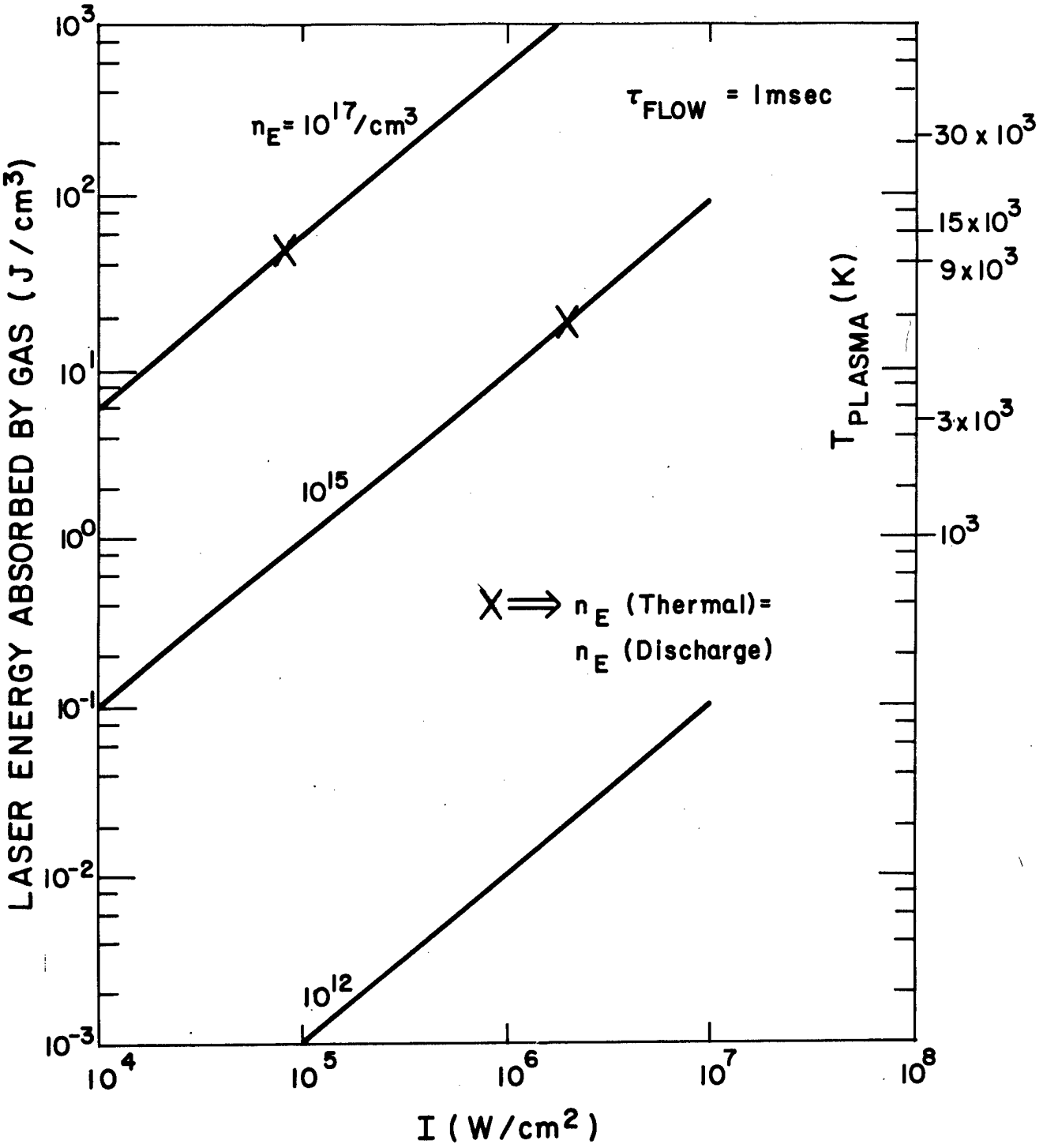

Fig. 2.4 Laser Energy Deposition for Various Discharge Electron Densities (Gas Density 4.9×10^{19} particles/cm^3)

3. PLASMA INITIATION BY LASER-INDUCED BREAKDOWN

3.1 INTRODUCTION

Free electrons can absorb laser radiation during collisions with heavy particles such as ions, atoms or molecules. In this process, known as inverse Bremsstrahlung, the role of the heavy particle is to conserve momentum. Little of the energy of the absorbed photon is transferred to the heavy particle. Free electrons transfer energy among themselves easily during collisions; therefore the laser energy absorbed by the electrons is rapidly distributed among all the free electrons. The electron distribution can then be characterized by an electron energy ϵ roughly equal to two-thirds the average electron energy just as kT is related to two-thirds the average energy in a Maxwellian distribution. (The factor of two-thirds relating ϵ and the average energy is exact only for Maxwellian distribution; nevertheless the characteristic energy ϵ is a useful concept.)

Energy transfer from the electrons to the heavy particles is less efficient than electron-electron transfer; hence it is possible for the gas temperature to lag behind the electron energy. For strong fields, electron heating occurs so rapidly that the few free electrons reach high characteristic energies, that is, a sizable fraction of the heavy particle ionization potential, without heating the gas noticably. At such energies a significant number of the electron - heavy particle collisions result in ionization. A chain reaction then occurs with both the original electron and the newly created electron absorbing laser energy and participating in further ionizing interactions. After a short time the avalanche created by electron - impact ionization leads to a sizable concentration of high energy electrons in a otherwise cold gas, i.e., to gas breakdown.

Experimentally, as laser intensity is increased from an initial low level an abrupt threshold is passed above which this breakdown occurs.[8] This threshold intensity can be estimated by balancing two important physical mechanisms. The first balance determines the number of electrons which remain in the laser - heated region. The rate of production of new electrons must equal the rate at which they are lost. The second balance determines the characteristic energy the electrons reach. They are heated by the laser, but lose heat by collisions with the gas molecules. From an analysis of there two balances, an estimate of the intensity for laser breakdown in hydrogen will be obtained.

3.2 ELECTRON PRODUCTION AND LOSS

In addition to production of electrons through electron - impact ionization, electrons may be freed by multiquanta absorption, the process in which an atom or molecule absorbs many low energy photons rather than one high energy photon. Whenever an appreciable number of electrons is present electron - impact ionization dominates. Multiquanta absorption is important only as a potential source of the initial electron population required for electron - impact ionization to dominate.[9]

In molecular gases the loss mechanisms generally are attachment of an electron to a neutral molecule, recombination of an electron with an ionized species (with or without the presence of a third particle) and electron diffusion out of the volume influenced by the laser. Attachment is unimportant in hydrogen. The recombination rate is also small, particularly during the initial stages of breakdown. Diffusion is the predominant loss process.

The net rate of electron production in hydrogen can thus be expressed as

$$\frac{\partial n}{\partial t} = \nu_i n_E + \nabla \cdot D \nabla n_E \ , \qquad (3.1)$$

where n_E is the number density of free electrons, ν_i is the ionization rate per electron (the concentration of neutral molecules is absorbed into the definition of ν_i) and D is the diffusion coefficient.

For rough estimates the diffusion loss mechanism can be approximated by

$$\nu_D n_E \equiv \vec{\nabla} \cdot (D \vec{\nabla} n_E) \sim \frac{D n_E}{R_b^2} \qquad (3.2)$$

where R_b is the radius of the laser beam. As long as the electron density is low the electron diffuses freely. At high concentrations diffusion proceeds at the slower ambipolar rate. For our estimates of threshold intensity we will use the free diffusion coeffient.

Breakdown requires electron production to exceed diffusion losses. The threshold electron energy for breakdown can be estimated by balancing losses and gains.

$$\nu_i(\epsilon) = \nu_D(\epsilon) \tag{3.3}$$

The quantities ν_i/n_M, Dn_M and ϵ, where n_M is the number density of free molecules, are known as functions of the electric field per particle, E/n_M, from experiments with static electric fields.[10,11,12] Despite the difference in the electron distribution function for DC fields as compared to AC fields calculations have indicated that the ionization rate for the same ϵ is very similar. We have thus used the DC experimental radius to determine ν_i/n_M and Dn_M as functions of electron energy ϵ.[13] In Fig. 3.1 we have plotted versus ϵ the diffusion frequency per molecule for an electron, ν_D/n_M, for various values of pR_b, (where $p = (3.034E\text{-}17)\, n_M$ at 293K), and the ionization frequency per molecule for an electron, ν_i/n_M. The extremely steep increase of ν_i/n_M with ϵ indicates why the threshold is abrupt. A small increase in ϵ above the temperature needed to balance diffusion losses results in ionization completely dominating diffusion. For example ionization and diffusion balance at $\epsilon \sim 2.7$ eV when $pR_b = 1$ torr-cm. If the electron temperature reaches 2.8 eV for the same pR_b, we find that

$$\frac{\nu_i}{n_M} - \frac{\nu_D}{n_M} \sim 2 \times 10^{-11}\ \text{cm}^3/\text{sec} \ . \tag{3.4}$$

For 1 atmosphere hydrogen at 293K, $n_M \sim 2.5 \times 10^{19}\ \text{cm}^{-3}$ so that solving the electron production Eq. (3.1) leads to

$$n \sim n_o \exp(5.0 \times 10^8\, t) \tag{3.5}$$

Thus if the breakdown requirements are exceeded by even a small amount the gas breaks down rapidly. [Of course other time scales are also involved - the time to heat the electrons and the time required to produce a reasonable initial electron population if one is not present.]

3.3 ELECTRON ENERGY BALANCE

The minimum laser intensity necessary to reach the breakeven electron energy is determined by equating the electron heating by the laser and the power lost through collisions with the molecules. The electron heating is described by

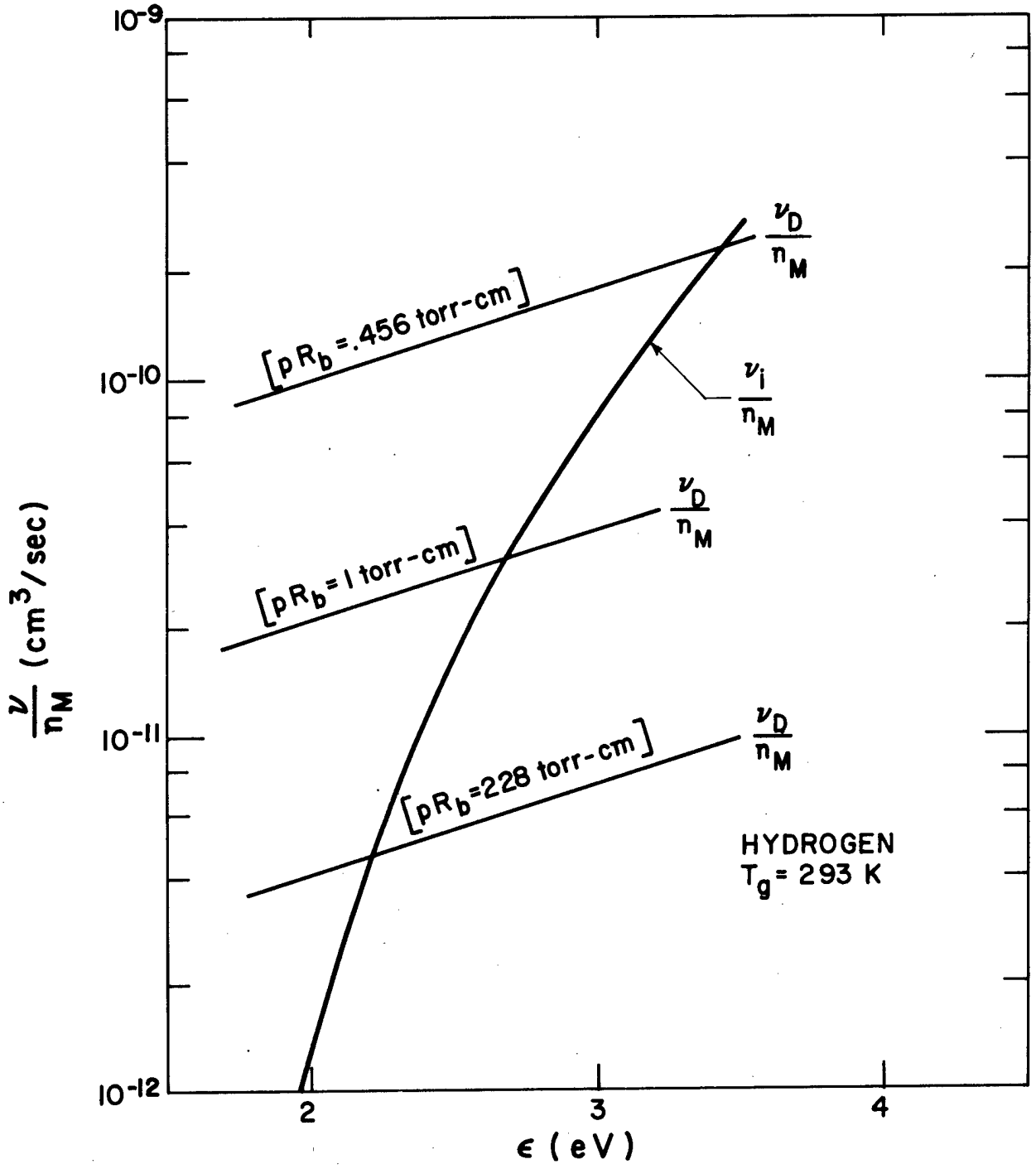

Fig. 3.1 Diffusion Frequency and Ionization Frequency in Hydrogen at Various Values of pR_b

$$\frac{d\epsilon}{dt} = \frac{e^2}{m_E} \frac{\nu_m E^2}{\nu_m^2 + \omega^2} - \nu_{in} \epsilon \qquad (3.6)$$

where e and m_E are the charge and mass of the electron, respectively, ω is the angular frequency of the laser radiation, E is the RMS electric field, ν_m the momentum transfer collision frequency per electron and ν_{in} the inelastic collision frequency per electron. The first expression on the right hand side represents inverse Bremsstrahlung which can be calculated from collision theory. For our purposes, however, it is simpler to use the expression given above and the experimentally determined values of ν_m and ν_{in} versus ϵ as determined from DC experiments.

The minimum laser intensity I necessary to reach ϵ is found by setting the right hand side of Eq. (3.6) equal to zero.

We have

$$I = cE^2/4\pi$$

$$= \left(\frac{\nu_{in}}{n_M}\right) \left(\omega^2 + \nu_m^2\right) \frac{m_E c \epsilon}{4\pi e^2} \Bigg/ \left(\frac{\nu_m}{n_M}\right) \qquad (3.7)$$

For I in watts/cm^2 and ϵ in eV, Eq. (3.7) becomes

$$I = 1.5 \times 10^{-18} \frac{(\nu_{in}/n_M)}{(\nu_m/n_M)} (\omega^2 + \nu_m^2) \epsilon \ . \qquad (3.8)$$

It is now possible to investigate qualitatively how close the breakeven intensity is to the true threshold intensity. In the eV range ν_{in} increases extremely rapidly with small increases in ϵ where as ν_m is almost constant. Hence the second term of Eq. (3.6) is negligible throughout most of the heating. It serves only to stop the heating abruptly at the final electron energy. Because of the sensitivity of both the production rate and the heating rate to small changes in ϵ, the two balances, Eqs. (3.3) and (3.6) should lead to accurate estimates of the threshold intensity. There is

greater uncertainty in the experimental values of ν_m, ν_i, ν_{in}, Dn_M and ϵ then in the identification of the threshold intensity with the breakeven intensity.

3.4 BREAKDOWN ESTIMATE

For a given beam radius R_b and pressure p, the laser intensity to produce breakdown can now be estimated. Using Fig. 3.1, the energy ϵ at the crossing point of the ν_i/n_M and ν_D/n_M curves is found. Using this energy, the quantities ν_{in} and ν_m are obtained from Refs. 10 or 11. Then the laser intensity I is calculated for the desired circular frequency ω from (3.8). Using this procedure the threshold intensity necessary to achieve breakdown in pure hydrogen initially at 293° K and 3 atmospheres pressure is plotted versus laser beam radius for a 10.6 μ laser in Fig. 3.2.

The threshold intensity is seen to decrease with increasing spot size until a plateau near $I = 4.5 \times 10^9$ W/cm^2 is approached. The decrease is caused by the lowering of the diffusion loss rate with increasing radius. The plateau represents the minimum intensity needed to raise the electron energy high enough for appreciable ionization to occur. The intensity of a 10 kW laser is also plotted as a function of beam radius. Over a limited range of pressure and wavelength the breakdown curve scales as follows: for a given laser intensity and wavelength, the beam radius is inversely proportional to pressure; for a given radius and pressure the threshold laser intensity is proportional to the wavelength squared.

Focussing a powerful laser unto a small volume will produce a high concentration of free electrons within a small volume. The effectiveness of laser induced breakdown in initiating an LSC wave is probably not limited by the electron concentration achievable but rather by the volume over which such a concentration can be sustained.

3.5 LASER-INDUCED BREAKDOWN WITH PARTICULATES

The effect of particle contaminants on the breakdown threshold for air is a subject which has recently received considerable attention. It has been found by numerous investigators[14 - 16] that the intensity threshold in the presence of particulates may be lowered as much as three orders of magnitude from the clean air threshold. Although there is no data for the effects of particulates upon the breakdown threshold in hydrogen, the mechanisms by which particules induce breakdown at lower intensities in air will also lead to lowering of the threshold in hydrogen.

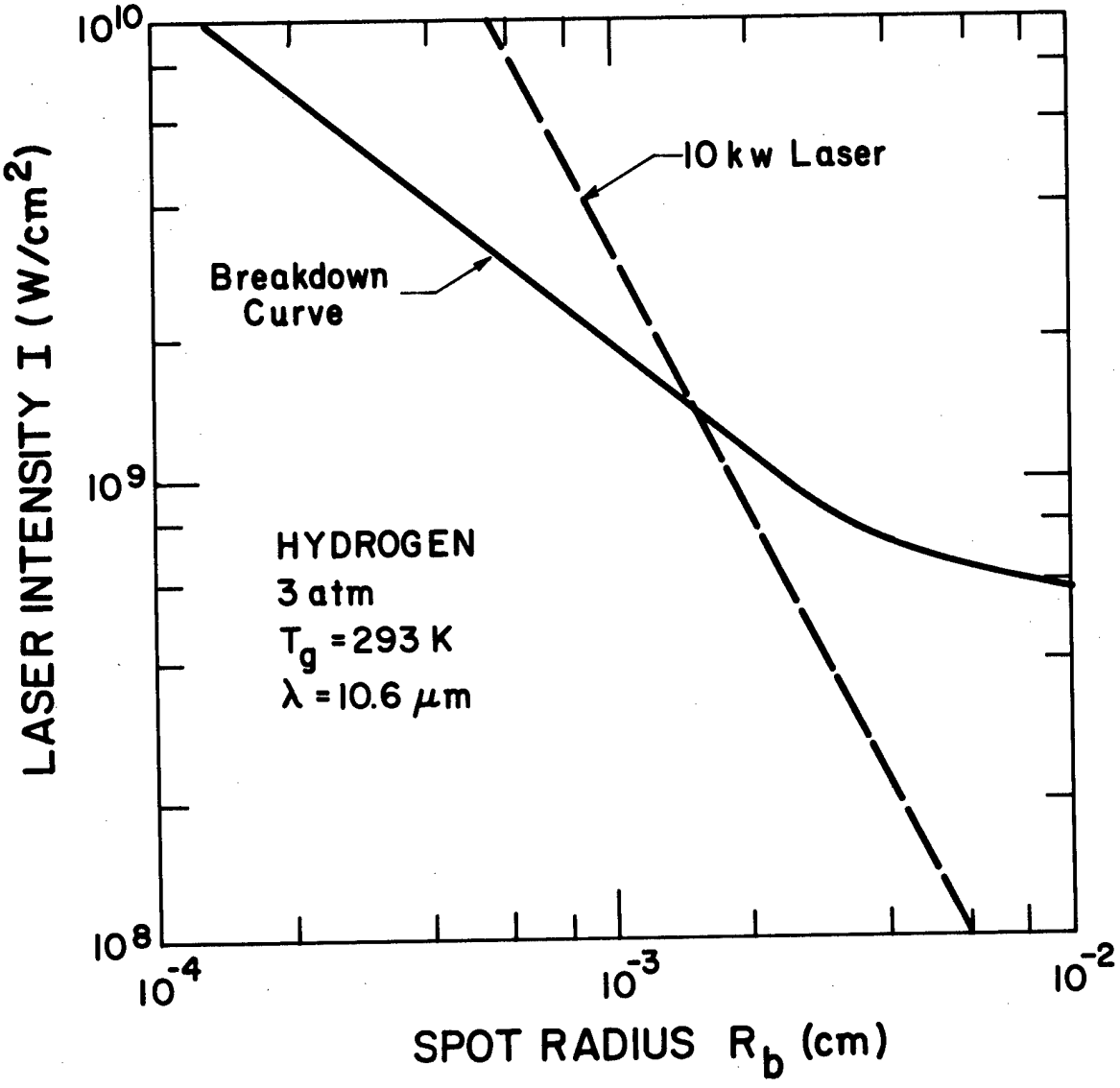

Fig. 3.2 Laser Intensity Required for Breakdown in Hydrogen and Laser Intensity Available from 10 kW Laser

A summary[17] of the observed breakdown data in air is presented in Fig. 3.3. The air breakdown threshold is a function of pulse time, beam diameter and particle size. The lowest observed threshold was of the order of a megawatt per cm^2; however, 30 μm particles were required to initiate the breakdown. In addition, it was observed[15] that no breakdown occurred with the larger particles at the lowest intensities until 10 μsec into the pulse. Shorter pulses do not yield breakdown with contaminants unless the flux is considerably higher.

The physics of particle induced breakdown is not well understood. For short pulses the particles evaporate rapidly, and cascade breakdown occurs in either the particle vapor or the air surrounding the particle. Triplett and Boni[18] have performed a theoretical study of the interaction of laser radiation with a single suspended particle. Their analysis applies only when the laser intensity is sufficiently large that the rapidly evaporating or "exploding" particle drives a strong shock wave into the surrounding air. Breakdown then occurs via a nonequilibrium cascade process (described above) in either the vapor or shock heated air. Calculations indicate that reductions in the breakdown threshold to slightly greater than one order of magnitude below that of clean air are feasible by this mechanism. It is not possible to predict with this mechanism the reduction in the threshold by the observed several orders of magnitude at longer laser pulses. In addition, an "incubation" time or delay time between laser turn-on and breakdown was observed with the long laser pulses[16] (10 μsec). Since the delay times are 10 - 30 μsec, the breakdown mechanism is nonequilibrium cascade ionization of shock heated air or vapor. It appears that the vapor formed by the evaporating particle heats in local thermodynamic equilibrium and transfers its energy to the surrounding air by conduction and radiative transport. The air ultimately heat via inverse Bremsstrahlung absorption until the formed plasma becomes opaque to laser radiation. However, at present there are not theoretical models capable of predicting the breakdown threshold under these conditions.

Therefore, although it is not possible to predict the breakdown threshold in particle seeded hydrogen, we would expect this to be a viable technique for igniting the plasma at lower intensities than predicted by Fig. 3.3.

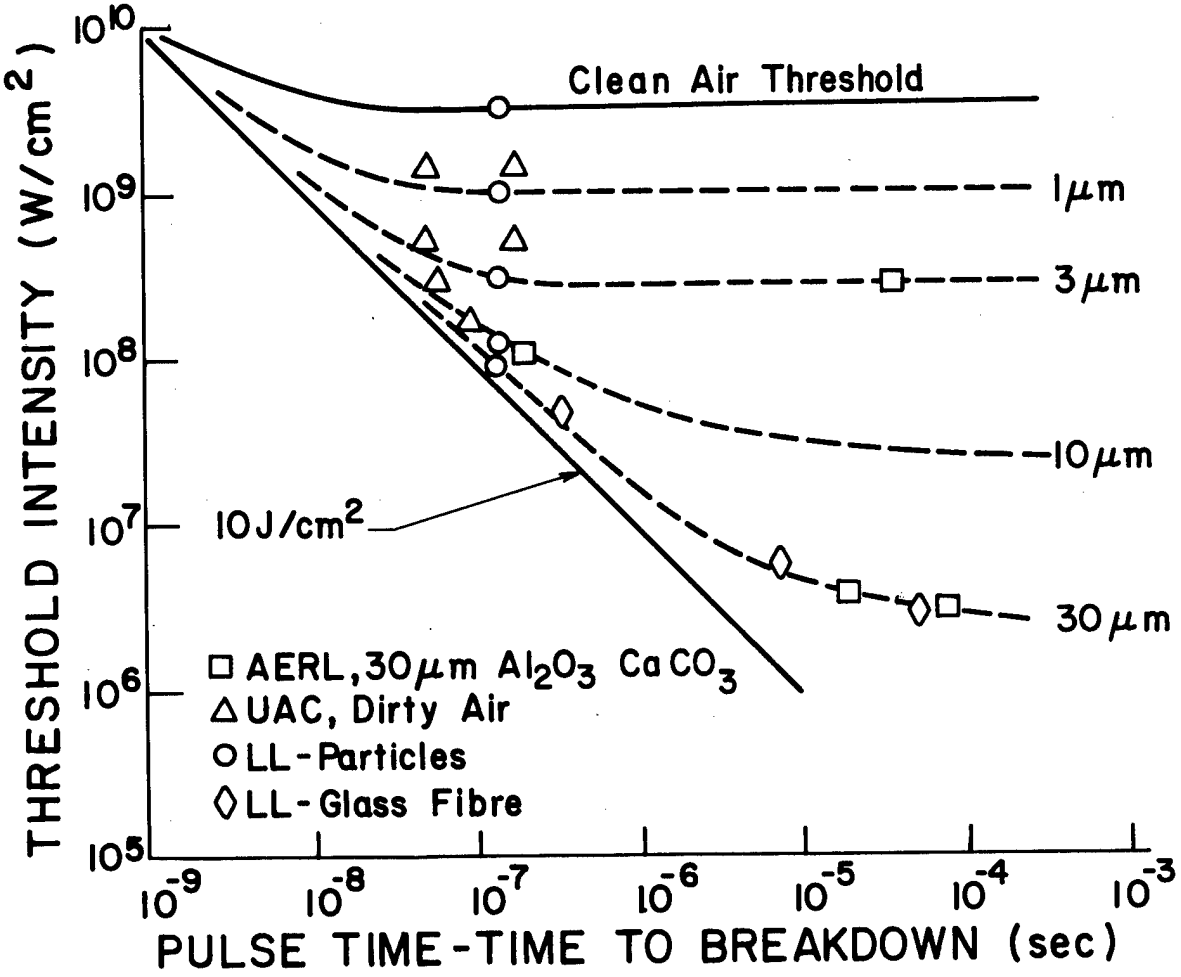

Fig. 3.3 Measurements of Air Breakdown in the Presence of Particulate Matter

4.0 PLASMA INITIATION BY MOLECULAR AND PARTICULATE ABSORPTION

The two methods of initiation discussed in the previous two sections, electric discharge and laser-induced breakdown, provide the electrons to initiate inverse Bremsstrahlung absorption by a nonequilibrium process. A third alternative is to provide the electrons in an equilibrium process by heating hydrogen into its ionization region. For pure hydrogen, that means heating to $T \sim 10,000$ K. If the hydrogen is seeded with an easily ionizable material, a much lower temperature would suffice. Cesium, for example, ionizes around 3000 K.

Such heating could be accomplished if one could find molecules or particles which would absorb 10.6 μm laser radiation, become hot and transfer their heat to the gas. In Ref. 1, Sec. 3, a study was made of possible molecular absorbers for 10.6 μm radiation. It was concluded that high temperatures could not be reached because the molecular absorbers dissociate (and so stop absorbing) at a few thousand degrees. No molecules which circumvent this limitation were identified in Ref. 1, nor have any come to light during performance of the work reported here. However, if seeded hydrogen is considered, then the gas need only be heated to a few thousand degrees for ionization to occur. Molecular absorption might be an effective means of accomplishing this heating.

Particulate absorption was also studied in Ref. 1, Sec. 4, as well as in Ref. 19. Here the particles absorb laser photons, get hot, and conduct heat to the hydrogen. Here again a temperature limitation was found. An upper bound for particle vaporization is 5000 K, limiting the temperature which can be reached to below the pure hydrogen ionization region, but within the ionization region of seed materials.

There was noted in Refs. 1 and 19 some possible benefits from hot particles, other than heating the gas. The vapor produced from hot particles may itself absorb the laser radiation, and may also have a lower ionization potential than the hydrogen. Furthermore, small particles can emit electrons thermionically as they are heated, though this emission is inhibited by electrostatic effects as the particle charge builds up. However, the electrons produced may be sufficient to support laser-induced breakdown.

Nevertheless, it seems at the present time that molecular or particulate absorption is not a favorable scheme for initiating an unseeded hydrogen plasma, compared to electric arc or laser-induced breakdown.

5. RADIATIVE EMISSION FROM HYDROGEN

5.1 INTRODUCTION

As the laser heats the hydrogen to high temperatures the radiation from the gas increases dramatically. In an ionized plasma, radiation contributes importantly as an energy transfer mechanism within the plasma and as a loss mechanism from the plasma. The radiative transfer within the gas affects both the axial and radial temperature gradients. Thus a precise description of the physical state of the gas in the rocket core requires that the radiation and fluid mechanics be coupled. It is beyond the scope of this report to deal with all aspects of the coupled problem. In keeping with approximations to be made in the fluid mechanics, such as the omission of the radial temperature gradients, we neglect radial radiative transfer within the plasma. Further-more, the axial radiative transfer within the hot gas is expected to be small compared to the laser heating; it will not be considered here. Axial radiative transport from the hot plasma to the cold incoming gas may be important. Its effect is included in the LSC wave properties discussed in the next section.

The only plasma-produced radiation remaining to be considered is the radial flux leaving the gas. This radiative transport enters into rocket engine analysis in two ways. First, the power lost radially must be absorbed somewhere else in the rocket, either in the walls or in a buffer gas. Second, the radial radiation which escapes the plasma must be accounted for in the fluid mechanical equations as a loss. At sufficiently high temperatures, in fact, it is the major loss mechanism and effectively limits the maximum temperature attainable.

The approach we follow here is first to study the local radiation properties of the plasma, and then to develop, using the local properties as guides, a reasonable approximation to the coupled radiating gas dynamic system.

5.2 LOCAL SPECTRAL RADIATION PROPERTIES

The spectral radiation properties of a hydrogen plasma are determined by the local state of the system. We assume that the plasma is in local thermodynamic equilibrium, so that temperature and pressure define the state of the gas. The concentrations of the various species is determined

through the equilibrium conditions. The temperatures and pressures of interest are those expected in a rocket heated by laser absorption; that is, temperatures between 10,000 K and 20,000 K and pressures between one and ten atmospheres. In the interest of simplicity we need only include effects which are expected to contribute 10% or more of the total radiation.

The basic ingredients for determining local radiative properties are the cross sections for the possible interactions and the number density of the various species. The use of local thermodynamic equilibrium assumes that collisions among the various species of the gas are frequent enough to ensure an equilibrium distribution of velocity and of species, corresponding to the local temperature and pressure. With this assumption and the principle of detailed balance the radiative transfer equation can be written in a simplified form involving only one function depending upon the concentration of species and the interaction cross-section. The radiative transfer equation has the following form:[20]

$$\hat{n} \cdot \nabla I_\omega (x, \hat{n}) = k'_\omega (T, p) [B_\omega (T) - I_\omega (x, \hat{n})] \qquad (5.1)$$

where $\omega = h_P \nu$ is the photon energy; I_ω is the spectral radiation intensity which depends on ω, x, and the direction specified by the unit vector $\hat{n}$; and $B_\omega (T)$ is the equilibrium spectral radiation intensity given by

$$B_\omega (T) = \frac{\omega^3}{c^2 \hbar^3 (e^{\omega/kT} - 1) 4\pi^3} \qquad (5.2)$$

where c is the velocity of light, $\hbar$ is the Planck constant divided by 2π and k is the Boltzmann constant. The effective absorption coefficient is related to $k_\omega (T, p)$, the absoption coefficient uncorrected for reabsorption, by

$$k'_\omega (T, p) = (1 - e^{-\omega/kT}) k_\omega (T, p) . \qquad (5.3)$$

The absorption coefficient $k_\omega (T, p)$ is, in turn, easily expressed as a sum of products of absorption cross sections and species concentrations. The temperature and pressure dependence of k_ω enter mainly through the concentration of species. However, secondary temperature variations occur whenever the cross section must be averaged over the relative flux of some of the involved species, as occurs in inverse Bremsstrahlung.

The first step in determining k_ω (T, p) is to detail which interactions are expected to be important for the range of temperatures and pressures expected. The interactions to be considered, in turn, depend upon the species which are abundantly present. When radiation is an important loss mechanism the concentration of molecules is several orders of magnitude lower than the atomic concentrations. We therefore consider a plasma in which only atoms, excited atoms, ions (protons) and electrons are present. Their relative abundance is determined through the Saha equation

$$\frac{n_E\, n_I}{n_A} = \frac{Q_{el\,I}\, Q_{el\,E}}{Q_{el\,A}} \left(\frac{k\, m_E}{2\pi \hbar^2} \right)^{3/2} T^{3/2}\, e^{-\theta_I/T} \qquad (5.4)$$

where n_E, n_I and n_A are respectively the concentration of electrons, ions and hydrogen atoms, $Q_{el\,E}$, $Q_{el\,I}$ and $Q_{el\,A}$ are the electronic partition functions of the electron, ion and the neutral atom and θ_I is the ionization portntial expressed in temperature units. (In more accurate calculations than are necessary here, θ_I would be replaced by $\theta_I - \Delta\,\theta_I$ where $\Delta\,\theta_I$ is the effective lowering of the ionization potential corresponding to terminating the sum in the electronic partition function of the neutral atom after a finite number of excited states).

The transitions which lead to emission can now be listed. They are:

1) capture of a free electron by an ion

2) Bremsstrahlung involving electron-ion collisions

3) Bremsstrahlung involving electron-atom collisions

4) radiative decay of an excited atom.

5.3 CONTINUUM TRANSITIONS

The spectral properties of the first three types of transitions, the transitions involving the electron continuum, can be estimated by semi-classical formulas. The quantum corrections to these formulas need only be included when the quantum correction is large and the radiation emitted is a sizeable portion of the total radiation produced.

From Kramer's semi-classical analysis of electron-proton Bremsstrahlung the absorption coefficient is given by[21]

$$k_\omega (T, p) = \left(\frac{2\pi}{3 m_E kT}\right)^{1/2} \frac{16\pi^2 e^6 n_I n_E \hbar^2}{3 c m_E \omega^3} \qquad (5.5)$$

where e is the charge of the electron and the pressure dependence enters only through the number densities.

Similar semi-classical formulas can be derived for bound-free absorption wherein an electron of energy E_n in the nth quantum state of an atom absorbs a photon of energy ω resulting in a free electron kinetic energy $\omega + E_n$ and a free ion. The semi-classical cross section for absorption is[22]

$$\sigma_{\omega, n} = \frac{8\pi e^{10} m_E}{3\sqrt{3} (\hbar)^3 c \omega^3 n^5} \qquad (5.6)$$

The total bound free absorption coefficient for radiation of given ω is then

$$\sum_{n \geq n_\omega^*} n_n \sigma_{\omega, n} \qquad (5.7)$$

where n_n is the number density of atoms in the nth quantum state, and where n_ω^* is the lowest quantum state which can be ionized by a photon of energy ω; that is

$$\frac{k\theta_I}{(n_\omega^*)^2} < \omega < \frac{k\theta_I}{(n_\omega^* - 1)^2} \; . \qquad (5.8)$$

The Bremsstrahlung due to ion-electron collisions Eq. (5.) can be re-expressed in a form similar to Eq. (5.7) by using the Saha Eq. (5.4) with $Q_{el\,I} = 1$ to convert the product $n_E n_I$ into the concentration of ground state atoms, n_{AG} and by similarly expressing n_n in terms of n_{AG}:

$$n_{AG} = \frac{2 n_A}{Q_{el\,A}} \qquad (5.9)$$

$$n_n = n_{AG}\, n^2\, e^{-\theta_I (1 - 1/n^2)/T} \tag{5.10}$$

The sum of the absorption coefficients for Bremsstrahlung and free-bound transitions is

$$k_\omega (T, p) = \frac{8\pi e^{10} m_E n_{AG} e^{-x_1}}{3\sqrt{3}\, c\omega^3 \hbar^3} \left[\frac{1}{2x_1} + \sum_{n=n_\omega^*}^{\infty} \frac{e^{x_n}}{n^3} \right] \tag{5.11}$$

where we define $x_n = \dfrac{\theta_I}{n^2 T}$, and we have used in (5.5) the expression for the ionization potential of hydrogen in terms of fundamental constants,

$$\theta_I = e^4 m_E / 2k\hbar^2 \tag{5.12}$$

to get the first term in brackets in (5.11).

If ω is given in eV and n_{AG} in cm^{-3}, then k_ω in cm^{-1} is

$$k_\omega = 1.99 \times 10^{-4} \frac{n_{AG}}{\omega^3} \left\{ \frac{1}{2x_1} + \sum_{n=n_\omega^*}^{\infty} \frac{e^{x_n}}{n^3} \right\} e^{-x_1}$$

(If the lowering of the ionization potential were important, Eq. (5.11) would have $1/2\, x_1$ replaced by $e^{\Delta\theta_I/T}/2x_1$).

The emission coefficient $\epsilon_\omega (T, p)$ is defined as

$$\begin{aligned} \epsilon_\omega (T, p) &= k'_\omega (T, p)\, B_\omega (T) \\ &= k_\omega (T, p)\, (1 - e^{-\omega/kT})\, B_\omega \end{aligned} \tag{5.13}$$

The semi-classical approximation to ϵ_ω (T, p) found from Eqs. (5.11) and (5.13) is shown in Fig. 5.1 for p = 3 atm and T = 14,000 K. The total continuum power emitted per unit volume, neglecting reabsorption effects, is found by integrating ϵ_ω over solid angle and over the photon spectrum.

$$P_{cc}(T, p) = \int d\Omega \int_0^\infty \epsilon_\omega (T, p)\, d\omega = 4\pi \int_0^\infty \epsilon_\omega (T, p)\, d\omega \qquad (5.14)$$

$$= 8.58 \times 10^{-9}\, n_{AG}\, \frac{e^{-x_1}}{x_1} \left\{ \frac{1}{x_1} + 2.404 \right\} \left(\frac{\text{watts}}{\text{cm}^3} \right)$$

In Fig. 5.2, P_{cc} (T, p) is plotted versus temperature for a hydrogen plasma at 3 atm.

If, on the other hand, the vacuum ultraviolet part of the spectrum ($\omega \geq 13.6$ eV) is effectively reabsorbed, the continuum power lost in the semi-classical approximation is

$$P'_{cc}(\omega \leq 13.6) = 4\pi \int_0^{13.6} \epsilon_\omega (T, p)\, d\omega$$

$$= 8.58 \times 10^{-9}\, n_{AG}\, \frac{e^{-x_1}}{x_1} \left\{ \frac{1}{x_1} + 0.404 \right\} \left(\frac{\text{watts}}{\text{cm}^3} \right) \qquad (5.15)$$

which is also shown in Fig. 5.2.

The relative magnitude of bound-free emission and Bremsstrahlung can now be determined. The contribution of ion-electron Bremsstrahlung to the emitted power, as compared to the bound-free emission, is estimated by comparing $1/x_1$ to 2.404 when no reabsorption occurs and to 0.404 when the vacuum ultraviolet is strongly reabsorbed. For the temperatures of interest we have $0.07 < x_1^{-1} < 0.14$. Thus Bremsstrahlung is not expected to be an important factor unless the bound free emission is inhibited by reabsorption.

The other continuum contribution, Bremsstrahlung associated with electron-neutral collisions, is much smaller than electron-ion Bremsstrahlung except when atoms are at least one hundred times more abundant than ions.[23] Only at low temperatures, such as 10,000 K, and high pressures

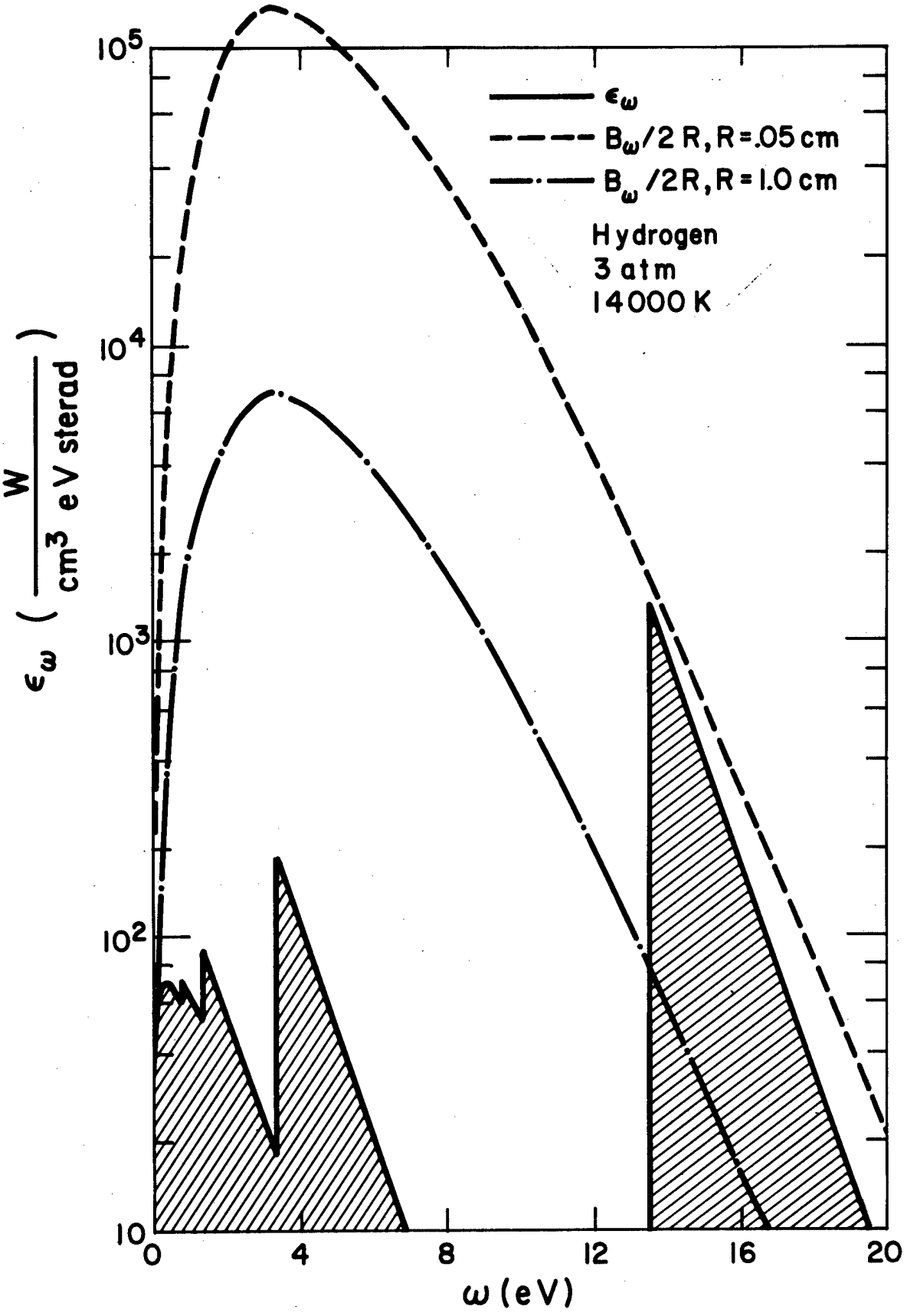

Fig. 5.1 Semi-classical Approximation for the Continuum Spectral Emissivity of Hydrogen and the Black Body Limits for Two Choices of Radius

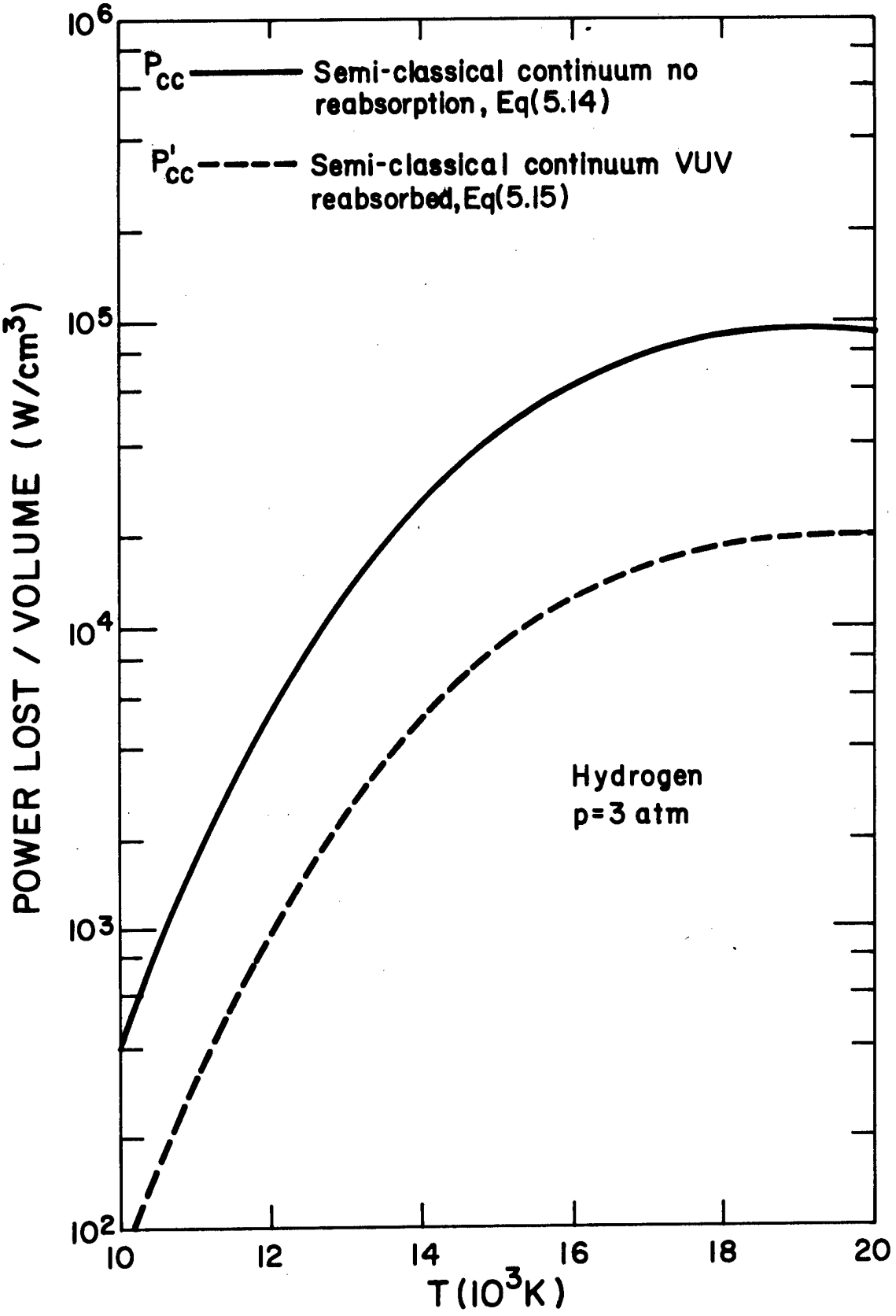

Fig. 5.2 Continuum Power Radiated per Unit Volume of Hydrogen

does the neutral concentration overwhelm the ion concentration sufficiently to make neutral Bremsstrahlung as important as electron-ion Bremsstrahlung, which itself is only a small fraction of the total radiation. Moreover, as can be seen from Fig. 5.2, plasma radiation is very small under these conditions. For our purposes, then, the contribution of neutral Bremsstrahlung can be safely omitted as an important radiation loss mechanism.

The expressions quoted above are semi-classical in origin. To include the quantum effects the cross-sections must be multiplied by a correction factor known as the Gaunt factor. For free-free transitions at the temperatures and pressures under consideration the Gaunt factor averaged over the range of ω is approximately 1.4. (The precise value varies with temperature and pressure.) Since this is a correction to an already small contribution it is not included in further computations.

The bound-free transitions also have Gaunt factors associated with them. The most important quantum correction, about 20%, concerns the transition to the ground state. Rather than using a Gaunt factor, however, it is more convenient in this case to begin with the correct quantum cross section for the region of ω where the bulk of the emission occurs. From Bethe and Salpeter[24] we have to replace the cross-section of (5.6) when $n = 1$ by

$$\sigma_{\omega,1} = 6.34 \times 10^{-18} \left(\frac{k\theta_I}{\omega}\right)^{8/3} \quad (cm^2) \tag{5.16}$$

We then separate off the continuum $n = 1$ term of the sum in (5.11) and find the absorption coefficient to be

$$k_\omega (T, p) = 1.99 \times 10^{-4} \frac{n_{AG}}{\omega^3} \left\{ \frac{1}{2x_1} + \sum_{\substack{n = n_\omega^* \\ n \neq 1}} \frac{e^{x_n}}{n^3} \right\} e^{-x_1}$$

$$+ 6.34 \times 10^{-18} \, n_{AG} \left(\frac{13.6}{\omega}\right)^{8/3} \quad cm^{-1} \tag{5.17}$$

The last term is, of course, only to be used when $n_\omega^* < 1$. This quantum correction is the only one we include in the calculations in Subsection 5.6.

5.4 ATOMIC TRANSITIONS

The final radiation process to be considered is the transition between two atomic bound states. The total power emitted in a spectral line corresponding to a transition from an upper state of quantum number n' to a lower state designated by quantum number n is easily computed from the well known $f_{nn'}$ number for atomic transitions.

The f numbers of the most important lines[25] are given in Table 5.1. The f number of the higher lines ($n' > 8$) in the first three series are given by

$$f_{nn'} = A_n \left(\frac{n'}{n'^2 - n^2} \right)^3 \qquad (5.18)$$

where $A_1 = 1.6$ for the Lyman series, ($n = 1$), $A_2 = 3.7$ for the Balmer series ($n = 2$), and $A_3 = 5.3$ for the Paschen series ($n = 3$). The $f_{nn'}$ numbers for transitions involving $n > 3$ can be approximated as

$$f_{nn'} = 1.96\, n \left(\frac{n'}{n^2 - n'^2} \right)^3 . \qquad (5.19)$$

From the $f_{nn'}$ number the cross section integrated over photon energy is found to be

$$\sigma_{nn'} = \frac{2\pi^2 e^2 \hbar}{m_E c} f_{nn'} .$$

and the power emitted per unit solid angle is given by

$$\int_{\text{line}\ \omega_{nn'}} \epsilon_\omega \, d\omega = (1 - e^{-\omega_{nn'}/kT}) \, B_{\omega_{nn'}}(T) \, \sigma_{nn'} \, n_{AG} \, (n^2 e^{-\omega_{1n}/kT}) \qquad (5.20)$$

where $\omega_{jl} = k\theta_I \left(\frac{1}{j^2} - \frac{1}{l^2} \right)$. By substituting for $B_{\omega_{nn'}}(T)$, Eq. (5.20) can be rewritten as:

TABLE 5.1

f NUMBERS FOR HYDROGEN FOR TRANSITIONS
FROM LOWER STATE n TO UPPER STATE n'
FROM REFERENCE 25

n	n'	$f_{nn'}$
1	2	.4162
"	3	.0791
"	4	.0290
"	5	.0139
"	6	.0078
"	7	.0048
"	8	.0032
2	3	.641
"	4	.1195
"	5	.0444
"	6	.02235
"	7	.0124
"	8	.0082
3	4	.8413
"	5	.150
"	6	.0554
"	7	.0271
"	8	.0162

$$\int_{\text{line } \omega_{nn'}} \epsilon_\omega \, d\omega = f_{nn'} \, n_{AG} \, e^{-\omega_{ln'}/kT} \left(\frac{\theta_I k}{\hbar}\right)^3 \frac{e^2 \hbar}{2\pi m_E c^3} \frac{1}{n^4} \left(\frac{n'^2 - n^2}{n'^2}\right)^3 \tag{5.21}$$

$$= 1.4 \times 10^{-9} \, n_{AG} \, f_{nn'} \, \frac{e^{(x_{n'} - x_1)}}{n^4} \left(\frac{n'^2 - n^3}{n'^2}\right) \left(\frac{\text{watts}}{\text{cm}^3 \text{ sterad}}\right) .$$

The power emitted (4π times Eq. (5.21)) in several of the low-lying lines dwarfs the total continuum contribution. In Table 5.2 we illustrate this feature for hydrogen at 14,000 K and 3 atm. However reabsorption, which will be discussed in the next subsection, reduces the magnitude of the losses due to line radiation. In order to adequately analyze line transport it is essential to know not only the total energy radiated but also the detailed profiles of the strong lines. The profile is modified by the influence of other particles. In the presence of atoms, ions and electrons the shape of the line is broadened from the narrow Lorentz characteristic of the natural line shape; however the change in total power emitted is negligible. In an ionized plasma such as in the hot core of the rocket the broadening is caused mainly by the charged particles and is commonly termed Stark broadening. Hydrogen lines are affected more strongly by Stark broadening than lines of other atoms, so that in ionized hydrogen other broadening mechanisms such as Doppler broadening are unimportant.

The profiles of hydrogen lines subject to Stark broadening serve as important diagnostic tools; as a result they have been thoroughly studied. Elaborate calculations of the profiles have been performed and the profiles carefully tabulated.[26] For our purposes, however, only the far wings of the Lyman lines are important. In the asymptotic far wings the profile S is adequately described by 2 times the Holtsmark profile:

$$S(\alpha) = 2 \, C_{nn'} / |\alpha|^{5/2} \tag{5.22}$$

where $C_{nn'}$ is a constant and α is the reduced wavelength defined in terms of the line center energy ω_o, the line center wavelength λ_o and the normal field strength

$$F_o = e(4\pi n_I/3)^{2/3} \quad , \quad \alpha = (\omega - \omega_o) \lambda_o / \omega_o F_o$$

TABLE 5.2

POWER EMITTED BY LINES IN TRANSPARENT APPROXIMATION.
HYDROGEN AT 3 ATMOSPHERES AND T = 14000 K

Line	n'	n	Power Emitted [watts/cm^3]
$L\alpha$	2	1	7.0×10^5
$L\beta$	3	1	4.62×10^4
$L\gamma$	4	1	2.4×10^4
$L\delta$	5	1	4.59×10^3
	6	1	2337
	7	1	1350
	8	1	866
	$9 \rightarrow \infty$	1	2463
$H\alpha$	3	2	5705
$H\beta$	4	2	1507
$H\gamma$	5	2	616
	6	2	314
	4	3	418
	5	3	176
	6	3	94.3
	$5 \rightarrow \infty$	4	80.4
Continuum			2.6×10^4

The profile is normalized by requiring

$$\int_{-\infty}^{\infty} S(\alpha)\, d\alpha = 1 \tag{5.23}$$

Thus in our spectral plots of the emission coefficient vs ω we have

$$\epsilon_\omega = \left| \frac{d\alpha}{d\omega} \right| S(\alpha) \int_{\text{line}} \epsilon_\omega \, d\omega \tag{5.24}$$

$$= \frac{\lambda_o}{\omega_o F_o} S(\alpha) \int_{\text{line}} \epsilon_\omega \, d\omega \tag{5.25}$$

The factor of two in Eq. (5.22) is required in order to include the electron broadening effects as well as the ion broadening. The values of $C_{nn'}$ for the first three Lyman lines[27] are given in Table 5.3. Typical line broadened profiles are illustrated in Fig. 5.3. Only the first four lines are shown isolated. The higher-lying lines are indistinguishable. They merge to form an extension of the bound-free continuum. When necessary more detailed line profiles can be found in Griem.[26]

5.5 SIMPLE MODEL OF RADIATIVE LOSSES

Using the spectral effective absorption coefficients found in the last subsection we can now proceed to model the radiation from the hot plasma core.

In principle we wish to find the spectral intensity $I_\omega(x, n)$ at each point x and direction $\hat{n}$ in the core by solving the equation,

$$\hat{n} \cdot \nabla I_\omega(x, \hat{n}) = k'_\omega(T, p) \left[B_\omega(T) - I_\omega(x, \hat{n}) \right] \tag{5.26}$$

subject to the boundary condition that at the outer surface of the plasma the radiant intensity I_ω directed into the plasma be zero. Rather than attempt such an ambitious task here, we are satisfied to develop a model in which the plasma radiation can be treated as a local loss term in the gas dynamic equations and in which the total flux of radiation at the edges can be estimated.

TABLE 5.3

COEFFICIENTS FOR ASYMPTOTIC HYDROGEN HOLTSMARK PROFILES = $\frac{C_{nn'}}{|\alpha|^{5/2}}$ FROM REFERENCE 27

n	n'	$\left(\frac{C_{nn'}}{\frac{\text{angstrom}}{\text{cgs field strength unit}}}\right)^{3/2}$
1	2	3.37×10^{-6}
1	3	1.80×10^{-5}
1	4	3.99×10^{-5}

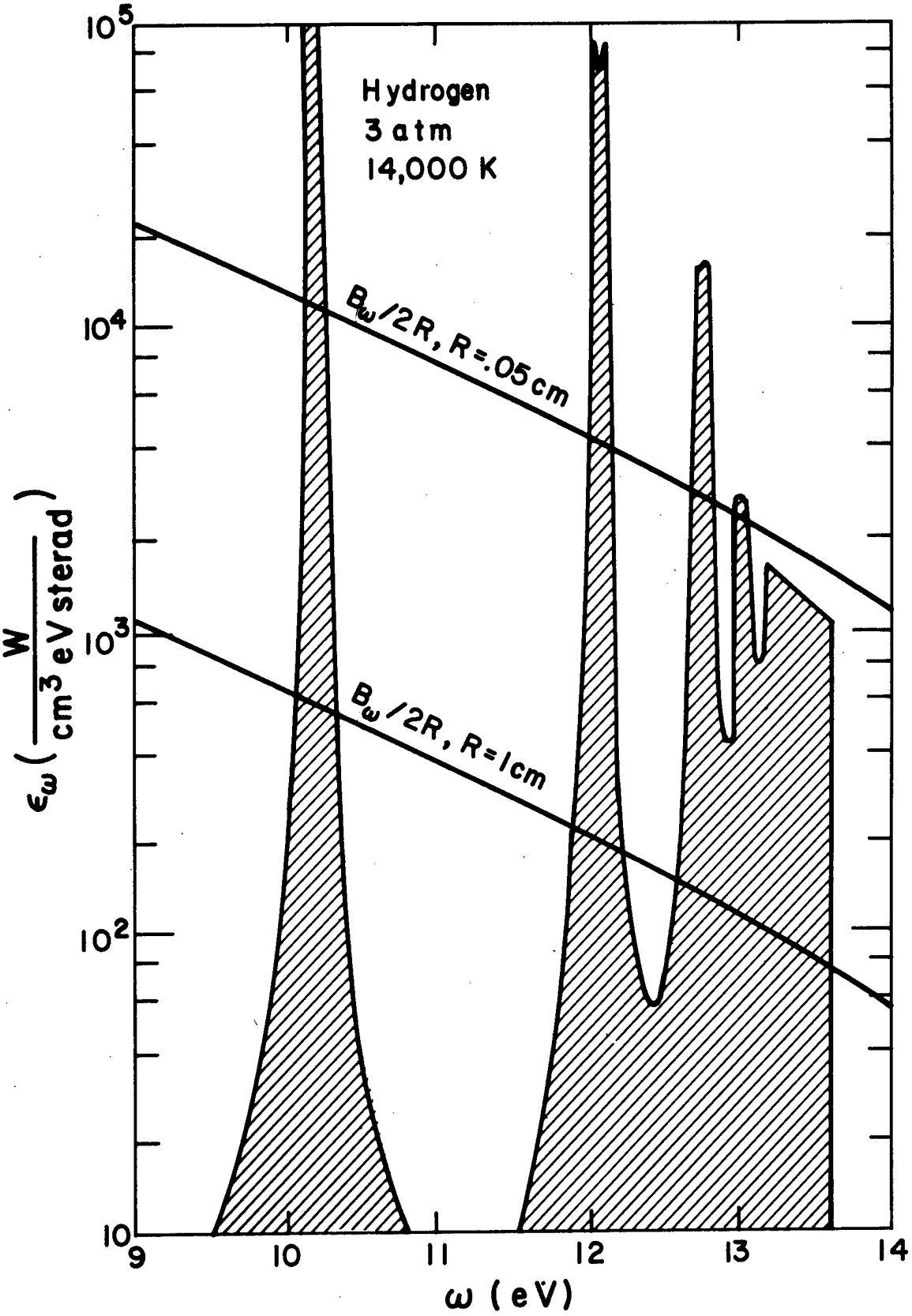

Fig. 5.3 Stark Broadened Profiles of Lyman Series in Hydrogen and the Black Body Limits for the Two Choices of Radius

To this end we consider the radiation lost per unit volume at temperature T and pressure p from the plasma to be equivalent to the average radiation loss per unit volume from an infinitely long cylinder of uniform temperature T, pressure p and radius r. In this way the major qualitative effects of reabsorption are estimated without including the effects of temperature variations.

The power emitted per unit length at a given ω is

$$P = 2\pi^2 B_\omega (T) R F[k_\omega' R] \tag{5.27}$$

where the function F is defined as

$$F\left(k_\omega' R\right) = 2\int_0^{\pi/2} d\theta \cos^2\theta \left\{ I_1\left(\frac{2k_\omega' R}{\cos\theta}\right) - L_1\left(\frac{2k_\omega' R}{\cos\theta}\right)\right\} \tag{5.28}$$

The function I_1 and L_1 are respectively the modified Bessel function of order one and the modified Struve function of order one. The function $F(k_\omega' R)$ gives the ratio of actual power emitted to the power emitted by a blackbody of the same radius. It is plotted in Fig. 5.4.

Two extreme limits are important. When k_ω' is sufficiently small so that $k_\omega' R \ll 1$ is satisfied, reabsorption effects are unimportant. The total emission per unit length is then equivalent to the emission per unit volume multiplied by the area:

$$P_{\omega\,(\text{volume})} = (4\pi\epsilon_\omega)(\pi R^2) = 4\pi^2 R^2 k_\omega' B_\omega \tag{5.29}$$

The other extreme is large k_ω'. When $k_\omega' R \gg 1$ reabsorption dominates and the cylinder looks like a blackbody surface radiator:

$$P_{\omega\,(\text{surface})} = (\pi B_\omega)(2\pi R) = 2\pi^2 B_\omega R \tag{5.30}$$

For comparison these two extreme limits are also plotted in Fig. 5.4 with the factor of $2\pi^2 R B_\omega$ divided out. Calculations using Eq. (5.25) to weight the various parts of the spectrum can be performed numerically; however, first estimates of the effect of radiation can be made by resorting

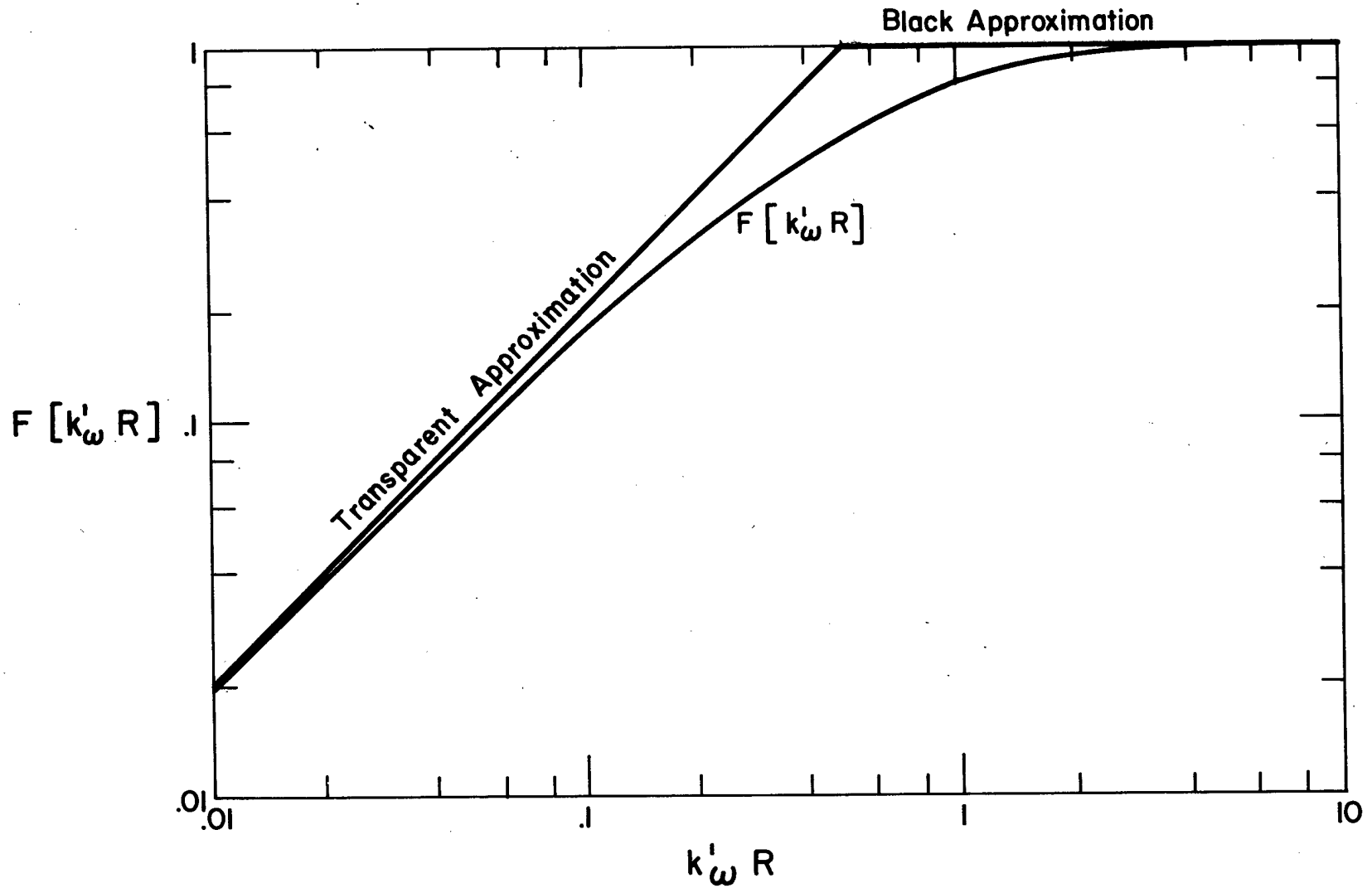

Fig. 5.4 Ratio of Actual Power Lost to Black Body Limit on Power Lost for an Infinite Cylinder. The Transparent and Black Body Approximations Are Also Shown.

to an even stronger approximation. The power lost per unit length will be approximated as the smaller of P_{ω} (volume) and P_{ω} (surface).

Using Eqs. (5.29) and (5.30) we find that the plasma is a transparent volume radiator for all ω such that $2 k'_{\omega} R \leq 1$ is true, or equivalently, such that

$$\epsilon_{\omega} (T, p) \leq \frac{B_{\omega} (T)}{2 R} \tag{5.31}$$

is satisfied. The transparent radiation losses can be immediately incorporated into the fluid dynamic equation as a loss term. The divergence of the plasma flux S_{ω} at any energy ω is simply

$$\nabla \cdot \underline{S}_{\omega} = 4 \pi \epsilon_{\omega} (T, p) \quad . \tag{5.32}$$

If the opposite inequality is valid, i.e.

$$\frac{B_{\omega} (T)}{2 R} \leq \epsilon_{\omega} (T, p) \quad , \tag{5.33}$$

the plasma acts as a blackbody radiator with effective volume radiation

$$2 \pi B_{\omega} (T)/R$$

It is not clear whether or not this loss should be included in the fluid mechanics as an effective volume loss. Even though it is a loss from the material, the loss occurs mainly at the surface; particularly when $2 k'_{\omega} R \gg 1$ is satisfied. Then most of the plasma in our model is unaffected since the temperature is assumed to be held fixed throughout the radius. In a more realistic approximation, radial temperature gradients must exist which then lead to heat transfer from the hotter interior to the cooler surface. The heat transfer is accomplished through both thermal conduction and radiative transfer. In this manner the surface losses do influence the interior. However a realistic radial profile may also result in photon trapping especially for regions of the spectrum where k'_{ω} is very large. Without additional information concerning the radial temperature profile it is difficult to assess accurately the role of the surface radiation in fluid equations, especially when the equations do not admit radial temperature gradients. This ambiguity suggests that two predictions of radiative losses should be made. For an upper limit on

the flux which leaves the plasma, both the blackbody and transparent radiation are included. For a reasonable lower limit on radiative loss only the transparent radiation and any borderline blackbody radiation (say $2 k_\omega' R < 3$) are to be included.

5.6 APPLYING THE MODEL

Our criterion is illustrated in Figs. 5.1 and 5.3 where, in addition to the contributions to the emission coefficient, we have plotted the function $B_\omega (T)/(2R)$ for two values of R of interest. In Fig. 5.1 where the classical approximation to the continuum radiation is shown, the low energy region of the spectrum is seen to lie below the curves $B_\omega (T)/2R$ for both radii. Therefore the transparent requirement is satisfied. The vacuum ultraviolet portion ($\omega \geq 13.6$ eV) lies slightly below $B_\omega (T)/2R$ for R = 0.05 mm but well above for R = 1 cm. Hence the VUV is barely transparent for the small radius and strongly black for the large radius. Four distinct Lyman lines are shown in Fig. 5.3. The three lowest lines are strongly black at their peak but they possess wide transparent wings. The higher lines tend to mimic an extension of the continuum. In our calculations of power lost we have lumped the higher Lyman lines, L_δ and above, with the true continuum insofar as determining whether they are black, marginally black, or transparent. To determine the power lost in the transparent limit for the region of $\omega \geq 13.6$ eV we have used the quantum-mechanical expression (5.17) for the continuum, and the sum of line strengths for $n' \geq 4$ for the high lying lines. For the three isolated lines the centers have been treated as black. Fortunately the transition between the black center and the transparent wing occurs far enough from the line center that the asymptotic Holtsmark profile is adequate to describe the line. The transition point $\Delta\omega$ where black turns to transparent can be determined by finding $\Delta\omega$ such that ϵ_ω as found from Eq. (5.25) satisfies the equality in Eq. (5.31).

The total power per steradian radiated by the wings is thus found by integration to be

$$P_{\text{line wings}} = \frac{8}{3} \frac{C_{nn'}}{(\alpha_T)^{3/2}} \int_{\text{line } nn'} \epsilon_\omega \, d\omega \qquad (5.34)$$

where α_T is the reduced wavelength corresponding to the transition from black to transparent.

The only other line which is strongly reabsorbed in our calculations is the first Balmer line H_α. The self absorption is important

only at high pressures and large radii. The asymptotic formulas are not sufficient to estimate the reabsorption, thus the detailed profiles of Griem[26] must be used.

The total power emitted per unit volume, including all transparent radiation and an effective vacuum ultraviolet radiation whenever it is marginally black, is illustrated in Figs. 5.5 and 5.6 as a function of temperature for two values of pressure and radius.* In the numerical fluid mechanical calculations of Section 7, the radiation loss terms are adequately approximated as constant factors multiplying one of the semi-classical formulas (5.14) or (5.15). These approximations are also indicated in Figs. 5.5 and 5.6. All the formulas are of the following form:

$$P_T = 8.6 \times 10^{-9}\ C_1 \left(\frac{T}{\theta_I} + C_2\right) \frac{T}{\theta_I}\ n_{AG}\ e^{-\theta_I/T} \left(\frac{W}{cm^3}\right) \qquad (5.35)$$

where n_{AG} is in cm^{-3}. The constants C_1 and C_2 used for various pressures and radii are converted to a different form, in mks units, in Eq. (7.38), and then listed in Table 7.3.

The calculations listed above are reasonable estimates of the effective loss term per unit volume from the bulk of the hot plasma. Radiation which is subject to strong reabsorption has not been included in these estimates. The blackbody surface contribution can be easily included by integrating $\pi B_\omega (T)$ over the region of the spectrum which satisfies our criterion for blackness. In order to compare the magnitude of the black and transparent losses, either the blackbody losses must be rewritten as effective volume losses, or the transparent losses must be transformed into an effective surface flux. In Table 5.4 we have compared the black and transparent effective surface fluxes for two situations of interest.

The transparent radiation accounts for the major portion of the total power lost. However the blackbody contribution is still a significant fraction of the total loss. Furthermore the fraction of the total emission which is blackbody radiation generally increases as the radius becomes

---

*Radiation which is black is not included because of uncertainty in the radial temperature gradients, as discussed below Eq. (5.33).

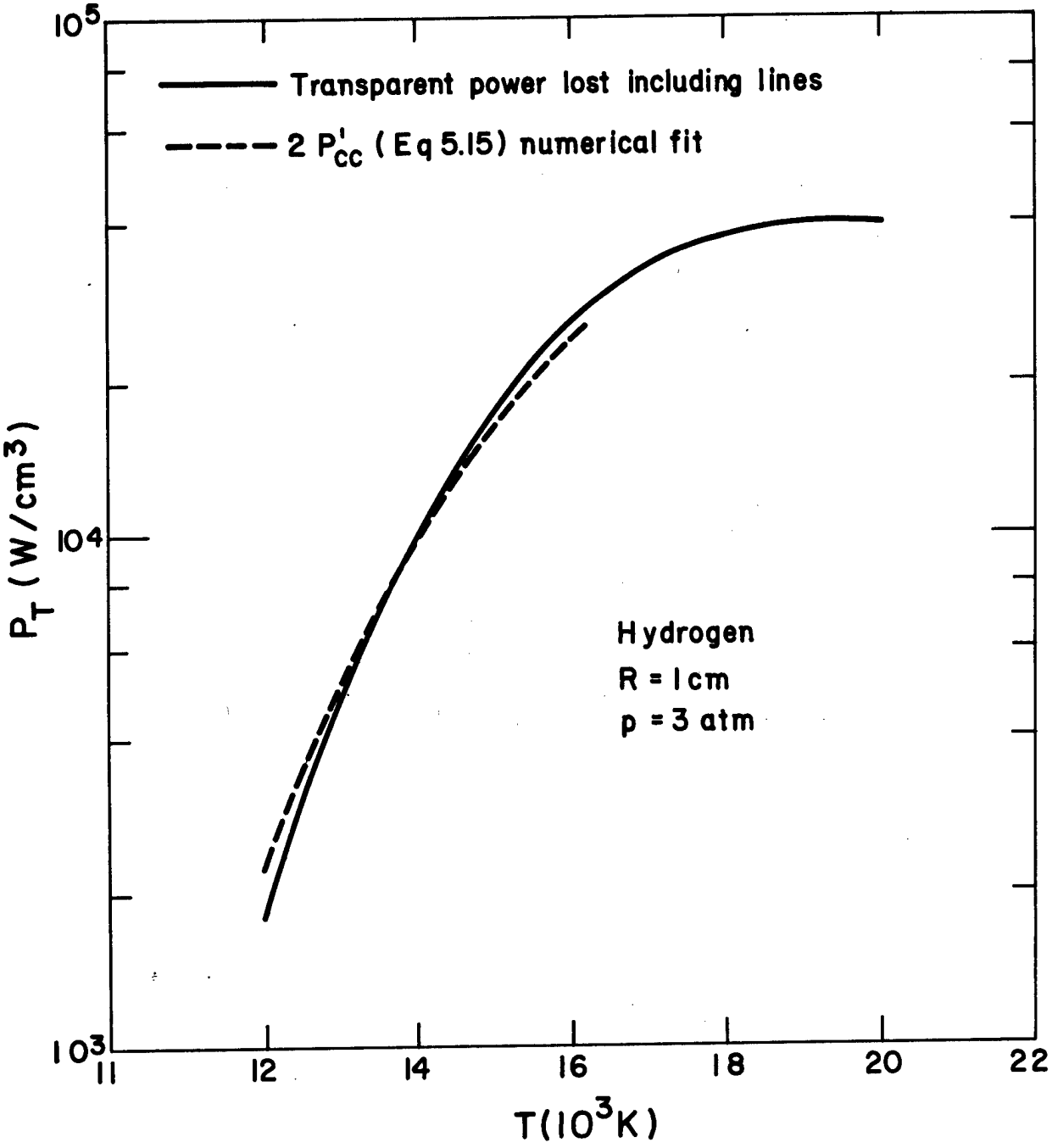

Fig. 5.5 Power Radiated from Hydrogen (3 atm, R = 1 cm) Showing Numerical Results and the Analytic Approximation

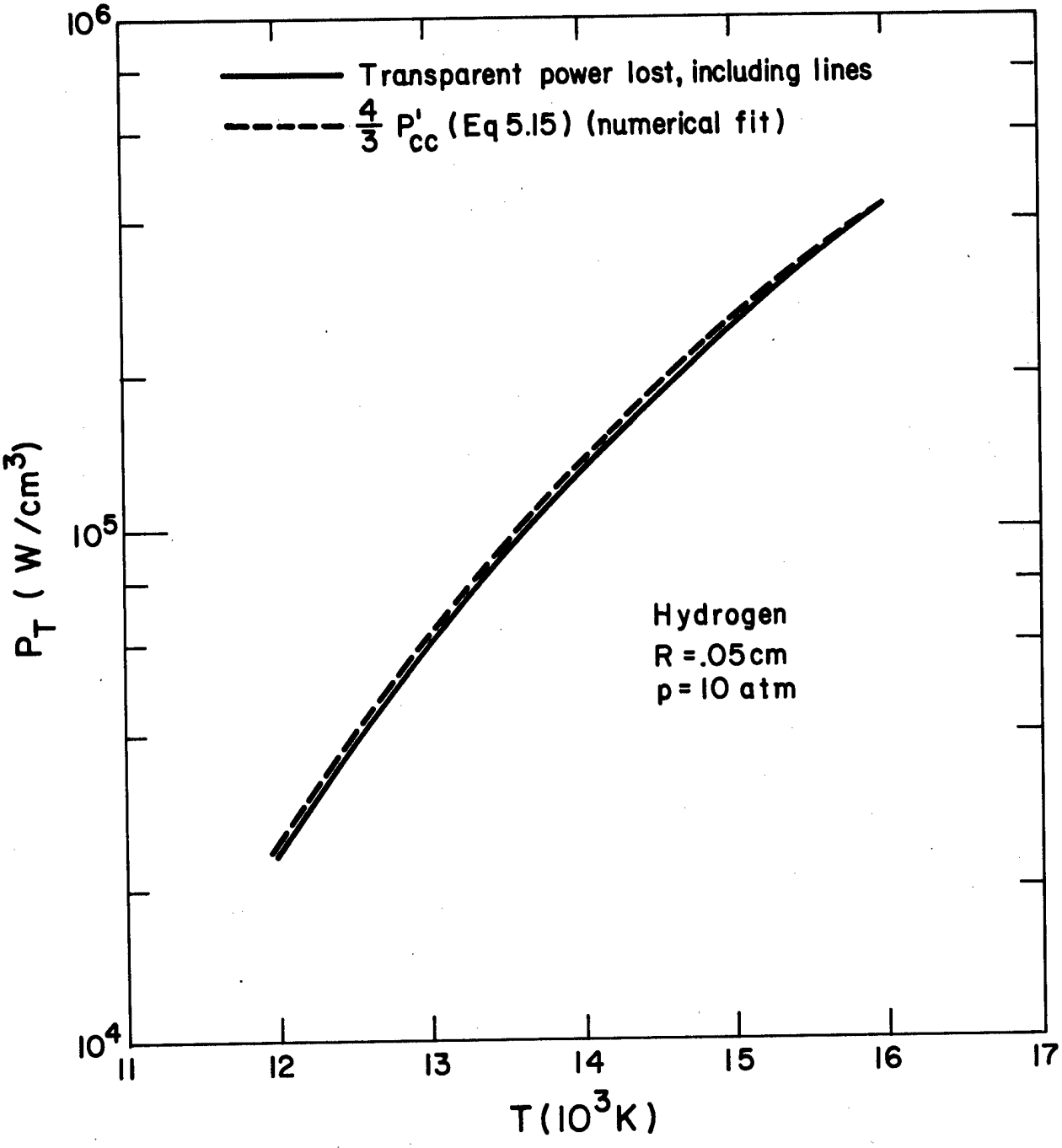

Fig. 5.6 Power Radiated from Hydrogen (10 atm, R = .05 cm) Showing Numerical Results and the Analytic Approximation

TABLE 5.4

EFFECTIVE SURFACE RADIATION LOSSES

LASER	10 kW	5 MW
Pressure	3 atm	3 atm
Temperature	14000 K	14000 K
Radius	.056 cm	1.25 cm
Transparent	1579 watts/cm^2	6507 watts/cm^2
Black	462 watts/cm^2	3356 watts/cm^2
Total	2041 watts/cm^2	9863 watts/cm^2

larger. For accurate results at larger radii it is necessary to include the blackbody radiation properly, but this is difficult unless one has knowledge of the radial temperature profile, as discussed below Eq. (5.33).

5.7 SUMMARY

Having analyzed the gross behavior of the spectral emission coefficient as a function of ω, T and p, we have obtained estimates of the volume power loss due to transparent radiation, and of the black body surface radiation. These estimates are based upon a simple model - one in which the radiation lost per unit volume from the core at given T and p is assumed to equal the radiation lost per unit volume from an infinite cylinder of equivalent T, p and R. The reabsorption effects included are those of the cylinder at uniform temperature and pressure. Only two extremes of reabsorption effects are recognized in the final calculations of power lost: the radiation of a given frequency is treated as being either transparent or black.

Our calculations show that radiation losses rise rapidly with temperature, peaking at approximately 18,000 K where ionization is complete. It is important therefore to know the operating temperature accurately. A small error in determining the operating temperature can lead to a large increase in radiation lost. Since the operating temperature is intimately related to the propagation mechanism, it is also important to understand thoroughly how LSC waves propagate.

Black body surface radiation is less important than transparent radiative losses for the configurations studied. However, the black body radiation is not negligible, and its importance increases with plasma diameter. Future work should include modeling of the radial temperature gradients so that better estimates of the surface radiation lost can be made.

6. ESTIMATE OF LASER SUPPORTED COMBUSTION WAVE PROPERTIES

To enable the flowing hydrogen core of the laser-heated rocket to absorb laser energy, it must be heated to a temperature where thermal ionization takes place, i.e., to temperatures of order 10,000 K. In steady state the mechanism for providing this heating is a laser supported combustion (LSC) wave, which is a zone of rapid temperature increase from ambient temperature to temperatures where absorption of the laser energy can take place. Laser energy flows through this zone from the cold side and is absorbed on the hot side. The hot plasma transmits energy forward to the cold gas by conduction and by radiation emission from the plasma, this providing the energy necessary to heat the cold gas up to temperatures where it can absorb laser energy. Thus the wave is supported by the laser energy, which indirectly converts cold flowing gas to hot flowing gas, using laser absorption in the hot gas, plasma emission, and conduction and plasma radiation absorption in the cold gas as mechanisms.

Such waves have been observed in air, in a non-steady geometry, by focusing laser intensities of 10^5 to 10^7 W/cm^2 on solid targets. Evaporation of the targets provides electrons which initiate absorption of laser energy in the gas in front of the target, and a temperature wave is observed to move away from the target toward the laser beam, at subsonic speeds. This wave is an LSC wave moving relative to the still air. It is observed to move at a definite speed, which depends on the laser intensity. (At intensities greater than 10^7 W/cm^2, the rapid energy deposition increases the pressure greatly and causes shock waves to precede the heated zone, a phenomenon called a laser-supported detonation (LSD) wave).

The laser-heated rocket flow is conceived to begin with a stationary LSC wave providing the mechanism to heat the flowing hydrogen. The wave is made stationary by flowing parallel to the laser beam at just the speed with which the wave would want to propagate towards the beam. This wave forms the initial condition for the flow in the plasma core, so it is necessary to know its speed for a given laser intensity, to establish the rate of mass flow into the core.

Experimentally, LSC waves in air have been observed by the non-steady method described above and curves of intensity vs. speed derived (Ref. 28). Theoretically, a number of attempts have been made to model air LSC waves [29, 30, 31], although their success in comparing with experiment has been limited. There is no information, either experimental or theoretical, on LSC waves in hydrogen. Since radiation from the gas plays

a crucial role in LSC wave properties, and since radiation properties of hydrogen are quite different from those of air, one cannot easily extrapolate from air to hydrogen. The lack of reliable information on the intensity vs. speed relation of LSC waves in hydrogen must be considered one of the major uncertainties in the study of the flowing core laser-heated rocket.

Nevertheless, it was necessary to estimate the intensity vs. speed curve for hydrogen in order to provide initial conditions for the plasma core streamtube calculation. For this purpose, the simple model of Jackson and Nielsen[30] was adapted to hydrogen. In this model we needed to characterize the high temperature emission and low temperature absorption of hydrogen. For the latter, a classical continuum absorption coefficient was assumed. For the former, the radiated power was taken to be the continuum radiated power per unit volume, as found by Yos in Ref. 32. With these assumptions the Jackson-Nielsen model was used to obtain the intensity vs. speed curve for hydrogen at 1 atm and 3 atm.*

The results are shown as the solid lines on Fig. 6.1. Also shown there is the Jackson-Nielsen result for air at 1 atm as the dashed line, and the data for 1 atm air of Ref. 28. It is seen that the hydrogen estimates do not differ much from the air theory in the range 4E5 to 1E6 W/cm^2. Also evident is the disagreement between the air theory and experiment, with the theory about a factor of 3 lower than the experimental results.

In spite of the uncertainty, a point near the 3 atm line at 3.67E5 W/cm^2 (3.67E9 W/m^2) and 1340 cm/s (13.4 m/s) was used for the initial conditions of the core calculation. This corresponds for T_o = 300 K to a mass flow per unit area of 0.3316 g/cm^2-s (3.316 kg/m^2-s).

For the 10 atm core calculations, it was assumed that the intensity vs. mass flow per unit area was the same as for 3 atm; this reduces the speed to 400 cm/s (4.0 m/s).

---

* These estimates were made before the work described in Sec. 5 was undertaken to define hydrogen radiation emission. That work could be used to develop a much more sophisticated model of LSC waves in hydrogen, which avoids most of the assumptions inherent in the model of Jackson and Nielsen, and which uses a much more accurate description of radiation emission and absorption than is possible with the formulas of Ref. 32.

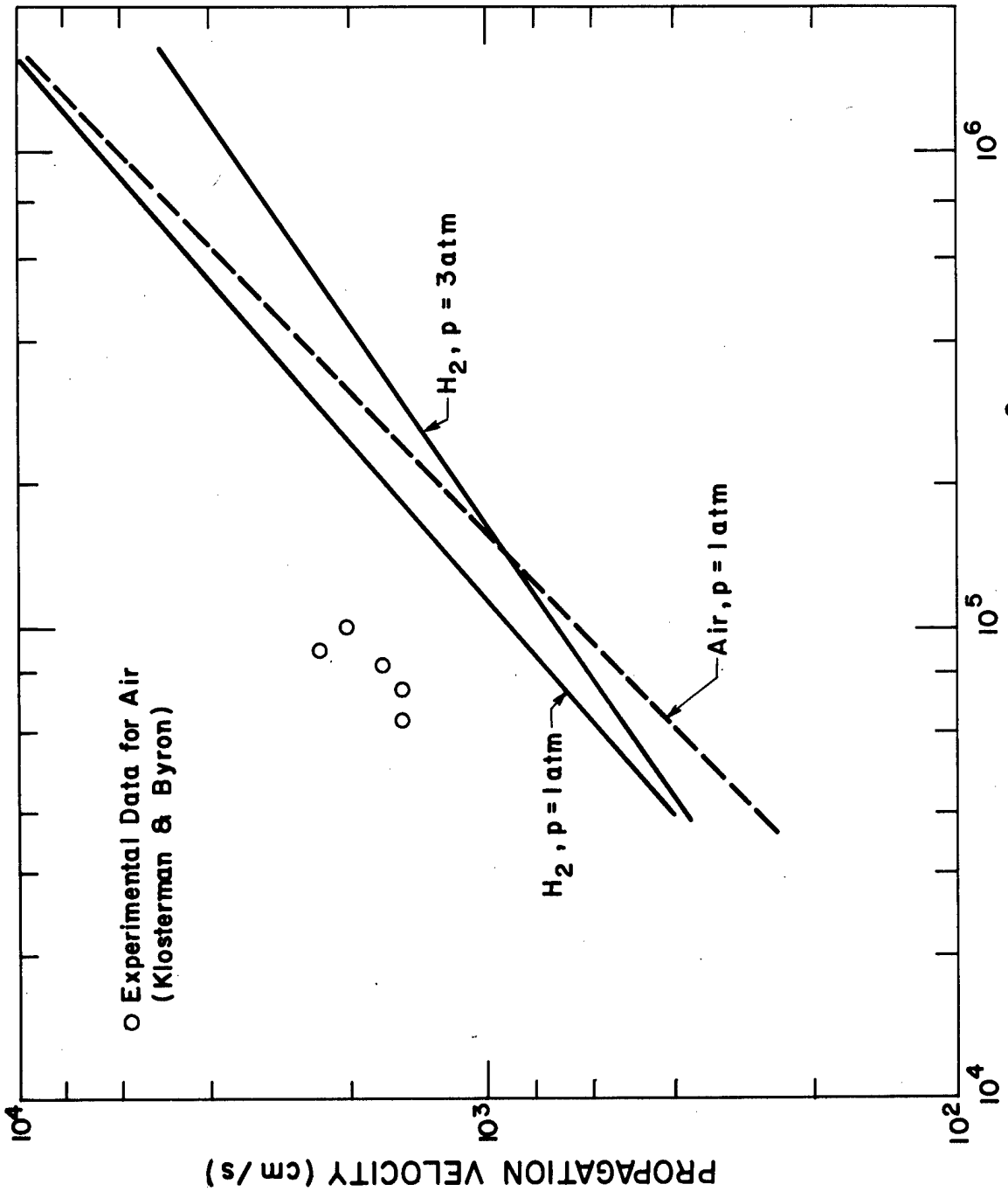

Fig. 6.1 Velocity of Laser Supported Combustion Waves

7. FLOWING CORE STREAMTUBE MODEL

7.1 INTRODUCTION

The central streamtube of the flowing-core laser-heated rocket combines a number of physical phenomena. It absorbs laser radiation, it dissociates and ionizes, it emits plasma radiation, and it flows through a variable area channel. All these phenomena must be included in a model to calculate the properties of the streamtube. The analysis described in the final report on the previous contract (Ref. 1) included laser radiation absorption in a variable area channel, but treated the gas as perfect, with constant specific heats, and did not include loss of energy by plasma radiation. Hydrogen is fully dissociated at about 8000K (with dissociation energy 2.16×10^8 J/kg) and is 50% ionized between 16,000 and 17,000K (with ionization energy 13.1×10^8 J/kg), while the total enthalpy change from 300K to 8,000K is 3.76×10^8 J/kg and from 8,000 to 16,000K is 8.37×10^8 J/kg. Thus it is clear that the dissociation and ionization processes are important energy sinks, and hydrogen should be treated as a real gas. The loss of energy by plasma radiation emission both reduces the energy in the streamtube and defines an energy loss against which the walls must be protected, so it is also important to include this physical phenomena.

A model of the flowing-core streamtube was constructed which included variable area, one-dimensional flow of dissociating and ionizing hydrogen in chemical equilibrium, with laser energy absorption by inverse Bremsstrahlung, and plasma radiation emission. This model was reduced to the solution of three first order differential equations which were solved by straightforward integration on a computer. This section will describe the model, and give the results of some calculations for configurations of interest.

7.2 BASIC EQUATIONS

The one-dimensional mass conservation equation for a gas of density ρ, speed u in a channel of area A gives the mass flow rate as

$$\dot{m} = \rho u A, \quad A = \pi R^2 \tag{7.1}$$

The momentum conservation equation relates the pressure gradient to the velocity gradient by

$$\frac{dp}{dx} + \rho u \frac{du}{dx} = 0 \tag{7.2}$$

The energy equation has laser absorption terms and plasma emission terms. The conservation of energy requires the divergence of the total energy flux to vanish. This total energy flux has three parts in the present problem. One is the total enthalpy flux of the gas, $\rho u AH$, where H is the total enthalpy. The second is the laser energy flux, AI, where I is the laser intensity per unit area, and the third is the plasma emission radiant energy flux vector $\underline{S}$. The energy equation is then

$$\frac{d}{dx} (\rho u AH + AI) + \int_0^R 2\pi v \nabla \cdot \underline{S} \, dr = 0 \tag{7.3}$$

The laser energy is absorbed with absorption coefficient k_L according to

$$\frac{d\,AI}{dx} = - k_L AI \tag{7.4}$$

whose solution is, with $(\ )_i$ denoting conditions at x = 0,

$$AI = (AI)_i e^{-\tau} , \quad \tau = \int_0^x k_L \, dx \tag{7.5}$$

Use of Eqs. (7.4), (7.5) and (7.1) in (7.3) allows the energy equation to be written as

$$\frac{dH}{dx} = \frac{dh}{dx} + \frac{udu}{dx} = \frac{dQ}{dx} \tag{7.6}$$

$$\frac{dQ}{dx} = \frac{k_L (AI)_i e^{-\tau}}{\dot{m}} - \frac{\int_0^R 2\pi r \nabla \cdot \underline{S} \, dr}{\dot{m}} \tag{7.7}$$

This is written so the laser absorption term is recognized as a heat addition, and the plasma emission term as a heat loss.

The problem is then one of heat addition to a one-dimensional nozzle flow, with the heat addition term coupled to the flow, since k_L and $\nabla \cdot \underline{S}$ depend on the local properties of the gas.

The conventional way to solve this problem, as described in Ref. 1, is to take the area A(x) as given, and solve for $d\rho$, du and dp from (7.1), (7.2) and (7.6). The results show the sonic singularity at M = 1, which makes for difficulties in the numerical integration of the equations when there is heat addition or real gas effects, both of which are present here. An alternative method of solution was therefore used, which led to simple numerical solutions.

Instead of taking the area as given, we take the velocity distribution u(x) as known. This leaves the thermodynamic variables p, ρ, T to be found from (7.2) and (7.6) and the equation of state. Then A(x) is found from (7.1), since the mass flow rate $\dot{m}$ is given. This is a perfectly acceptable method of solving the problem, as long as one chooses u(x) so the resulting area distributions are realistic, and this can be accomplished with a little experience.

Equations (7.2) and (7.6) can be written easily in terms of dp and dT by using the equation for the enthalpy of equilibrium hydrogen in the form

$$h = h\,(p,\ T)$$

$$dh = \left(\frac{\partial h}{\partial T}\right)_p dT + \left(\frac{\partial h}{\partial p}\right)_T dp\,, \quad \left(\frac{\partial h}{\partial T}\right)_p = c_p \tag{7.8}$$

If this is inserted into (7.6), and (7.2) used to eliminate dp, (7.2) and (7.6) become

$$\frac{dp}{dx} = -\rho u \frac{du}{dx} \tag{7.9a}$$

$$\frac{dT}{dx} = \left\{ \frac{dQ}{dx} + \left[\rho \left(\frac{\partial h}{\partial p}\right)_T - 1 \right] u \frac{du}{dx} \right\} \Big/ c_p \tag{7.9b}$$

When the thermodynamic properties of hydrogen and the radiation properties which are contained in dQ are defined, the specification of u(x) enables a straightforward integration of these two equations from any given initial condition. From their solution and the gas law, the radius of the stream-tube is obtained from (7.1) as

$$R = (\dot{m}/\pi \rho u)^{1/2} \tag{7.10}$$

Actually the emission term in (7.7) involves R, so (7.10) is used for R during the course of the integration.

7.3 THERMODYNAMIC PROPERTIES OF EQUILIBRIUM HYDROGEN

We need the derivatives of enthalpy with respect to p and T, the equation of state which relates ρ and T, and the composition of the mixture of hydrogen molecules, atoms, ions and electrons. The pressure derivative of h can be expressed in terms of the equation of state by a classical use of reciprocity relations between the derivatives of h and entropy, which are in turn obtained from the second law. These lead to

$$\left(\frac{\partial h}{\partial p}\right)_T = \frac{1}{\rho} + \frac{1}{\rho}\left(\frac{\partial \ln \rho}{\partial \ln T}\right)_p$$

so that

$$\rho\left(\frac{\partial h}{\partial p}\right)_T - 1 = \left(\frac{\partial \ln \rho}{\partial \ln T}\right)_p \tag{7.11}$$

We characterize the hydrogen as a mixture of perfect gases whose components have number densities: molecules n_M, atoms n_A, ions n_I and electrons n_E. We do not expect to get to a temperature where other species are significant, nor are there multiply ionized atoms, so $n_I = n_E$. As reaction coordinates we use the fraction of molecules dissociated β and the fraction of atoms ionized, α:

$$\beta = \frac{(n_A + n_I)/2}{n_M + (n_A + n_I)/2} \quad , \quad \alpha = \frac{n_I}{n_A + n_I} \tag{7.12}$$

In terms of the original number of particles per unit volume,

$$n_o = n_M + (n_A + n_I)/2 \tag{7.13}$$

the number density of the species are

$$n_M = n_o (1 - \beta) , \qquad n_A = 2 n_o \beta (1 - \alpha) , \qquad n_I = n_E = 2 n_o \beta \alpha \tag{7.14}$$

and the corresponding partial pressure are found from

$$p_i = n_i kT \tag{7.15}$$

where k is the Boltzmann constant. The partial mass densities are, in terms of the particle masses m_i,

$$\rho_M = n_M m_M , \quad \rho_A = n_A m_A , \quad \rho_I = n_I m_I , \quad \rho_E = n_I m_E \tag{7.16}$$

and the total number and mass densities are

$$n = n_o [1 + \beta (1 + 2\alpha)] , \quad \rho = n_o m_M \tag{7.17}$$

Whenever convenient we will use the facts that to an excellent approximation for hydrogen, $m_A = m_I = m_M/2$.

The equation of state is the sum of the partial pressures,

$$p = \rho Z R_M T , \quad Z = 1 + \beta (1 + 2\alpha) , \quad R_M = k/m_M \tag{7.18}$$

where Z is the compressibility factor and R_M the gas constant for the molecules. We have now expressed ρ in terms of p, T through α and β by (7.18). Since p and T are the dependent variables in the basic differential equations (7.9), we need α, β in terms of T, p.

Since we deal with hydrogen in thermochemical equilibrium, α and β are determined by the Law of Mass Action in terms of the thermodynamic variables of the mixture. There are two reactions occuring, dissociation and ionization:

$$H_2 \rightleftharpoons 2H \qquad\qquad H \rightleftharpoons H^+ + E^-$$

For each the equilibrium constant provides a relation between the partial pressures and the partition functions of the species, involving the heat of reaction. These relations are

$$\frac{p_A^2}{p_M} = \left(\frac{\pi m_A}{h_P^2}\right)^{3/2} \frac{(kT)^{5/2} Q_{elA}^2}{Q_v Q_r Q_{elM}} e^{-h_D^o m_M/kT} \tag{7.19a}$$

$$\frac{p_I p_E}{p_A} = \left(\frac{2\pi m_E}{h_P^2}\right)^{3/2} (kT)^{5/2} \frac{Q_{elI} Q_{elE}}{Q_{elA}} e^{-h_D^o m_I/kT} \tag{7.19b}$$

where h_p is Planck's constant, Q_v and Q_r are the vibrational and rotational partition functions of H_2, Q_{eli} are the electronic partition functions of the species, h_D^o is the heat of dissociation of a molecule per unit mass and h_I^o is the heat of ionization of an atom per unit mass. From (7.14), (7.15), (7.17) and (7.18) the partial pressure ratios are

$$\frac{p_A^2}{p_M} = \frac{4\beta^2 (1-\alpha)^2}{1-\beta} n_o kT = \frac{4\beta^2 (1-\alpha)^2}{1-\beta} \frac{p}{Z} \tag{7.20a}$$

$$\frac{p_I p_E}{p_A} = \frac{4\beta^2 \alpha^2}{2\beta(1-\alpha)} n_o kT = \frac{2\beta\alpha^2}{1-\alpha} \frac{p}{Z} \tag{7.20b}$$

The rotational partition function Q_r may be approximated by $T/2\,\theta_r$ where $\theta_r = 87.62K$ for H_2 and the factor of 2 comes from the symmetry of the molecule. This is a valid approximation for $T \gg \theta_r$; it is about 10% low at 300K but only 0.5% low at 1000K. The vibrational partition function is

$Q_v = \left(1 - e^{-\theta_v/T}\right)^{-1}$ where $\theta_v = 5983K$ for H_2. The electronic partition function for the molecule may be replaced by its ground-state statistical weight 1, since its first excited state lies very high (132,000K). For the electron $Q_{elE} = 2$ because of the two electron spin states, and for the ion, there are no internal states, $Q_{elI} = 1$.

For the atom

$$Q_{elA} = 2 S_1 \exp(-h_I^o m_I/kT) \tag{7.21}$$

$$S_1 = \sum_{j=1}^{17} j^2 \exp(h_I^o m_I/kT\, j^2)$$

The first term is the usual ground-state weight 2. The subsequent terms are needed here, even though $h_I^o m_A/k = 158,000K$, because we may be interested in hydrogen atoms up to 20,000K. The upper limit cut-off of the sum can be obtained in various ways, and may depend on temperature. Here we took it constant at 17, since the effect of the sum is rather small. If (7.20) and (7.21) are used in (7.19) we have

$$\frac{\beta^2 (1-\alpha)^2}{(1-\beta) Z} = \left(\frac{\pi m_A k}{h_P^2}\right)^{3/2} 2kT_r \frac{T^{3/2}}{p} e^{-\theta_D/T} \left(1 - e^{-\theta_v/T}\right)\left(S_1 e^{-\theta_I/T}\right)^2 \tag{7.22a}$$

$$\frac{2\beta\alpha^2}{(1-\alpha) Z} = \left(\frac{2\pi m_E k}{h_P^2}\right)^{3/2} \frac{kT^{5/2}}{pS_1} \tag{7.22b}$$

$$\theta_D = h_D^o m_M/k, \quad \theta_I = h_I^o m_I/k$$

These two relations express α, β in terms of p, T, as desired, and could be used. However, they are algebraically complicated, and difficult to solve for α, β. For hydrogen they can be considerable simplified with little loss in accuracy. Hydrogen in equilibrium dissociates almost completely before it ionizes significantly. We can thus separate the two reactions and take $\alpha = 0$ in the first one while β goes from 0 to 1. Then in the second, we can take $\beta = 1$ while α increases from zero. These two are separated by a temperature T^* below which there are only molecules and atoms, and above which there are only atoms, ions and electrons. Additionally, in the non-ionizing region, the temperature is too low for the higher electronic states of atom to contribute, so the squared term on the right of (7.22a) can be taken as unity. Then we have

$$T < T^*: \quad \frac{\beta^2}{1-\beta^2} = \frac{f_D(T)}{p}, \quad \alpha = 0 \tag{7.23a}$$

$$f_D(T) = \left(\frac{\pi m_A k}{h_P^2}\right)^{3/2} 2kT_r T^{3/2} \left(1 - e^{-\theta_v/T}\right) e^{-\theta_D/T}$$

$$T \geq T^*: \quad \frac{\alpha^2}{1-\alpha^2} = \frac{f_I(T)}{p}, \quad \beta = 1 \tag{7.23b}$$

$$f_I(T) = \left(\frac{2\pi m_E k}{h_P^2}\right)^{3/2} \frac{kT^{5/2}}{S_1}$$

These are both linear in β^2 or α^2, and yield

$$T < T^*: \quad \alpha = 0, \quad Z = 1 + \beta, \quad \beta = (1 + p/f_D)^{-1/2} \tag{7.24a}$$

$$T > T^*: \quad \beta = 1, \quad Z = 2(1 + \alpha), \quad \alpha = (1 + p/f_I)^{-1/2} \tag{7.24b}$$

which are very simple expressions for α, β in terms of p and T, the primary dependent variables.

From (11), we need the derivative of ln ρ with ln T at constant pressure, which from the gas law (7.18) is

$$\left(\frac{\partial \ln p}{\partial \ln T}\right)_p = -1 - \left(\frac{\partial \ln Z}{\partial \ln T}\right)_p \tag{7.25}$$

The derivate of Z is easily found from (7.24) in terms of the derivatives of α, β, which are obtained by differentiating (7.24) and using the definitions of f_D, f_I given in (7.23). The results are

$$T < T^* : \left(\partial \alpha / \partial T\right)_p = 0, \; \psi_v = \left(\theta_v / T\right) \Big/ \left(e^{\theta_v / T} - 1\right)$$

$$\left(\frac{\partial \beta}{\partial \ln T}\right)_p = \frac{\beta \left(1 - \beta^2\right)}{2} \left[\frac{3}{2} + \frac{\theta_D}{T} - \psi_v\right] \tag{7.26a}$$

$$\left(\frac{\partial \ln Z}{\partial \ln T}\right)_p = \frac{1}{1 + \beta} \left(\frac{\partial \alpha}{\partial \ln T}\right)_p = \frac{\beta \left(1 - \beta\right)}{2} \left[\frac{3}{2} + \frac{\theta_D}{T} - \psi_v\right]$$

$$T > T^* : \left(\partial \beta / \partial T\right)_p = 0 , \quad S_2 = \sum_{j=1}^{17} \exp\left(\theta_I / T_j^2\right)$$

$$\left(\frac{\partial \alpha}{\partial \ln T}\right)_p = \frac{\alpha \left(1 - \alpha^2\right)}{2} \left[\frac{5}{2} + \frac{S_2}{S_1}\right] \tag{7.26b}$$

$$\left(\frac{\partial \ln Z}{\partial \ln T}\right)_p = \frac{1}{1 + \alpha} \left(\frac{\partial \alpha}{\partial \ln T}\right)_p = \frac{\alpha \left(1 - \alpha\right)}{2} \left[\frac{5}{2} + \frac{S_2}{S_1}\right]$$

The remaining thermodynamic property needed is c_p, the temperature derivative of the enthalpy. The translation specific heats of the atoms, ions and electrons are $5k/2$ per particle. This is the total contribution for the ions and electrons, which thus have a specific heat per unit mass of

$$c_{pI} = 5k/2m_I , \quad c_{pE} = 5k/2m_E = c_{pI} \, m_I/m_E \tag{7.27}$$

Their enthapies are the integrals with respect to T, plus the dissociation energy h_D^o and the ionization energy h_I^o for the ions

$$h_I = c_{pI} \, T + h_D^o + h_I^o , \quad h_E = c_{pE} \, T \tag{7.28}$$

The atoms have a translational contribution $5kT/2m_A$, carry the dissociation energy h_D^o, and also have a contribution from the electronic states derived from Q_{elA} of (7.21) by

$$h_{elA} = \frac{kT^2}{m_A} \frac{\partial \ln Q_{elA}}{\partial T} = h_I^o \left(1 - \frac{S_2}{S_1}\right)$$

where S_2 has been defined in (7.26b). The resulting atom enthalpy is

$$h_A = \frac{5kT}{2m_A} + h_D^o + h_I^o \left(1 - \frac{S_2}{S_1}\right) \tag{7.29}$$

Finally the molecules have a translational contribution $5kT/2m_M$, a rotational contribution $2kT/2m_M$ for the two rotational degrees of freedom, corresponding to $Q_r = T/2\theta_r$, and a vibrational contribution found from $Q_v = (1 - e^{-\theta_v/T})^{-1}$ as

$$h_v = \frac{kT^2}{m_M} \frac{\partial \ln Q_v}{\partial T} = \frac{kT}{m_M} \psi_v$$

where ψ_v is defined in (7.26a). Thus the molecular enthalpy is

$$h_m = \frac{7kT}{2m_M} + \frac{kT}{m_M} \psi_v \tag{7.30}$$

The enthalpy of the mixture is the sum of the species enthalpies weighted by their mass fractions in the mixture:

$$h = \sum h_i \rho_i / \rho \tag{7.31}$$

The mass fractions are found in terms of α and β by (7.14), (7.16) and (7.17):

$$\frac{\rho_m}{\rho} = 1 - \beta, \quad \frac{\rho_A}{\rho} = \beta(1 - \alpha), \quad \frac{\rho_I}{\rho} = \beta\alpha, \quad \frac{\rho_E}{\rho} = \beta\alpha \frac{m_E}{m_I} \tag{7.32}$$

Using (7.28), (7.29), (7.30) and (7.32) in the enthalpy expression (7.31), we find the enthalpy for this mixture as

$$h = c_{pI}\, T \left\{ \beta\,(1+\alpha) + (1-\beta)\,(0.7 + 0.2\,\psi_v) + 0.4\,\beta\,\left[\theta_D/2\,T + (\alpha + (1-\alpha)\,\psi_{elA})\,\theta_I/T\right]\right\} \tag{7.33}$$

$$c_{pI} = 5k/2m_I\,, \qquad \psi_{elA} = 1 - (S_1/S_2)$$

The equilibrium c_p is obtained by differentiating h with respect to T at constant p:

$$c_p = c_{pI}\left[(1-\beta)\,(0.7 + 0.2\,\varphi_v) + \beta\,(1+\alpha) + 0.4\,\beta\,(1-\alpha)\,\frac{\theta_I^2}{T^2}\left(\frac{S_4}{S_1} - \frac{S_2^2}{S_1^2}\right)\right]$$

$$+ c_{pI}\, T \left(\frac{\partial \beta}{\partial T}\right)_p \left[0.3 - 0.2\,\psi_v + \alpha + 0.2\,\frac{\theta_D}{T} + 0.4\,\frac{\theta_I}{T}\left(\alpha + (1-\alpha)\,\psi_{elA}\right)\right]$$

$$+ c_{pI}\, T\beta \left(\frac{\partial \alpha}{\partial T}\right)_p \left[1 + 0.4\,\frac{\theta_I}{T}\,(1 - \psi_{elA})\right] \tag{7.34}$$

$$\varphi_v = (\theta_v/T)^2\, e^{\theta_v/T} \Big/ \left(e^{\theta_v/T} - 1\right)^2\,, \qquad S_4 = \sum_{j=1}^{17} j^{-2} \exp\left(\theta_I/T\,j^2\right)$$

Equations (7.11), (7.18), (7.23), (7.24), (7.25), (7.26) and (7.34) express ρ, $(\partial h/\partial p)_T$ and c_p in terms of p, T, and thus express all the unknowns except dQ in the basic differential equations (7.9) in a form usable for numerical integration

A check on the thermodynamic properties used can be obtained by comparing some calculations made using the present formulas with those of Patch (Ref. 33). (The enthalpies of Ref. 33 have had $h_D^o = 2.16$ E 5 J/g added, since in that reference the H atom is taken as the reference for enthalpy, while here we have taken the H_2 molecule.) The comparison is made in Table 7.1 for β, α and h, with $T^* = 8000$K. Comparison shows the errors to be mostly a few percent, compared to the very elaborate scheme of Ref. 33. The worst errors are at high values of T and p. The applications in the present report do not exceed 16,000K at 10 atm, and are all above 8,000K, so the approximations appear satisfactory. The major source of error is probably the use of 17 terms in the sums of S_1 and S_2, instead of a variable cut-off.

7.4 ABSORPTION OF LASER ENERGY

The first term in the heat addition expression, Eq. (7.7), gives the absorption of the incident laser energy by the plasma. It is dependent on k_L, the absorption coefficient of the plasma. Based on the studies of Ref. 1, we use as the absorption mechanism inverse Bremsstrahlung, both electron-ion and electron-neutral. The expressions for k_L have been given in Ref. 1. The electron-ion absorption is given in Eq. (2.1) of Ref. 1 as

$$k_{LEI} = \sigma_{EI}\, n_E\, n_I \left[\exp\left(h_P \nu / kT\right) - 1\right]$$

where σ_{EI} is the electron-ion absorption cross-section and ν is the laser frequency (for 10.6 μm in the present case). The cross-section is given in Eq. (2.2) of Ref. 1 as

$$\sigma_{EI} = \frac{4}{3}\left(\frac{2\pi}{3 m_E k T}\right)^{1/2} \frac{Z^2 e^6}{h_P c\, m_E \nu^3} = \frac{1.63 \times 10^{-32}}{T^{1/2}} \ (\mathrm{cm}^5)$$

where Ze is the ion charge, e is the electron charge and c is the speed of light. Combining these two equations we find

$$k_{LEI} = \frac{1.63 \times 10^{-32}}{T^{1/2}}\, n_E\, n_I \left(e^{1357/T} - 1\right) \ (\mathrm{cm}^{-1})$$

where T is in K and n_E, n_I are in cm^{-3}.

TABLE 7.1

COMPARISON OF α, β, h WITH REFERENCE 33

p (atm)	T (K)	β	β (Ref. 2)	% Error
1	2000	8.34E-4	8.10E-4	3.0
10	2000	2.64E-4	2.56E-4	3.1
1	4000	0.645	0.622	3.8
10	4000	0.258	0.243	6.0
1	6000	0.99389	0.99251	0.14
10	6000	0.9435	0.9319	1.2
1	8000	0.99994	0.99926	7.3
10	8000	0.9945	0.9927	1.9

p (atm)	T (K)	α	α (Ref. 2)	% Error
1	10,000	0.2126E-1	0.2192E-1	-3.0
10	10,000	0.672E-4	0.706E-4	-4.8
1	14,000	0.2922	0.3050	-4.2
3	14,000	0.174	0.185	-5.9
10	14,000	0.0962	0.105	-8.4
1	20,000	0.895	0.922	-2.9
10	20,000	0.535	0.651	-17.8

p (atm)	T (K)	h (J/g)	h (J/g) (Ref. 2)	% Error
3	12,000	5.604E5	5.57E5	0.5
10	12,000	5.199E5	5.16E5	1.1
3	14,000	8.123E5	8.03E5	0.8
10	14,000	6.908E5	6.74E5	2.5

The electron and ion number densities are related to the density by (7.14) and (7.17) as

$$n_E = n_I = 2 \beta \alpha \rho / m_M$$

The above expression for k_{LEI} is a semi-classical result. To account for quantum - mechanical effects we multiply by a Gaunt factor of 1.5, which is an average value for the range of interest. The final expression for the electron-ion inverse Bremsstrahlung absorption coefficient is then

$$k_{LEI} = 8.7 \times 10^{a} \frac{\alpha^2 \beta^2 \rho^2}{\sqrt{T}} \left(e^{1357/T} - 1\right) \qquad (7.35a)$$

a = 15 for cgs units, a = 11 for mks units.

Of course, this expression is only valid where there are ions, $\alpha \neq 0$, so in our approximation for the chemistry, it is to be used only above T^*, where $\beta = 1$.

The absorption coefficient for electron-neutral inverse Bremsstrahlung is also given in Ref. 1, Eq. (2.6), as

$$k_{LEN} = Q_{EN} n_E n_N \left[1 - \exp\left(-h_P \nu / kT\right)\right]$$

where Q_{EN} is the absorption cross-section and n_N is the neutral number density. Equation (2.8) of Ref. 1 gives

$$Q_{EN} = \frac{2.96 \times 10^{-45} T}{1 - \exp\left(-h_P \nu / kT\right)} \left(\frac{h_I^o m_I}{h_P \nu}\right)^2 e^{-\xi} \left(\frac{m_I h_I^o}{kT}\right)^{1/2} \quad (cm^5)$$

where ξ may be approximated by the first term of Eq. (2.9) of Ref. 1, when $\sqrt{T/158,000}$ is small, as

$$\xi = 4.862 \left(kT / m_I h_I^o\right)^{1/2}$$

Since for hydrogen $m_I h_I^o/k = 158,000\,K$, then we have

$$k_{LEN} = 1.6 \times 10^{-38} \sqrt{T}\; n_E\, n_N \exp(-0.0122\sqrt{T})\ (cm^{-1})$$

where n_E, n_N are in cm^{-3}.

The number densities are found from (14) and (17), where we recognize that our chemical model has $\beta = 1$ whenever there are electrons present, so

$$n_E = 2\alpha\rho/m_M, \quad n_N = n_A = 2(1-\alpha)\rho m_M \quad .$$

Then the final expression for k_{LEN} is

$$k_{LEN} = 5.7 \times 10^{b}\, \alpha(1-\alpha)\rho^2 \sqrt{T} \exp(-0.0122\sqrt{T}) \qquad (7.35b)$$

b = 9 for cgs units b = 5 for mks units

The expression for k_L to be used in the first term of (7.7), and in the definition of optical depth τ, Eq. (7.5), is the sum

$$k_L = k_{LEI} + k_{LEN} \quad . \qquad (7.36)$$

A plot of k_{LEI} (dashed lines) and k_{LEN} (solid lines) is given in Fig. 7.1 as k_L/p vs T. It can be seen that electron-ion absorption dominates at temperatures above 11,000K at 10 atm, and above 9,000K at 1 atm. The sum k_L follows the k_{LEI} curves closely above 12,000K.

7.5 PLASMA RADIATION EMISSION

The second term in dQ, Eq. (7.7), is the loss of energy caused by emission of radiation from the plasma

$$\int_0^R 2\pi r\, \nabla \cdot \underline{S}\, dr$$

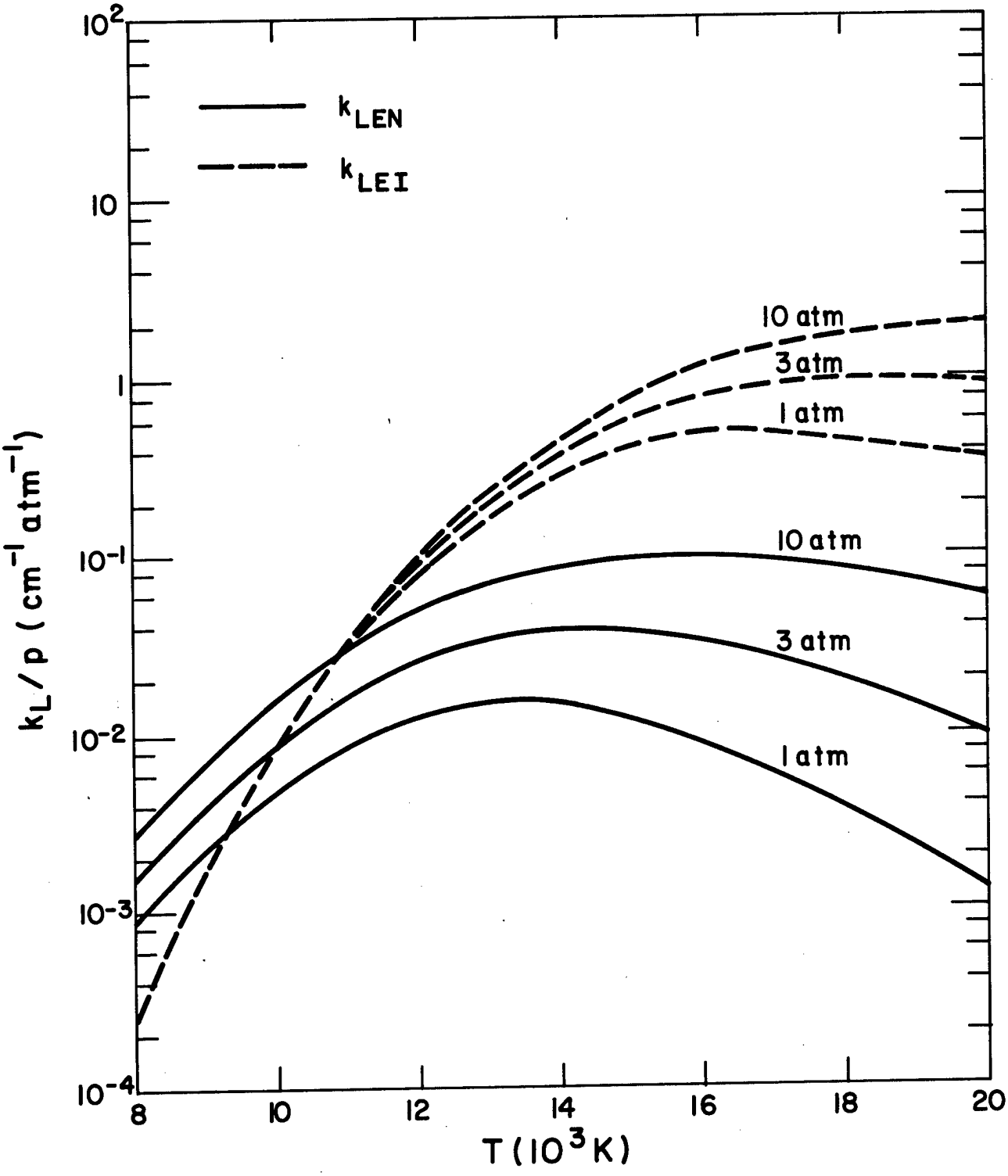

Fig. 7.1 Inverse Bremsstrahlung Absorption Coefficient

The model used for this term is discussed in the section of this report entitled Radiative Emission. The model is one of a uniform cylinder of plasma, so the emission at any station is expressed in terms of a volume emission P_T and the cross-sectional area

$$\int_0^R 2\pi r \, \nabla \cdot \underline{S} \, dr = \pi R^2 P_T \tag{7.37}$$

The general form of P_T, as deduced in the section on Radiative Emission, from Eq. (5.32), is

$$P_T = 8.6 \times 10^{-9} C_1 \left(\frac{T}{\theta_I} + C_2 \right) n_{AG} \frac{T}{\theta_I} e^{-\theta_I/T} \left(\frac{W}{cm^3} \right)$$

where n_{AG} is the atom ground state population, in cm^{-3}, and the constants C_1 and C_2 depend on the pressure level and the relative importance of line and continuum radiation. The relation between n_{AG} and n_A is through the electronic partition function Q_{elA} of (7.21), whose first term relates to the ground state.

$$n_{AG} = n_A \frac{2}{Q_{elA}} = \frac{n_A}{S_1 \exp(-h_I^o m_I/kT)}$$

When n_A is expressed in terms of α, β and ρ from (7.14) and (7.17), the expression for P_T is, in mks units,

$$P_T = 5.1 \times 10^{18} C_3 \left(\frac{T}{\theta_I} + C_2 \right) \frac{T}{\theta_I} \frac{\beta (1 - \alpha) \rho}{S_1} \left(\frac{W}{m^3} \right) \tag{7.38}$$

The values of the constants C_3, C_2 depend on the pressure level and laser power, as described in the section on Radiative Emission from Hydrogen. The particular values used for the cases calculated will be given when the results of the calculations are discussed.

7.6 SPECIFICATION OF VELOCITY DISTRIBUTION

As described above, in the subsection on Basic Equations, the velocity distribution in the plasma core streamtube is chosen as the independent parameter rather than the area distribution, since it greatly simplifies the calculation of the flow, by avoiding the explicit appearance of the singularity at the station at which M = 1.

Several forms of u were tried, to see if reasonable nozzle shales were attained. The simplest and most satisfactory was a logarithmic distribution.

The calculations were done with the optical depth τ, rather than distance x, as the independent variable. This choice eliminates the explicit appearance of k_L from the differential equations when the plasma emission term ϵ is not taken into account, as can easily be seen from Eqs. (7.5), (7.7) and 7.9). It was used in Ref. 1, where ϵ was not considered. In the present case where ϵ was included, there is no simplification afforded by using τ, since it will require the explicit appearance of k_L in the plasma emission term, but it was used to provide some continuity with Ref. 1. However, in the future, it probably would be better to use x as the independent variable.

In terms of τ, the u distribution was taken as

$$u = u_i \left(\frac{u_f}{u_i} \right)^{\tau/\tau_f} \tag{7.39a}$$

which goes from u_i at $\tau = 0$ ($x = 0$), the initial station, to u_f at the final station τ_f. This is a linear variation of ln u with τ. The nozzle shapes obtained with this can be quite reasonable, as will be seen when the results of the calculations are presented.

The derivative is easily obtained from

$$\ln u = \ln u_i + (\tau/\tau_f) \ln (u_f/u_i)$$

as

$$\frac{du}{d\tau} = \frac{u \ln (u_f/u_i)}{\tau} \tag{7.39b}$$

7.7 SUMMARY OF THE MODEL

All the quantities necessary for the integration of the differential equations (7.9) have now been defined. In terms of τ as the independent variable, (7.9) becomes, using (7.5), (7.7), (7.10), (7.11), (7.18), (7.25) and (7.37):

$$\frac{dp}{d\tau} = \frac{-pu}{R_M Z T} \frac{du}{d\tau} \tag{7.40a}$$

$$\frac{dT}{d\tau} = \left\{ \frac{(AI)_i}{\dot{m}} e^{-\tau} - \frac{\pi R^2 \epsilon}{k_L \dot{m}} - \left[1 + \left(\frac{\partial \ln Z}{\partial \ln T} \right)_p \right] u \frac{du}{d\tau} \right\} \Big/ c_p \qquad (7.40b)$$

$$\frac{dx}{d\tau} = \frac{1}{k_L} \quad , \quad R = \left(\frac{\dot{m} R_M Z T}{p u} \right)^{1/2} \qquad (7.40c)$$

Z is given in terms of α, β by (7.24), and those equations also give α, β in terms of p, T. Equation (7.34) gives c_p, while the derivatives of α, β and Z are in (7.26). With u and $du/d\tau$ from (7.39), a forward integration of the three differential equations can be performed from a starting station $\tau = 0$ at which $x = 0$, $T = T_i$, $p = p_i$, $u = u_i$, to a final station τ_f, where $u = u_f$. The mass flow rate constant $\dot{m}$ is determined by the given initial conditions and the initial radius R_i as

$$\dot{m} = \pi R_i^2 \rho_i u_i = A_i \rho_i u_i \qquad (7.41)$$

which shows that only R/R_i is determined by the solution. Of course, if the laser power P is given, R_i is related to the incident laser intensity by

$$I_o = P/\pi R_i^2 \qquad (7.42)$$

The incident laser intensity I_o is not the same as the initial intensity I_i, because energy has been added to the incident gas in the LSC wave before the stream tube calculation is started, and we must be careful to conserve energy. If the calculation is begun at T_i, p_i, u_i, the initial total enthalpy flux is $\dot{m}(h_i + u_i^2/2)$, where h_i is obtained from (7.33). If the gas is supplied at p_o, T_o, h_o, u_o, then its total enthalpy flux is $\dot{m}(h_o + u_o^2/2)$, and the amount of energy added up to the initial state must have come from I_o. Thus

$$I_i = I_o - \dot{m}_A (h_i + u_i^2/2 - h_o - u_o^2/2) \qquad (7.43)$$

where $\dot{m}_A$ is the mass flow per unit area,

$$\dot{m}_A = \dot{m}/A_i = \rho_i u_i = \rho_o u_o \quad . \tag{7.44}$$

If the initial conditions are at a temperature of order 10,000K, the reduction in I_o, caused by the heating of the incident gas by the LSC wave, is substantial.

The initial conditions for the streamtube are determined by the properties of the LSC wave which pre-heats the gas. As is customary with LSC wave properties, we assume it causes no pressure change, but only temperature and density changes, so $p_i = p_o$. In addition the LSC wave propagates against the flow at a speed dependent on laser intensity and pressure level, so I_o and p_o determine $\dot{m}_A$. If T_o is also given then ρ_o and $u_o = \dot{m}_A/\rho_o$ $u_i = \dot{m}_A/\rho_i$. Finally, (7.43) gives I_i, and we have all the necessary initial conditions. This scheme shows that the properties of the LSC wave, plus a choice of I_o, p_o and T_o are all the conditions necessary to integrate the streamtube equations, once u_f and τ_f are chosen. The integration then determines the distribution of all gas properties along the streamtube including the plasma emission ϵ, and also determines the streamtube shape R/R_i. The scale of the streamtube can only be found when the laser power P is also given, whence R_i follows from (7.42). However, it should be noted that some idea of the size of the streamtube, is necessary to perform the integration, because its size influences the degree of opacity of the plasma, and thus influences the choice of constants in the expression for ϵ.

Although it is not used in the integration, the Mach number is an interesting parameter which can be calculated when p and T are known, since they determine the speed of sound a. For a gas in thermochemical equilibrium, the second law of thermodynamics and the expression of h as a function of ρ and p shows that

$$a^2 \equiv \left(\frac{\partial p}{\partial \rho}\right)_s = \frac{(\partial h/\partial \rho)_p}{\rho^{-1} - (\partial h/\partial p)_\rho}$$

Conversion of these derivatives to h as a function of T and p, and use of (7.11) shows that

$$a^2 = \left[\left(\frac{\partial \rho}{\partial p} \right)_T - \frac{1}{c_p T} \left(\frac{\partial \ln \rho}{\partial T} \right)_p^2 \right]^{-1}$$

The second derivative has already been expressed in terms of Z by (7.25). From the gas law (7.18) it is easy to see that

$$\left(\frac{\partial \rho}{\partial p} \right)_T = \frac{1}{R_M Z T} \left[1 - \left(\frac{\partial \ln Z}{\partial \ln p} \right)_T \right]$$

Thus the Mach number squared is

$$M^2 = \frac{u^2}{a^2} = \frac{u^2}{T} \left\{ \frac{1}{R_M Z} \left[1 - \left(\frac{\partial \ln Z}{\partial \ln p} \right)_T \right] - \frac{1}{c_p} \left[1 + \left(\frac{\partial \ln Z}{\partial \ln T} \right)_p \right]^2 \right\} \quad (7.45)$$

The T derivative of Z is given in (7.26). Similar differentiation of Z, α and β in (7.24) with respect to p gives

$$T < T^*: \left(\frac{\partial \ln Z}{\partial \ln p} \right)_T = \frac{1}{1+\beta} \left(\frac{\partial \beta}{\partial \ln p} \right)_T = - \frac{\beta (1 - \beta^2)}{2} \quad (7.46a)$$

$$T > T^*: \left(\frac{\partial \ln Z}{\partial \ln p} \right)_T = \frac{1}{1+\alpha} \left(\frac{\partial \alpha}{\partial \ln p} \right)_T = - \frac{\alpha (1 - \alpha^2)}{2} \quad (7.46b)$$

Thus the Mach number can be calculated as the integration progresses.

7.8 RESULTS OF CALCULATIONS

A computer program has been written to integrate Eqs. (7.40), and has been used for six cases of varying laser power and incident gas pressure level. All the cases were done for the same incident laser intensity of $I_o = 3.67 \times 10^9$ w/m^2 (3.67×10^5 w/cm^2) and the same mass flow rate per unit area, $\dot{m}_A = 3.316$ kg/m^2 (0.3316 g/cm^2), based on an estimate of the properties of LSC waves in hydrogen, as described in the section on LSC Wave Properties. In all cases the incident temperature was $T_o = 300$K

and the initial temperature was T_i = 12,000K. (It is believed that the effect of lowering T_i by a few thousand degrees will not change the major results of the calculations.)

The parameters varied were the laser power P and the incident gas pressure level $p_o = p_i$. Therefore the initial radius R_i (and area A_i), and the total mass flow rate is also varied. The calculation matrix is given in Table 7.2.

The range of power varied from the experimental device of 10 kw to a 5000 kw device of operational size, with an intermediate size of 100 kw. The pressure of 3 atm corresponds to the experimental device, while 10 atm was chosen to show the effect of operating pressure. The initial densities and velocities are determined by p_o, T_i and $\dot{m}_A$, as explained above. In all cases, the integration was carried out to a final value of optical depth $\tau_f = 4$, with a velocity there of u_f = 1.47 E4 m/s. The attempt was to perform the calculations to the throat of the streamtube, and in all cases the minimum area was in fact reached. The choice of $\tau_f = 4$ means that the laser energy still unabsorbed at that point is down from the initial value by a factor of e^{-4} = 1.8 E-2, so only 2% of the initial laser energy is not absorbed. From there one, there is no longer significant heat addition to the gas. There are still losses due to radiation.

The constants C_3 and C_2 used in Eq. (7.38) to express the plasma emission ϵ were taken from the material described in the section on Radiative Emission, and were appropriate to the sizes of plasma core for each power level. They are given in Table 7.3.

The properties of hydrogen needed were taken from standard references, and are:

k = 1.305 E-23 J/K, $\quad m_A = m_I = m_M/2$ = 1.673 E-27 kg

m_E = 9.109 E-31 kg, $\quad h_P$ = 6.6256 E-34 Js

θ_r = 87.62 K, $\quad \theta_v$ = 5983 K

θ_D = 52,000 K, $\quad \theta_I$ = 158,000 K

The value used for θ_v includes the correction for anharmonicity.

TABLE 7.2

CASES CALCULATED

Case	P (kW)	p_o (atm)	R_i (cm)	A_i (cm^2)	$\dot{m}$ (g/cm^2-s = 10 kg/m^2-s)
1	10	3	9.31 E-2	2.72 E-2	9.03 E-3
2	5000	3	2.08	1.36 E1	4.51
3	100	3	2.94 E-1	2.72 E-1	9.02 E-2
4	10	10	9.31 E-2	2.72 E-2	9.03 E-3
5	100	10	2.94 E-1	2.72 E-1	9.02 E-2
6	5000	10	2.08	1.36 E1	4.51

TABLE 7.3

CONSTANTS IN PLASMA EMISSION

Case	P (kW)	p_o (atm)	C_3 (W/m^3)	C_2
1	10	3	2	2.4
2	5000	3	2	0.4
3	100	3	1	2.4
4	10	10	4/3	2.4
5	100	10	3/4	2.4
6	5000	10	2.2	0.4

The integration of the differential equations was performed at steps in τ of 0.05, so there were 80 steps from $\tau = 0$ to 4.

The profiles of T and R/R_i vs x are given in Figs. 7.2 and 7.3. Figures 7.2a and 7.2b are the temperature profiles for 3 and 10 atm respectively. The location of the throat, and the station at which 90% of the initial laser energy is absorbed are marked. They all show an increase to a rather flat maximum, followed by a drop to the throat, although the throat is still at temperatures of 13,000 to 15,000 K. The maxima are quite flat, and occur near the 90% absorbed station. The larger the power, the larger is the temperature at any station, as might be expected. Also, the large the power, the shorter the distance to the throat, though this effect is not great. These distances vary from 3.2 to 4.0 cm for 3 atm and from 0.49 to 0.54 cm for 10 atm. This points up the major effect of pressure level. Because the absorption coefficient k_L increases with pressure, the laser energy is absorbed in shorter distances at the higher pressure, and the converging part of the streamtube is shorter. The 10 atmosphere streamtubes are nearly one-tenth the length of the 3 atmosphere streamtubes.

When one combines the initial radii given in Table 7.2 with the throat lengths given in Fig. 7.2, the small size of these devices becomes evident. The lengths are determined by the pressure level through the absorption coefficient, as just mentioned. The radius is determined by the power and the incident intensity I_o. If I_o of order 10^5 W/cm^2 is required to support the LSC wave, then radii of order 0.1 to 2 cm will follow. To enlarge the size, it is crucial to operate at as small values of I_o as possible which means as near as possible to the threshold intensity of the LSC wave. This emphasizes the importance of having a reliable theory to estimate the threshold of LSC waves in hydrogen.

Figures 7.2a and 7.3b show the normalized radius distribution R/R_i for 3 and 10 atm respectively. It can be seen that only small variations of shape with power occur, and the shapes seem very reasonable. Notice the vertical scale is not physical size, though the horizontal scale is, so angles on the figure are not necessarily correct. For the 5 MW power $R_i = 2.08$ cm, so the streamtube shown on the 3 atm figure, Fig. 7.3a, has very nearly the same scales on both axes. The same is approximately true of the 100 kW power on the 10 atm figure, Fig. 7.3b, where $R_i = 0.294$ cm. Other streamtube shapes can be produced by varying the assumed velocity distribution, and more experience with calculations would show what range of shapes can be achieved.

Notice that at 10 atm the higher power cases lead to fat, stubby streamtubes, such as one which is 2.08 cm in initial radius and only 0.5 cm

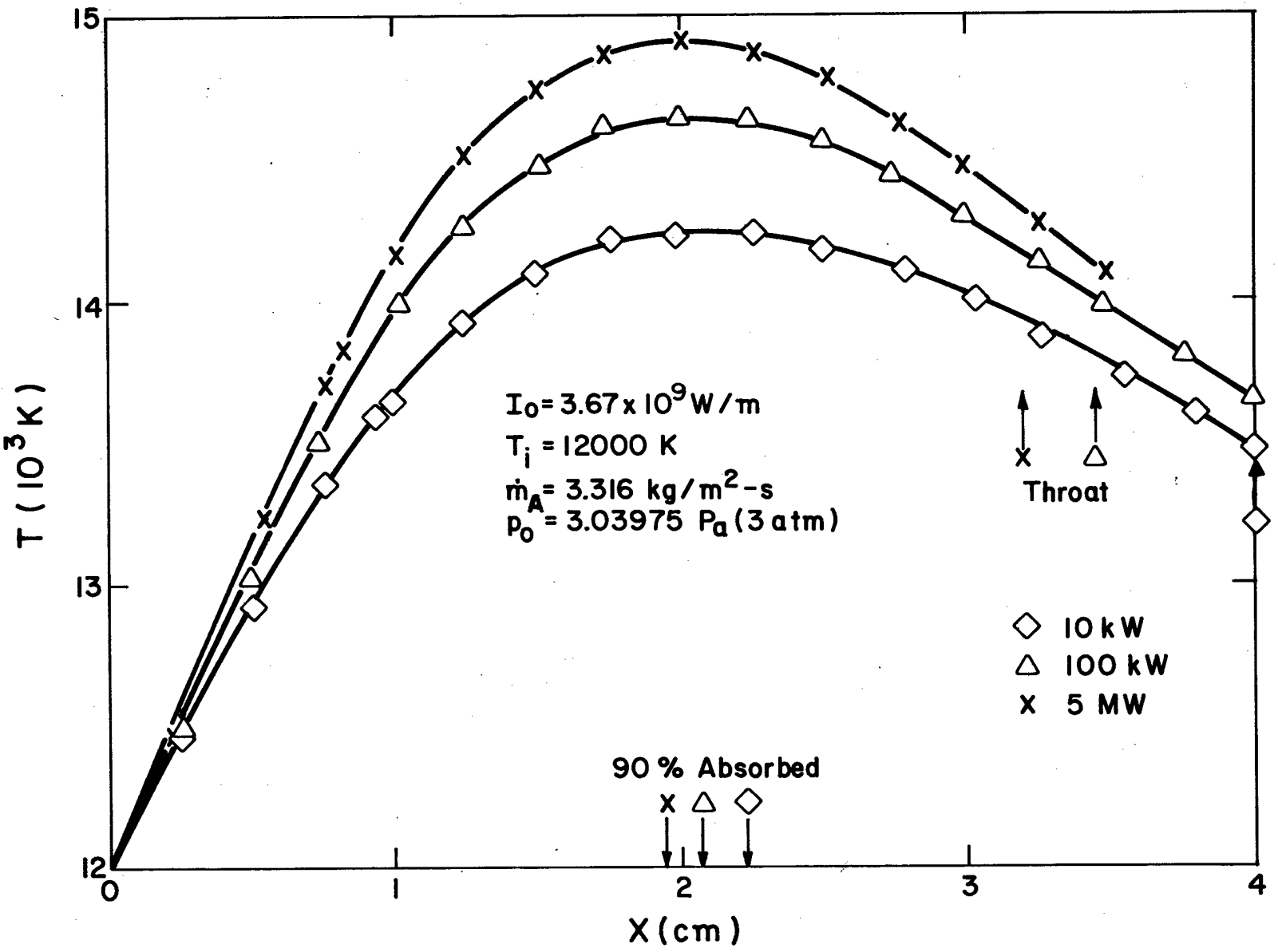

Fig. 7.2a Laser-Heated Streamtube Temperature Distribution for 3 atm Initial Pressure

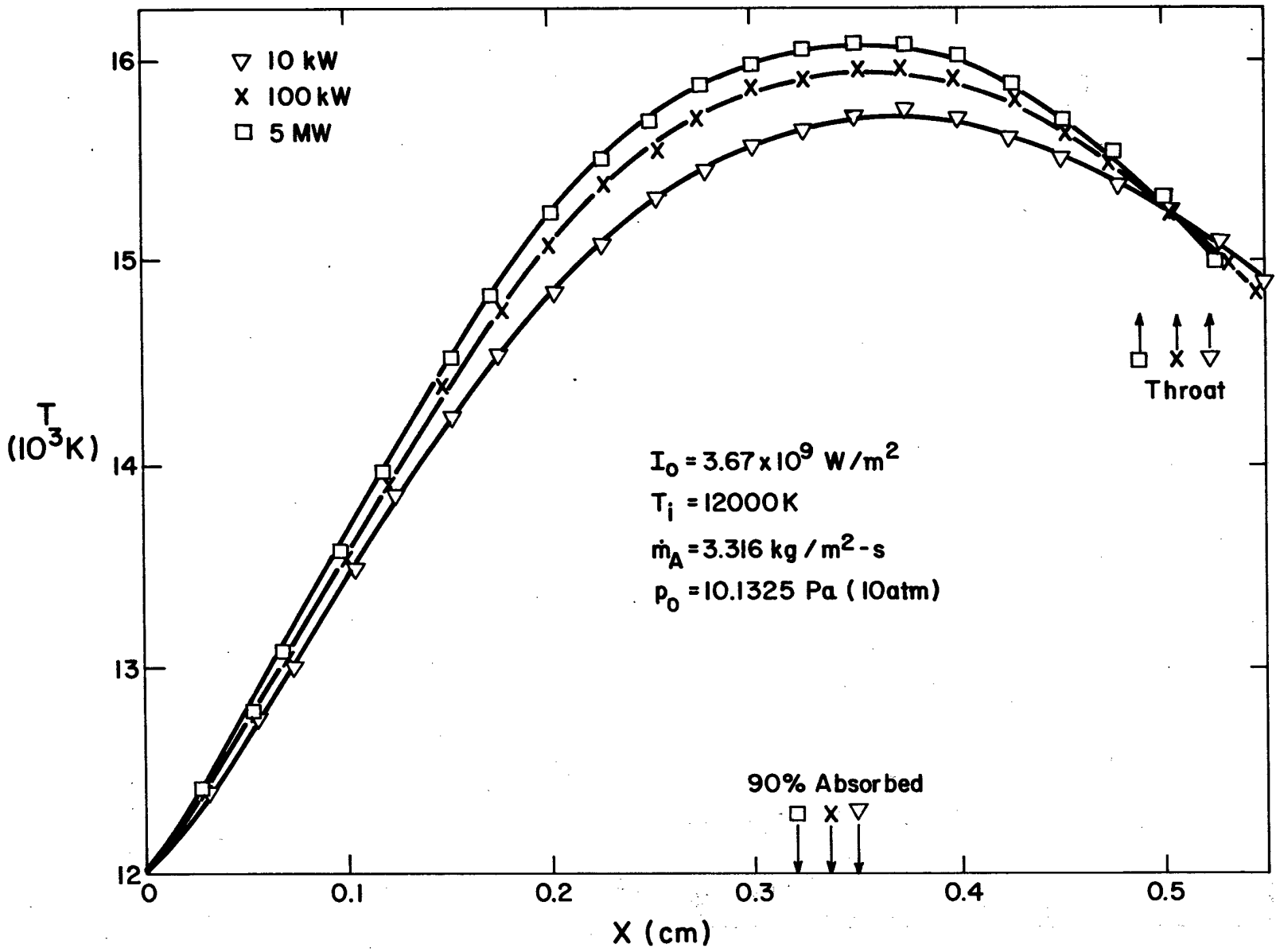

Fig. 7.2b Laser-Heater Streamtube Temperature Distribution for 10 atm Initial Pressure

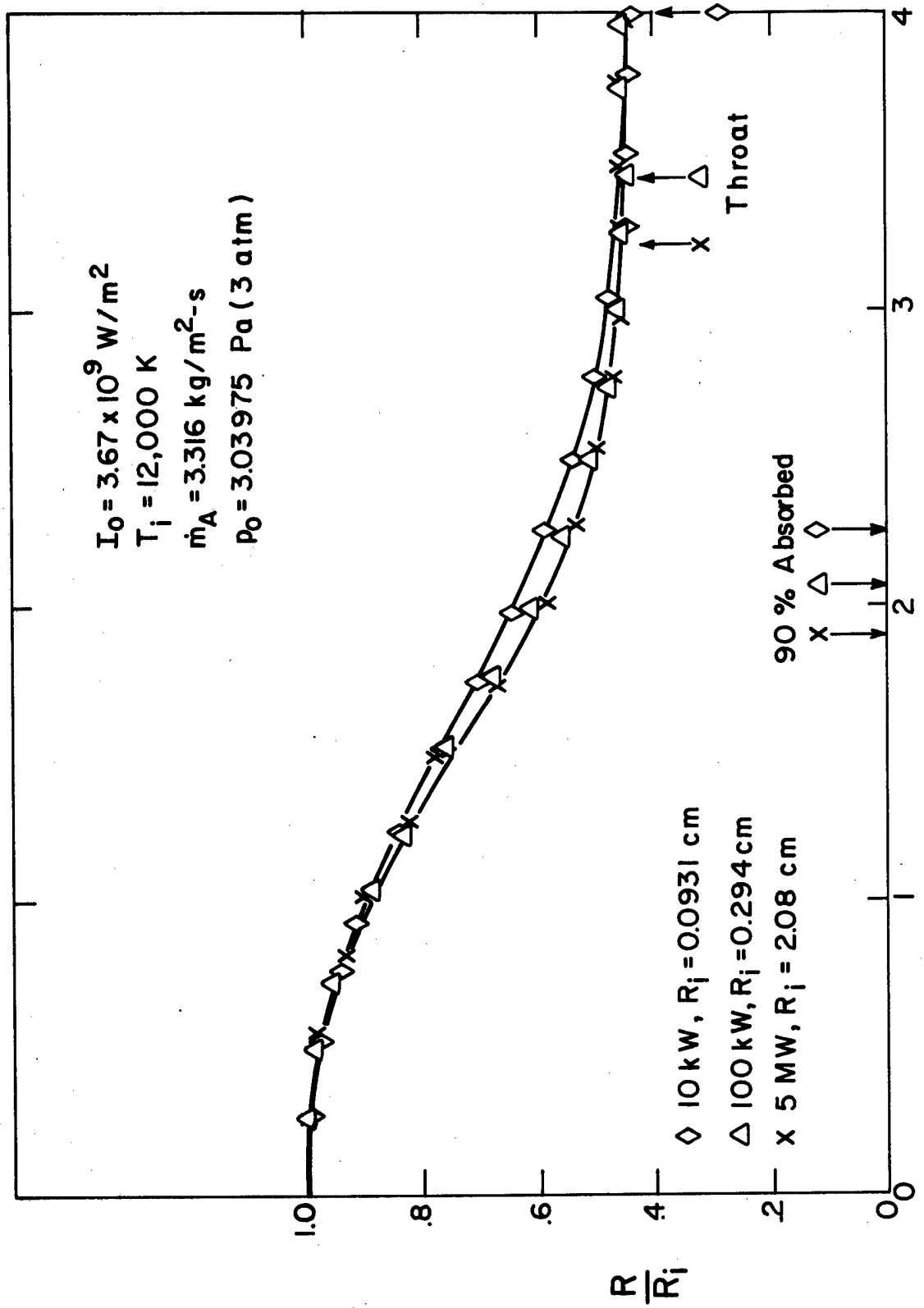

Fig. 7.3a Laser-Heated Streamtube Radius Distribution for 3 atm Initial Pressure

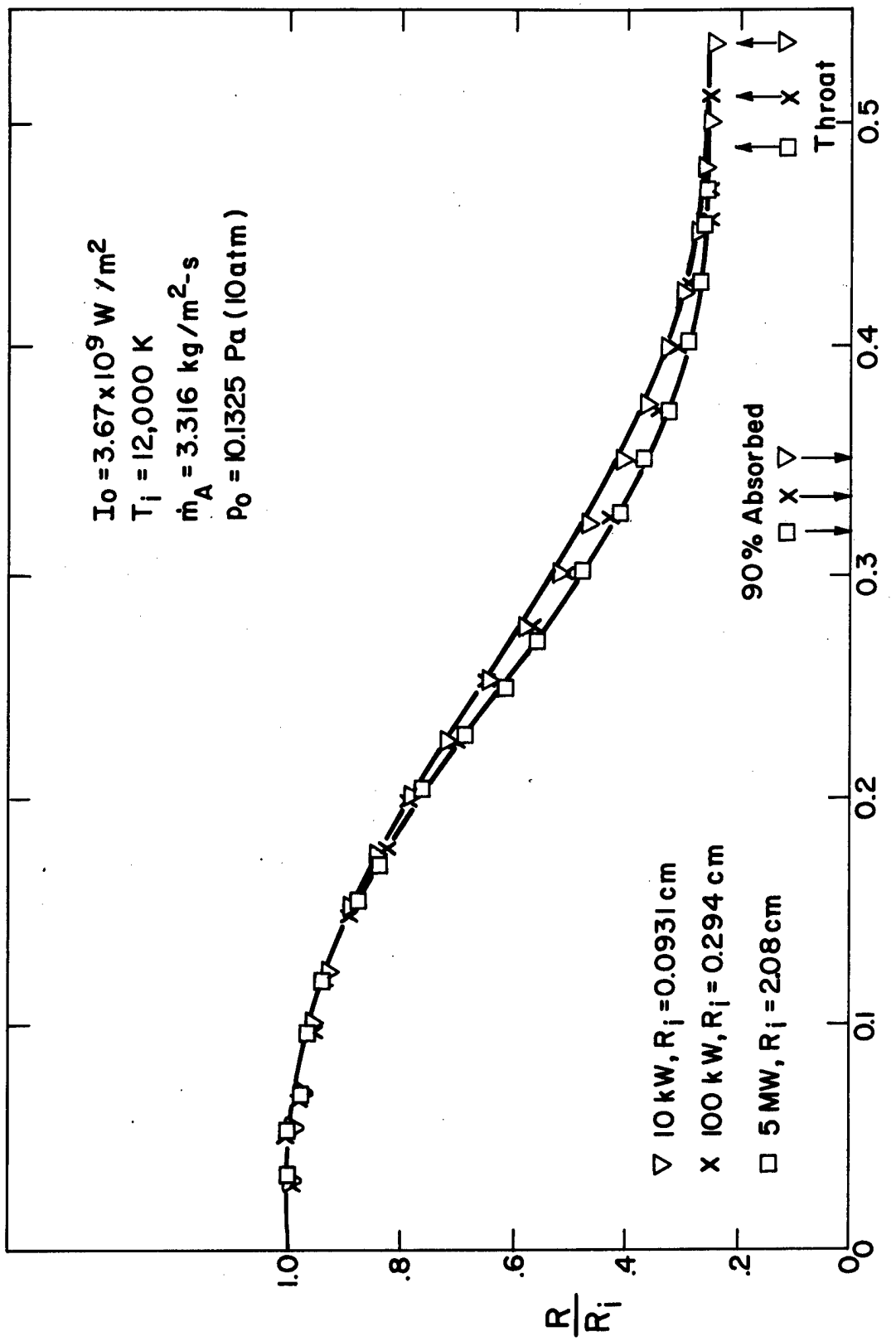

Fig. 7.3b Laser-Heated Streamtube Radius Distribution for 10 atm Initial Pressure

long for 5 MW. This may be undesirable geometry from flow criteria, and may indicate that high pressure operation at large powers is not a useful combination.

It can be concluded that this rather small program can calculate the core streamtube quite easily.

Other results of the calculations are described in the sections on Radiative Heating and on Performance.

8. HEAT LOSSES

8.1 INTRODUCTION

The flowing plasma core loses heat by emission of plasma radiation, and by convenction of heat to whatever surface is in contact with the hot plasma. The walls of the rocket must be protected from this heat load. In order to define what method of protection should be used, the size of the heat load must be known. This section is devoted to calculation of the heat load from both emission and convection.

The emission has already been used in the plasma core streamtube calculation, where it was coupled to the plasma core temperature and geometry to provide the energy loss term. The explicit calculation of the amount of energy lost and the resulting heat load is easily obtained from the results of the core streamtube calculation, as described in Subsection 8.2.

No convective heat loss was taken into account in the core calculation. In order to decide if this loss is of sufficient size to require it also to be coupled to the core calculation, an uncoupled calculation was made by using the temperature and pressure distributions found from the core model. These conditions were used as external conditions in a hydrogen boundary layer calculation to estimate the heat loss to a cool surface placed in contact with the plasma core. If the resulting energy loss is large compared to the core energy, it indicates a coupling of the convective loss and the core flow is needed. If the loss is small compared to the core energy, such a coupled model is not necessary. In addition to an impervious wall boundary layer, some cases of gas injection into the boundary layer were calculated to see if that was a feasible method of reducing the convective heat loss. These hydrogen boundary layer calculations are described in Subsection 8.3.

Finally, the possibility of protecting the walls from the radiative emission by particles in a buffer gas region surrounding the plasma is considered in Subsection 8.4.

8.2 RADIATIVE HEAT LOSS

One of the results of the core streamtube calculation is the radiative energy emission from the plasma. At any station, the plasma emission

term is $\pi R^2 P_T$, as shown in Eq. (7.37). The streamtube program calculates both R and P_T as function of x, and the quantity $\pi R^2 P_T$ is shown in Fig. 8.1a for 3 atm and in Fig. 8.1b for 10 atm. Notice that in Fig. 8.1a, the 5 MW curve is plotted as $\pi R^2 P_T/100$, while in Fig. 8.1b the 100 kW curve is $\pi R^2 P_T/10$ and the 5 MW curve is $\pi R^2 P_T/100$.

These curves show that the station emission has a maximum somewhat earlier than the temperature profiles shown in Fig. 7.2, because R decreases steadily. At the throat, the values are below the initial values because of the small radius there.

In order to estimate the heating received by the wall or the buffer gas by plasma emission we divide the station emission by the circumference $2\pi R$ of the steamtube at the same station, to get the distributions of

$$q_{rad} = \pi R^2 P_T/2\pi R \qquad (8.1)$$

The results are shown in Fig. 8.2a for 3 atm and Fig. 8.2b for 10 atm. (The 5 MW curve on Fig. 8.2b is 1/10 of q_{rad}). This is not exactly the radial heat flux at the station, because the radiation is emitted in all directions, not only radially. However, the includsion of the geometrical effects necessitates a complicated calculation which is not warranted at the present stage of the theory. For long, narrow streamtubes the approximation is a good one since most of the solid angle is radial, and the axial energy transport out of one station is compensated by axial transport in from other stations. For short, stubby streamtubes like the 5 MW, 10 atm one, the approximation is not so good, but these are probably not desirable geometries to use.

The total energy lost to the streamtube by plasma emission up to the throat can be obtained by integrating the curves of Fig. 8.1 from x = 0 to the throat station. The average energy flux at the streamtube surface is likewise obtained by integrating the curves of Fig. 8.2 to the throat, and dividing by the throat station x_{th}.

$$Q_{rad} = \int_0^{x_{th}} \pi R^2 P_T \, dx \,, \quad \bar{q}_{rad} = \frac{1}{x_{th}} \int_0^{x_{th}} q_{rad} \, dx \qquad (8.2)$$

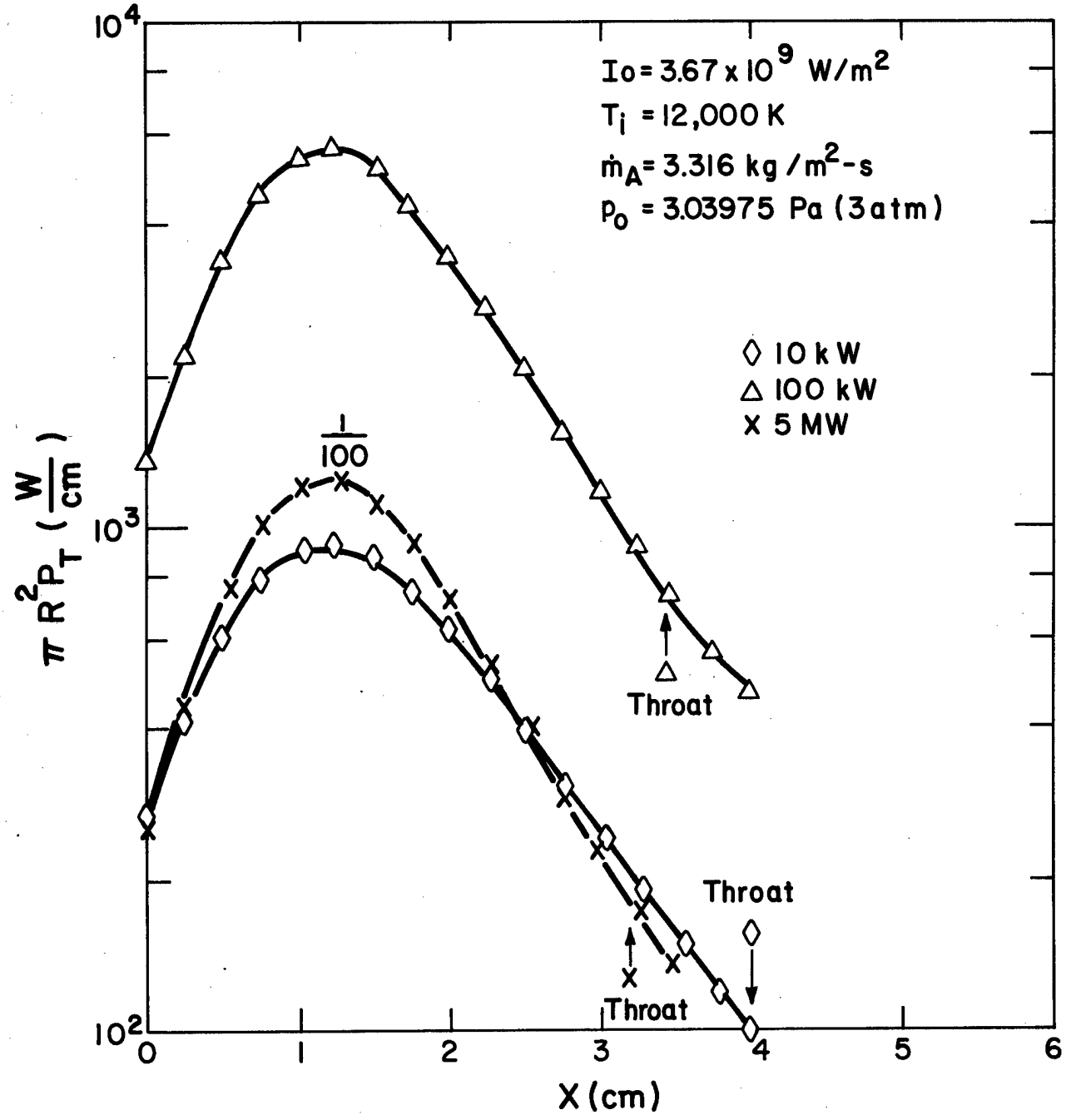

Fig. 8.1a Station Radiance of Laser-Heated Streamtube for 3 atm Initial Pressure

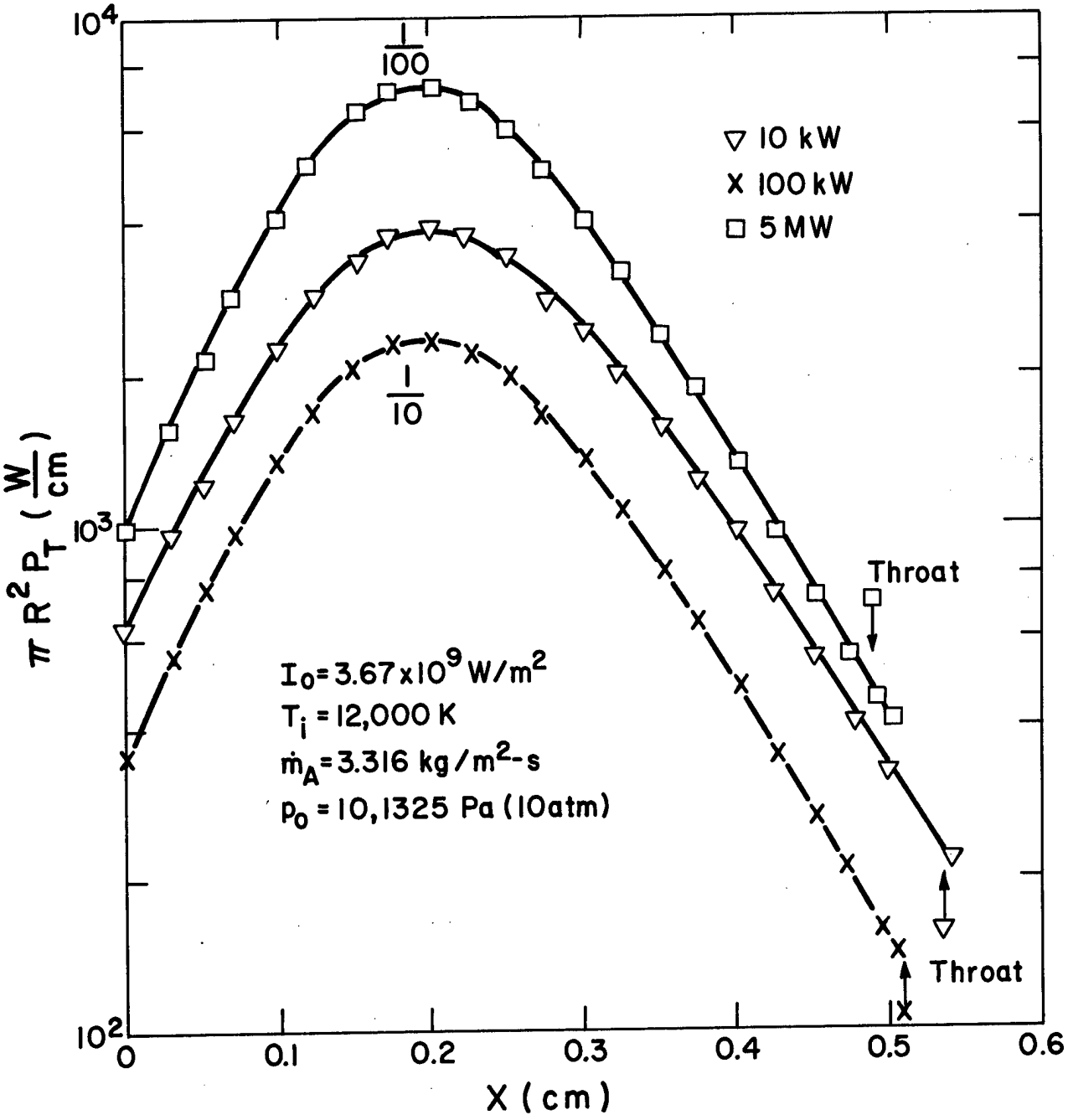

Fig. 8.1b Station Radiance of Laser-Heated Streamtube for 10 atm Initial Pressure

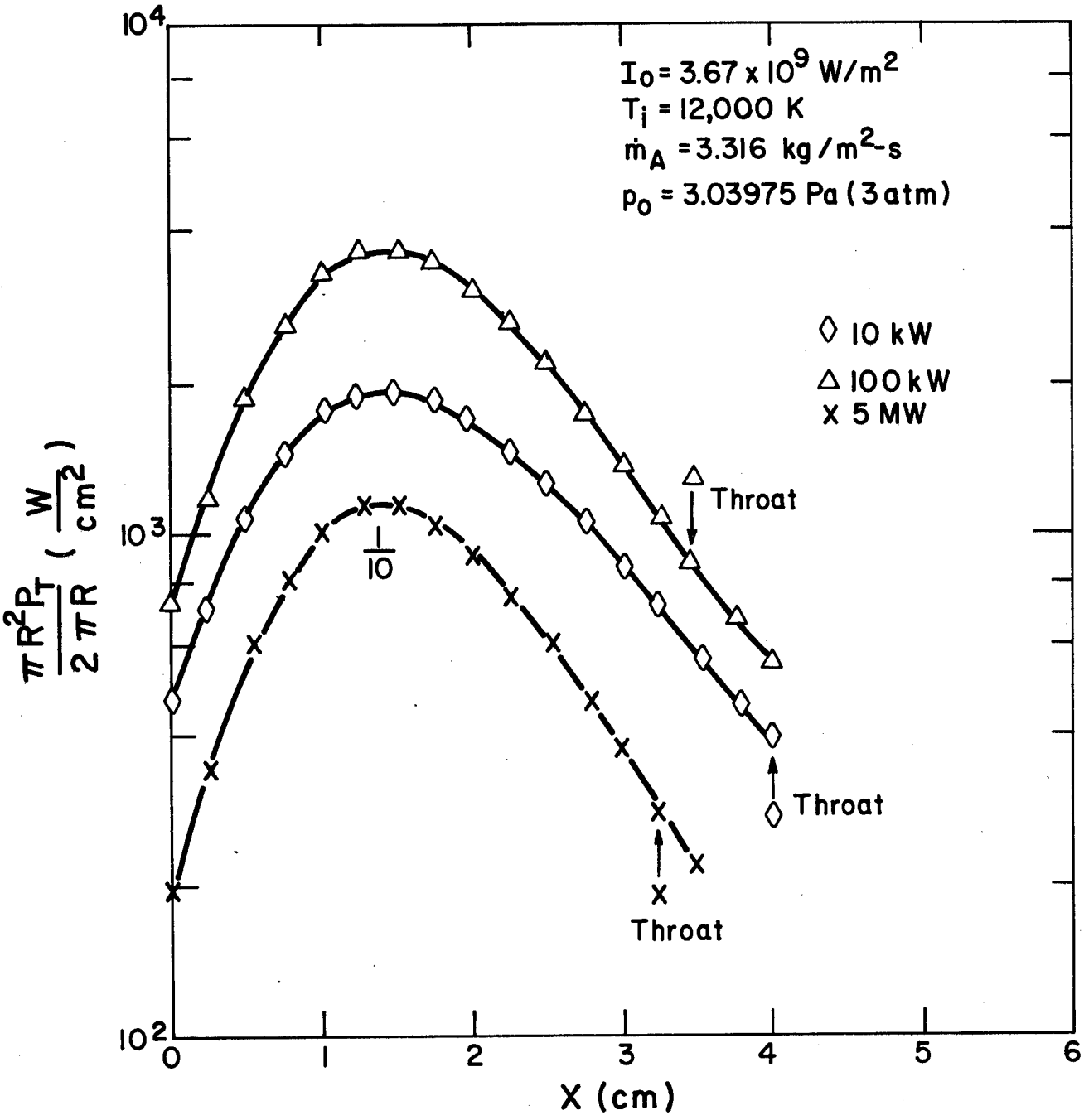

Fig. 8.2a Station Radiant Energy Flux of Laser-Heated Streamtube for 3 atm Initial Pressure

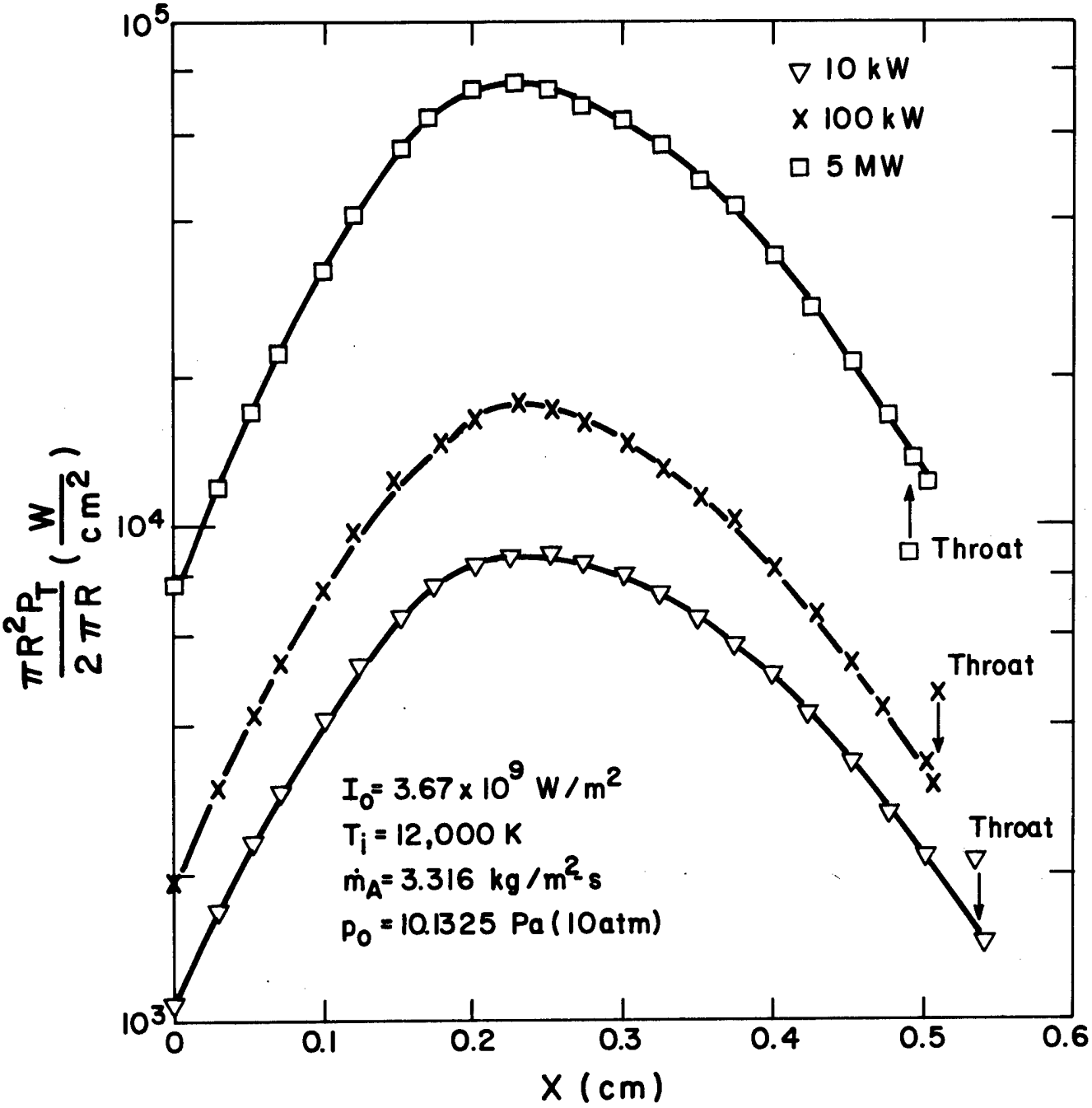

Fig. 8.2b Station Radiant Energy Flux of Laser-Heated Streamtube for 10 atm Initial Pressure

Table 8.1 presents these quantities for the six cases calculated, as well as the maximum value of the energy flux

$$\left(q_{rad}\right)_{max} = \left(\pi R^2 P_T / 2\pi R\right)_{max} \qquad (8.3)$$

and the fraction of the laser power radiated. The radiative losses are small fractions of the power input, indicating that the incident power is converted efficiently into hot plasma, which is then available for propulsion. The larger engines are the most efficient; even though the absolute amount of power they radiate is larger, the fraction of the incident power is smaller. The reverse is true for the energy flux; the larger engines have the highest fluxes. This is a surface to volume ratio effect at any one pressure. The higher fluxes at the higher pressure are a result of the shorter length of the streamtube. The magnitude of the fluxes at the higher powers indicate that some form of active heat protection will be needed, either by absorbing some of this energy in a buffer gas, or by some suitable scheme of cooling the walls.

8.3 CONVECTIVE HEAT LOSS

The hydrogen boundary layers grow on the sides of the core streamtube starting at the initial station, with the flow external to the boundary layer given by the core properties. For the six cases calculated by the core streamtube program, the Reynolds number based on conditions in the core at the throat station varies from 2800 for the 10 atm, 5 MW case to 8500 for the 3 atm, 10 kW case. This indicates that laminar flow will prevail, so a laminar compressible boundary layer model is appropriate.

Since the primary purpose of this calculation is to estimate the heating, and to see if a coupled calculation is necessary, it is appropriate to use as simple a model as will include the important physical effects. We have therefore assumed that a "local similarity" solution will be satisfactory. That is, at any station, the boundary layer is calculated as if it was a similar boundary layer with the local external properties as parameters. This reduces the numerical problem to one of ordinary, rather than two - variable partial, differential equations, which is a great simplification. This approximation has proved to be very useful in calculating heating from high temperature gases, and can be found discussed in books on boundary layer theory.

Although many cases of similar boundary layers have been calculated, none known to us is useful for the present case of very high temperature hydrogen, because they do not include the transport properties of hydrogen

TABLE 8.1

RADIATION HEAT LOSSES

	p_o = 3 atm			p_o = 10 atm		
Power (kW)	10	100	5000	10	100	5000
Throat Station x_{th} (cm)	3.99	3.46	3.24	0.54	0.51	0.49
Power Loss Q_{rad} (kW)	2.00	10.8	225	1.01	5.84	174
Max Energy Flux $(q_{rad})_{max}$ (kW/cm^2)	1.9	3.6	11.0	8.8	17.5	75
Av. Energy Flux $\bar{q}_{rad}$ (kW/cm^2)	1.19	2.31	7.16	5.11	9.95	43.1
% Power Loss	20	11	4.5	10	5.8	3.5

in the dissociated and ionized state. We have therefore made calculations including these properties, which play an important role in determining the heating, since the temperature variation, and therefore the property variation, across the boundary layer is so large.

A simple set of boundary layer equations is obtained in the standard way by transforming from the wall - oriented coordinates s, y along and normal to the wall to the similarity coordinates ξ, η. This transformation is given in terms of velocity u_e, viscosity μ_e, and density ρ_e at the edge of the boundary layer by

$$\xi(s) = \int_0^s \rho_e \mu_e u_e \, ds, \quad \eta(s,y) = \frac{\rho_e u_e}{\sqrt{2\xi}} \int_0^y \frac{\rho}{\rho_e} \, dy \tag{8.4}$$

The dependent variables velocity u and total enthalpy H are written in normalized form as

$$u/u_e = f_\eta \ , \quad H/H_e = g \tag{8.5}$$

where the subscript η denotes differentiation with respect to η. The boundary layer momentum and total enthalpy equations are transformed using (8.4) and (8.5). The "local similarity" assumption is that f and g depend only on η; the equations are then

$$(C f_{\eta\eta})_\eta + f f_{\eta\eta} + \beta^* \left(\frac{\rho_e}{\rho} - f_\eta^2 \right) = 0 \tag{8.6a}$$

$$\left(\frac{C g_\eta}{Pr} \right)_\eta + f g_\eta + \frac{u_e^2}{H_e} \frac{\partial}{\partial \eta} \left[C \left(1 - \frac{1}{Pr} \right) f_\eta f_{\eta\eta} \right] = 0 \tag{8.6b}$$

where we have defined

$$Pr = c_p \mu / k \ , \quad C = \rho\mu / \rho_e u_e \ , \quad \beta^* = 2 d \ln u_e / d \ln \xi \tag{8.7}$$

and k denotes the thermal conductivity, μ the viscosity.

The hypothesis of "local similarity" has enabled us to convert the partial differential equations of momentum conservation parallel to the wall,

and energy conservation, into ordinary differential equations in the variable η. The variable ξ, which depends only on distance along the wall, s, by (8.4), appears as a parameter in u_e and in β^*, which involves the derivative of u_e with respect to ξ. The gas property functions Pr, C and ρ_e/ρ depend only on the state of the gas, so are functions of p and T (or p and enthalpy $h = H - u_e^2 f_\eta^2/2$) and so can be written as functions of g at each value of $\xi(s)$. Thus, when the properties external to the boundary layer are specified as functions of s, Eq. (8.6) can be integrated to find $f(\eta)$, $g(\eta)$.

Two further simplifications are useful. Since u_e^2/H_e is small, and Pr is near unity for hydrogen over the range of interest, we will put Pr = 1 in (8.6b). Further, the third term in (8.6a), the pressure gradient term, is small so we will approximate ρ_e/ρ by h/h_e. When this is expressed in terms of g, a new pressure gradient parameter β appears,

$$\beta = \frac{H_e}{h_e}\beta^* = 2\,\frac{H_e}{h_e}\,\frac{d\ln u_e}{d\ln \xi} \tag{8.8}$$

Now the boundary layer equations are

$$(C f_{\eta\eta})_\eta + f f_{\eta\eta} + \beta\,(g - f_\eta^2) = 0 \tag{8.9a}$$

$$(C g_\eta)_\eta + f g_\eta = 0 \tag{8.9b}$$

The boundary conditions are no slip at the wall, a given wall enthalpy h_w based on the wall temperature T_w, and approach to the external conditions at large η:

$$f_\eta(0) = 0, \quad g(0) = h_w/H_e = g_w, \quad f_\eta(\infty) = g(\infty) = 1 \tag{8.10a}$$

For the case where there is no flow through the wall, we have the fifth condition that the normal velocity is zero there, which is given by

$$f(0) = 0 \tag{8.10b}$$

When the external conditions ρ_e, μ_e, u_e are given from the core streamtube solutions, and the ρ and μ are defined in terms of h, then (8.9) and (8.10) can be integrated. The $\rho(h)$ function was found from the equilibrium properties for hydrogen given in Ref. 33, as was the function h(T). The viscosity was found from Ref. 32 as a function of T and p, completing the necessary information. The integration was performed by the method of quasi-linearization.

The results of the integration for $T_e = 14,000$K $p = 3$ atm, are shown in Fig. 8.3 as plots of the shear and heat transfer parameters $f_{\eta\eta}(0)$ and $g_\eta(0)$ against the pressure gradient parameter β, for various values of g_w. These are related to the shear stress τ_w and heat flux q_w by

$$\tau_w = \frac{\rho_w \mu_w u_e^2}{\sqrt{2\xi}} f_{\eta\eta}(0) \qquad q_w = \frac{\rho_w \mu_w u_e H_e}{\sqrt{2\xi\,Pr}} g_\eta(0) \qquad (8.11)$$

In addition to the solid curves for equilibrium hydrogen properties, the dashed curves show the results of assuming that the $\rho\mu$ product does not vary across the layer, i e., C = 1. For the small values of wall to external enthalpy ratio g_w in which we are interested ($g_w \approx 0.02$ for $T_w = 1,300$ K, the melting point of copper) it is very important to consider the variation of C. This is not surprising, since for 3 atm, $T_e = 14,000$K, $T_w = 1,300$K, C varies from unity (by definition) at the outer edge of the boundary layer, to 7.4 at the wall. Another notable feature is the very slight dependence of $g_\eta(0)$ on pressure gradient parameter β, especially for $g_w \sim 0.02$.

Based on calculations like those shown in Fig. 8.3, and the use of Eq. (8.11), the heat transfer distribution along a 1,300K wall in contact with the plasma core was calculated for the 3 atm, 10 kW case. Because conditions in the core for the 100 kW and 5000 kW cases are only slightly different, the resulting heating rate is also a good estimate for these two cases at 3 atm. The distribution of q_w is shown in Fig. 8.4, and gives fluxes from 10 kW/cm^2 to a peak of 34 kW/cm^2 near the throat. If these values are integrated over the surface, the total convective heat loss rate is found from

$$Q_c = \int_0^{x_{th}} 2\pi R\, q_w\, dx \qquad (8.12)$$

The values that result for the 10 kW, 100 kW and 5000 kW cases (each of which have a different radial size), for integration from x = 1.5 to x_{th}, are 17, 53 and 374 kW respectively.

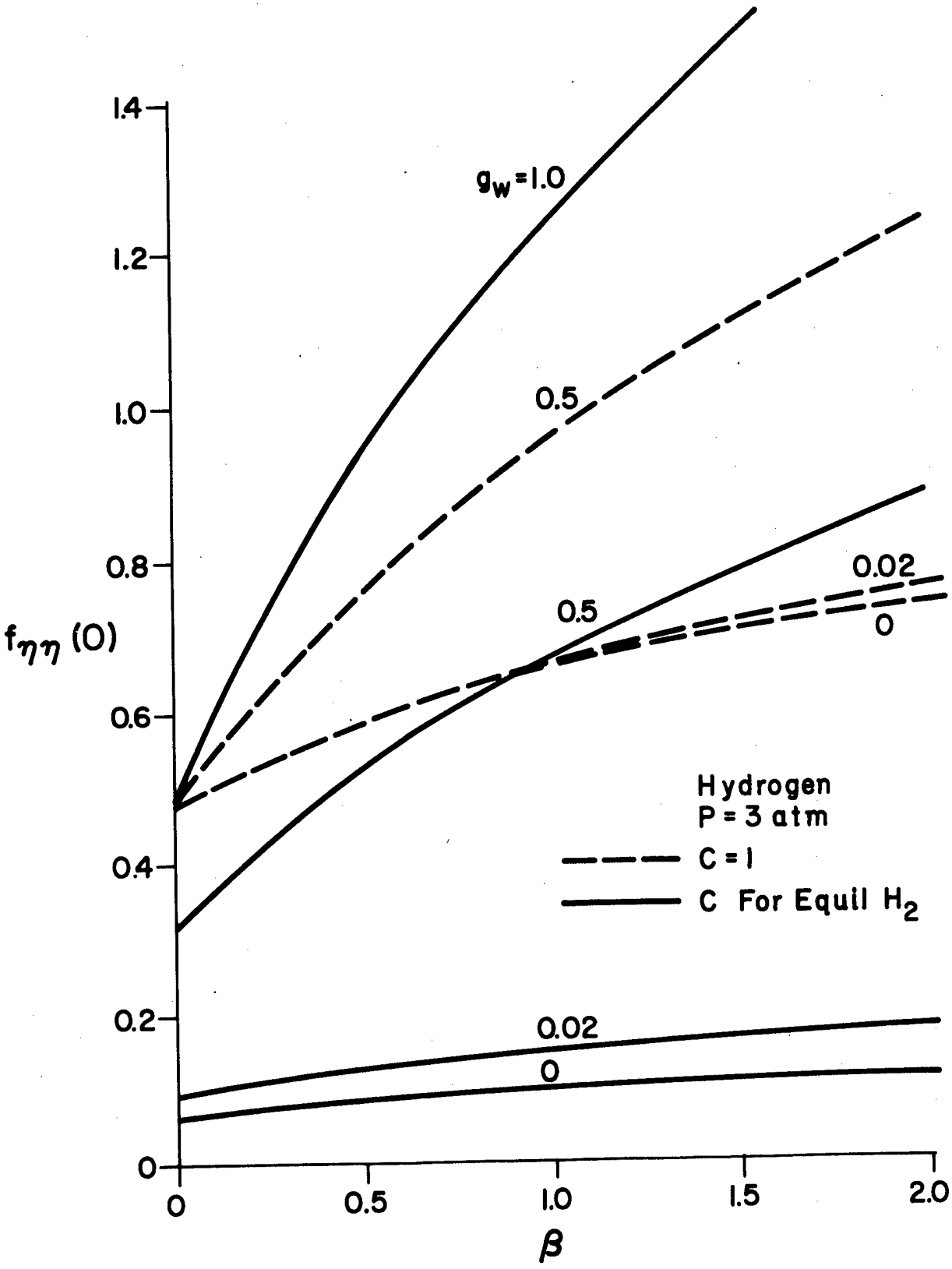

Fig. 8.3a Shear Parameter for Hydrogen Boundary Layer

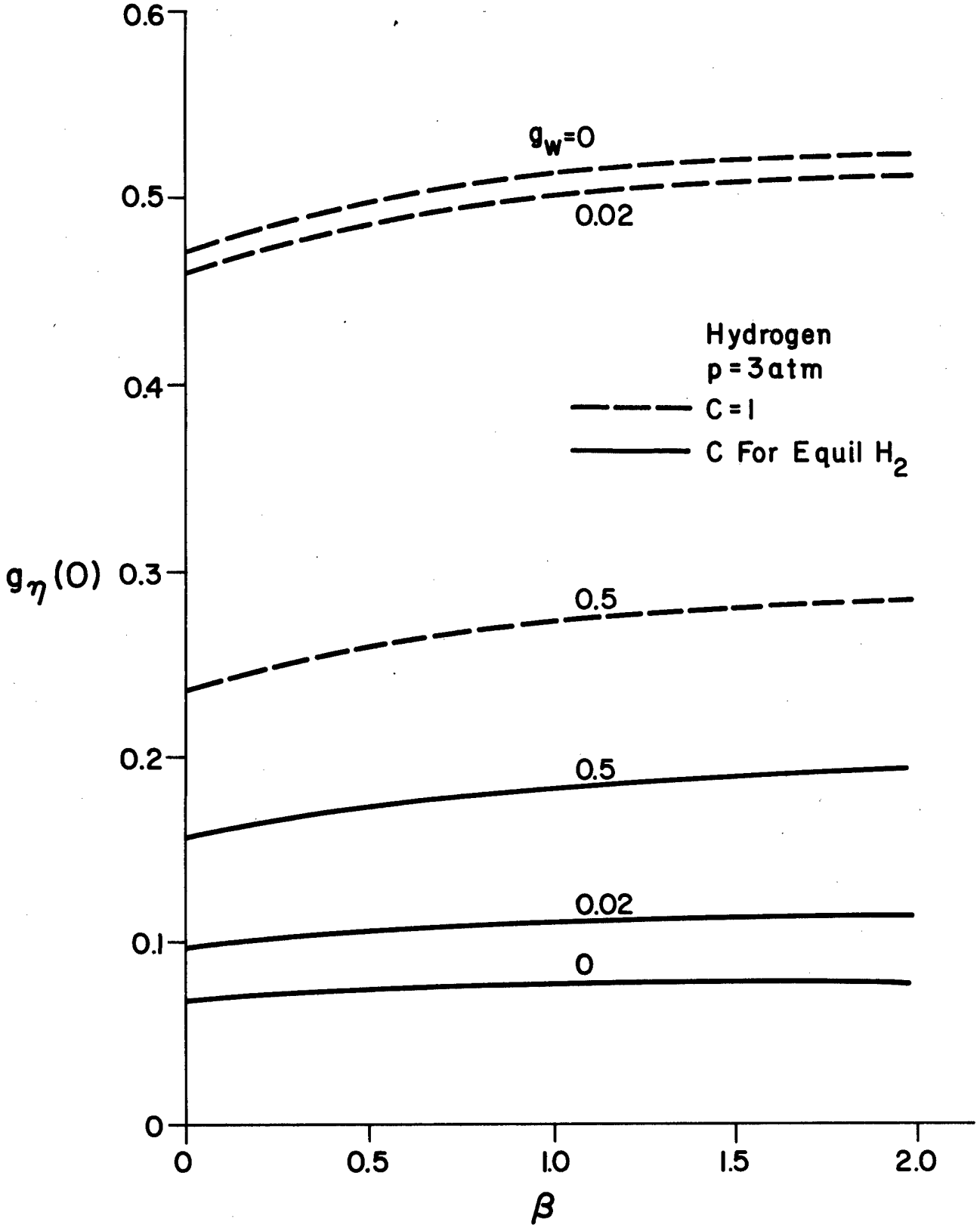

Fig. 8.3b Heat Transfer Parameter for Hydrogen Boundary Layer

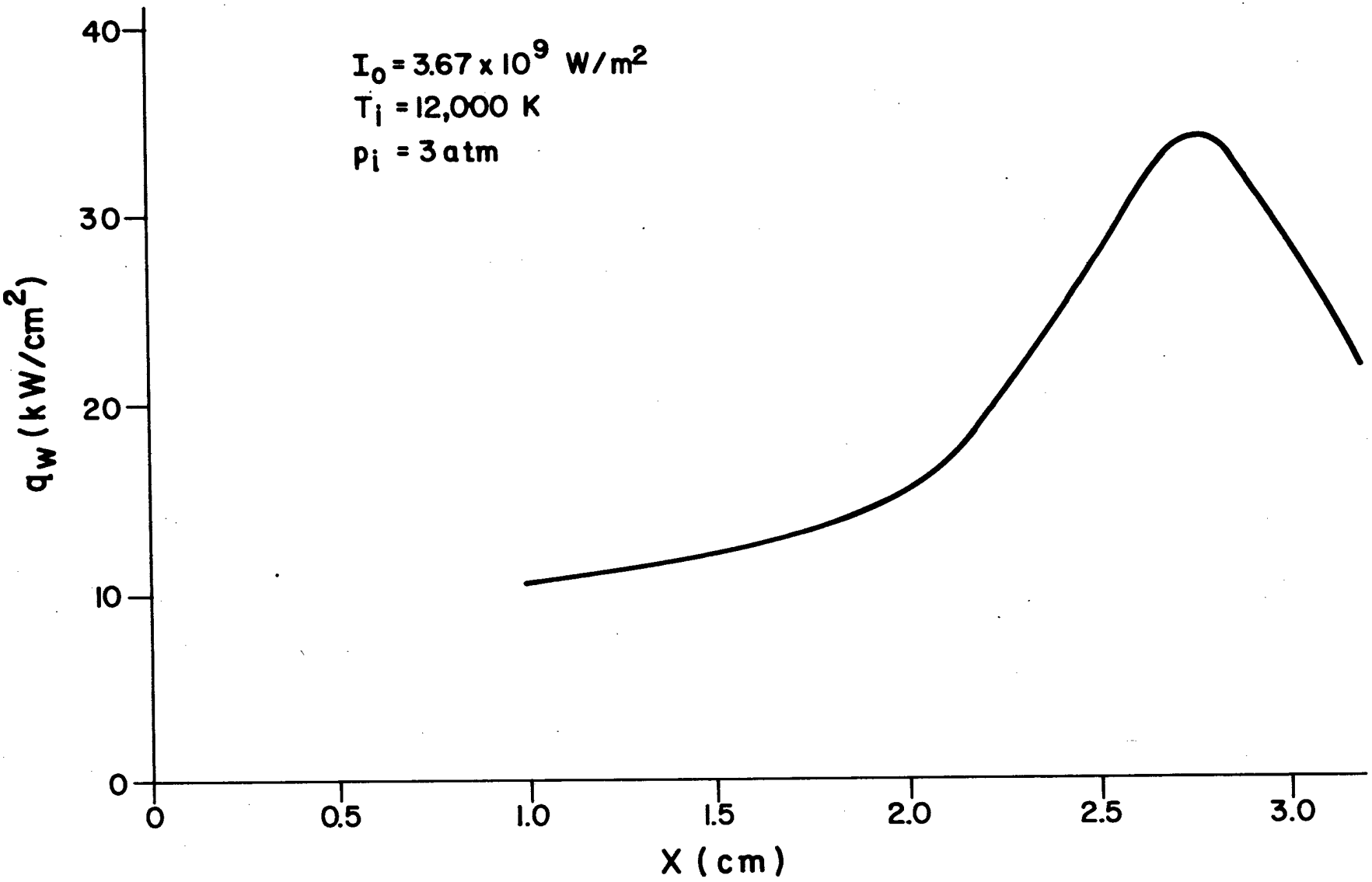

Fig. 8.4 Heat Flux Distribution from Hydrogen Boundary Layer of Laser-Heated Streamtube

It is immediately evident that this uncoupled calculation produce unrealistic results for both the 10 kW and 100 kW cases, since the calculated heat loss rate is a large fraction of the total power. Such a loss rate would decrease the core temperature, which in turn would decrease the loss. For the low power cases, then, the convective loss must be coupled to the core calculation for a realistic model of the fluid mechanics. For the 500 kW case, however, the loss calculated is only 7.5% of the laser power, which is probably not a large enough loss to require coupling to the core. For this case, the heating distribution shown in Fig. 8.4 is probably realistic. This certainly indicates the need for some protection of the rocket walls, since rates of 30 kW/cm^2 cannot be handled by simple means. However, the larger rates do occur near the throat, where the streamtube is of small radius, so the area to be protected is not large. The throat radius for the 3 atm, 5000 kW case is about 1 cm.

Realistic heat fluxes for the lower power engines can only be determined by a coupled calculation of the core and boundary layer, which was not undertaken under the present contract.

The boundary layers for the 10 atm cases were not calculated, but for laminar heating, the heat fluxes should scale like the square root of pressure, increasing them by a factor of about 2. But the areas of the streamtube surface are nearly 10 times smaller because of the short length, so the values of Q_c should be about one fifth of those for 3 atm. This means the coupled calculation is still necessary for the 10 kW case at 10 atm, might not be necessary for the 100 kW case, and of course is not necessary for the 5000 kW case. The heat protection of the walls will be even more important though, since q_w is higher by a factor of 2.

One method of heat protection is the injection of cold gas normal to the wall, which alters the temperature profile and blocks some of the heat. Some sample calculations have been made to illustrate the effect of this method of reducing the heat flux. The only change in the calculation is the introduction of a non-zero value of f (0) to replace the boundary condition (8.10b), because now the mass flux through the wall is not zero, but is related to f (0) by

$$(\rho v)_w = -\rho_w \mu_w f(0) / \sqrt{2\xi} \qquad (8.13)$$

This introduces another parameter into the equations, f (0). The results of two calculations, at stations x = 1 and x = 2.7, are given in Fig. 8.5 as curves of g_η (0) against f (0). The left end of these curves is the zero injection or solid wall case f (0) = 0. It can be seen that the heat transfer

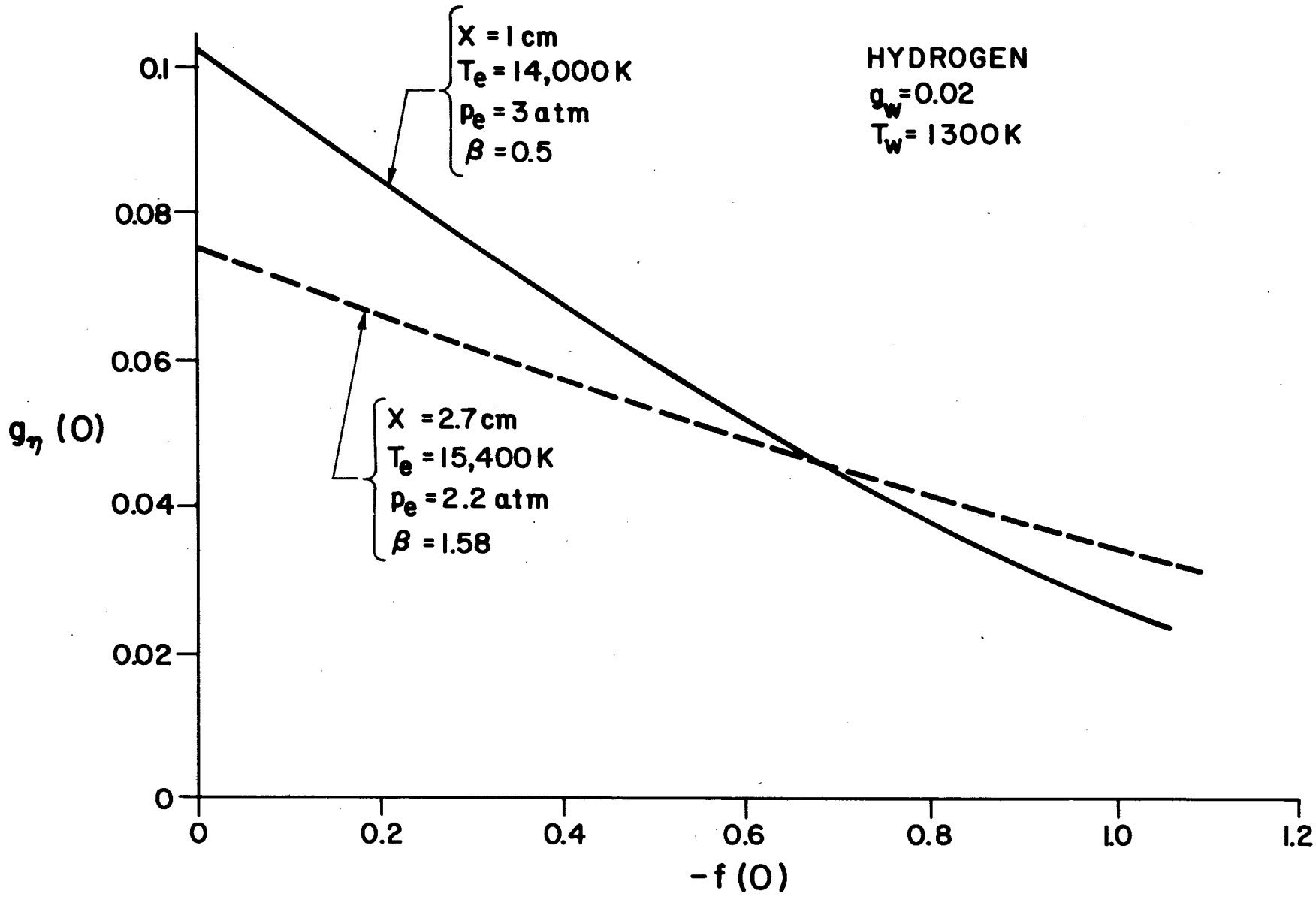

Fig. 8.5 Effect of Normal Hydrogen Injection on Heat Transfer Parameter for Hydrogen Boundary Layer

parameter g_η (0) drops sharply as f (0) decreases, which means the injection velocity increases by (8.13). If we look at injection with f (0) = - 1, g_η (0) at x = 1 is reduced by a factor of 4, leading to a heat flux of about 2.5 kW/cm^2 for an injection rate of 0.014 gm/cm^2-s, from (8.13). At x = 2.7, g_η (0) is reduced by a factor of 2, yielding 17 kW/cm^2 with an injection rate of 0.017 g/cm^2-s.

To see the magnitude of this rate of injection, one may compare it to the mass flow in the core, which is 0.3316 g/cm^2-s over the initial area. Thus for the 10 kW case, the core mass flow is 9.0 E-3 g/s, while an injection of 0.015 g/cm^2-s over the surface area of the streamtube up to the throat is 22 E-3 g/s, more than twice the core mass flow. On the other hand, for the 5000 kW case, the core mass flow is 500 times larger, 4.5 g/s, while the area is only $\sqrt{500}$ = 22 times larger, so the injected mass would be about 0.49 g/s, or only 11% of the core mass flow. The surface to volume effect favors injection in the large engines, and it appears to be one possibility for reducing the wall heat load by a factor of 2 or more. Notice also, that large reductions in heat flux are only needed in the limited regions of high heating, not over the whole streamtube surface, so injection is not needed over the whole nozzle surface, which reduces the mass which must be injected.

The purpose of the present calculation was to show how much heating reduction can be achieved by mass injection. Considerable additional calculation would be needed for an engineering analysis of the proper amount and distribution of injection for efficient heat protection.

8.4 ABSORPTION BY PARTICLES IN BUFFER GAS

It appears that for specific device configurations the radiation escaping from the plasma will be of sufficiently high intensity that some sort of shielding mechanism will be required in order to maintain wall integrity. One possibility would be to introduce small carbon particles into a buffer gas flowing around the plasma. In this event the carbon particles would intercept the plasma radiation, heat up and conduct heat energy to the surrounding buffer gas. These particles would also radiate with an intensity corresponding to their own characteristic temperature and could further reach vaporization temperatures depending on the particle flow time and their radiative flux loading.

In the following analysis first order estimates are provided for the particle mass loading required to protect the walls against plasma radiation. The particles are assumed to have constant absorption properties, velocities and size. An understanding of the phenomenology of the

plasma/particle/buffer gas interaction, including the all-important question of particle survival, will require a significantly more sophisticated analysis of the mixing region between the plasma and buffer gas flows. When such an analysis is performed the required particle mass loadings can be more accurately defined.

Small carbon particles, of the order of 1 μm, are very efficient absorbers of radiation in the visible and near infrared wavelength regions, approximately acting as black-body absorbers. A large fraction of the hydrogen plasma radiation will unfortunately originate in the far UV where little is known about the absorptive properties of carbon. In the following analysis it will be assumed that the carbon particles absorb as black bodies at all wavelengths.

The configuration considered is a cylindrical plasma of radius r_1 surrounded by a particle seeded buffer flow of thickness Δr. The particles are taken to be spherical with radius R_p and to have a constant number density n_p in the buffer flow. Each particle has an absorption cross section of πR_p^2 and thus the optical depth, τ, across the buffer layer is defined by

$$\tau = n_p \pi R_p^2 \Delta r \tag{8.14}$$

An optical depth of 3 is sufficient to absorb 95% of the plasma radiation and this condition is met when the particle number density is given by

$$n_p = \frac{3}{\pi R_p^2 \Delta r} \sim \frac{1}{R_p^2 \Delta t} \tag{8.15}$$

It is perhaps more interesting to examine this quantity in terms of the total mass/cc of particles in the buffer flow, M_p,

$$M_p = n_p \rho_p (4/3) \pi R_p^3 \tag{8.16}$$

where ρ_p is the specific density of carbon which is ~2 gm/cc. Combining Eq. (8.15) and (8.16) results in

$$M_p = 4 \rho_p \frac{R_p}{\Delta r} \sim 8 \frac{R_p}{\Delta r} \tag{8.17}$$

Equation (8.17) can readily be extended to deduce the mass flow of particles required to absorb the plasma radiation.

$$\dot{M}_p = M_p u_b A_b \tag{8.18}$$

where

$$A_b = \pi (2 r_1 \Delta r + (\Delta r)^2) \tag{8.19}$$

and u_b is the buffer flow velocity. Since it is desirable to maintain a configuration such that $\Delta r / r_1 \ll 1$, the approximation

$$A_b \approx 2 \pi r_1 \Delta r \tag{8.20}$$

is made. Combining Eq. (8.17), (8.18) and (8.20) results in

$$\dot{M}_p = 8 \pi \rho_p u_b R_p r_1 \approx 48 u_b R_p r_1 \tag{8.21}$$

It can be seen from Eq. (8.21) that as long as $\Delta r \ll r_1$, the particle mass flow required to absorb the plasma radiation is independent of the buffer flow thickness and linearly proportional to both the particle and plasma radii. In the interest of optimizing thrust one wishes to minimize the buffer flow; hence, it is clear that the smallest particle size consistent with the assumption of blackbody absorption should be used.

Another interesting feature is that since the required buffer flow is linearly proportional to plasma radius, the ratio of buffer flow to plasma flow is size dependent; i.e.

$$\frac{\dot{M}_p}{\dot{M}_{pl}} = \frac{8 \rho_p R_p u_b}{\rho_{pl} r_1 u_{pl}} \tag{8.22}$$

where u_{pl} is the plasma flow velocity. For example, for a 14,000°K hydrogen plasma at a pressure of 3 atm.

$$\frac{\dot{M}_p}{\dot{M}_{pl}} \sim 10^7 \frac{R_p u_b}{r_1 u_{pl}} \tag{8.23}$$

Note that relationship (8.23) implies that for small devices, i.e. $r_1 \lesssim 1$ cm, the buffer mass loading would of necessity be orders of magnitude larger than that of the plasma for reasonable particle sizes unless $u_b \ll u_{pl}$. Thus these preliminary numbers suggest that particulate absorption may not represent a viable technique for wall protection in the flowing plasma configuration. Note that even if the buffer flow had a velocity two orders of magnitude lower than the plasma, a condition difficult to maintain along the flow length, there may still be an unacceptable constraint on particle size.

Although the analysis presented above is admittedly crude it would suggest that particle shielding would provide too large a weight penalty for proposed operating conditions. A more detailed analysis would be required to confirm this. Furthermore the possibility of operating under different conditions, for instance at higher plasma pressures, should also be considered.

9. PERFORMANCE OF FLOWING CORE ROCKET

The performance of the flowing-core laser-heated rocket is affected by many more variables than the ones considered in this report. Most of the effort reported here has dealt with the fluid mechanics, laser radiation absorption and plasma emission of the flowing core, and the convective heat transfer from the core streamtube. Based on this work, only the performance obtained from the core streamtube can be obtained, that is, the thrust and specific impulse of the core gas when it is expanded to some exit condition. The resulting values will be high estimates because no losses past the throat are considered, nor has the convective heating loss been properly coupled to the core streamtube for the lower power levels as yet. On the other hand, added thrust which might be supplied by a buffer gas layer used for heat protection is not included either. With the understanding of the partial nature of the performance which can be calculated here, we can describe the method for the calculations.

We begin at the throat of the streamtube with the enthalpy h_{th} and velocity u_{th} found from the program described in the section on the Flowing Core Streamtube. The flow is then expanded isentropically to a specified exhaust pressure p_{ex} by linear interpolation in hydrogen property tables in Ref. 33. This provides the exhaust conditions of enthalpy and temperature h_{ex}, T_{ex}. Conservation of total enthalpy during the expansion (no losses) then provides the exhaust velocity as

$$u_{ex} = \left[2 (h_{th} - h_{ex}) + u_{th}^2 \right]^{1/2} \tag{9.1}$$

The thrust is then

$$Th = (p_{ex} - p_{am}) A_{ex} + \dot{m} u_{ex}$$

where p_{am} is the ambient pressure. We will give the so-called ideal thrust, for which $p_{ex} = p_{am}$, so that

$$Th = \dot{m} u_{ex}, \quad I_{sp} = u_{ex}/g \tag{9.2}$$

give the thrust and specific impulse, where g is the acceleration of gravity.

The conditions at the throat, as calculated by the core streamtube program, the mass flow rate from Table 7.2 and the entropy s from Ref. 33 are given in Table 9.1. The exhaust conditions, I_{sp} and Th for p_{ex} = 1 atm, as found from Ref. 33, and Eqs. (9.1) and (9.2) are given in Table 9.2. The maximum thrust is obtained by expanding to $p_{ex} = 0$, since all energy is then converted into velocity, h_{ex} being zero. This limiting case is given in Table 9.3, as obtained from Eqs. (9.1) and (9.2) by setting $h_{ex} = 0$.

Table 9.2 shows that the expansion to 1 atm of the 3 atm cases is really a very small expansion, since the throat is at about 1.7 atm. Therefore, the gas in the exhaust is still very hot (near 13,000 K) and its enthalpy is only a few percent less than at the throat. It is this few percent which is converted to additional velocity, so the increase from the throat velocity to the exhaust velocity is also only a few percent. However, this velocity is sufficient to produce I_{sp} in the range of 1400 to 1500 s. Because of the small mass flow rate, the thrust is in the range 0.1 to 66 N (0.03 to 15 lbs.).

The 10 atm cases have a greater expansion ratio, since the throat is at 5.6 to 5.8 atm, so they have a greater conversion of enthalpy to velocity, exhausting somewhat cooler gas, at speeds nearly double the throat speed. They then produce higher values of I_{sp}, in the range 2400 to 2500 s, and somewhat larger thrusts, 0.2 to 100 N (0.05 to 25 lbs.).

For the maximum possible expansion, in Table 9.3, we see much less difference between the 3 atm and 10 atm cases, since the expansion ratio is infinite for both. They all yield I_{sp} in the range 3000 to 3300 s. In fact, the 100 and 5000 kW cases have nearly the same at I_{sp} at both pressures. Only the highest percent loss case, 10 kW, has noticeable difference in I_{sp} with pressure. The thrusts for the vacuum exhaust cases are also higher than the atmospheric exhaust cases since thrust is proportional to u_{ex}.

Even though a number of loss mechanisms were omitted from this calculation, and they will reduce the performance calculated here, it seems quite clear that values of I_{sp} above 1000 s can be obtained, even over a 3 atm to 1 atm expansion.

The thrusts produced may seem rather small, because of the very small mass flow rates. However, the Th/P ratio for the vacuum expansion core is in the range 20 to 30 mN/kW, which seems to be typical for electric propulsion schemes, to which the laser-heated rocket is the most comparable. Of course, the laser-heated rocket does not have to carry its own power supply, so its weight for a given mission should be smaller than an electric propulsion engine.

TABLE 9.1

THROAT CONDITIONS

P(kW)	p_o (atm)	h_{th}(J/kg)	p_{th}(N/m^2)	T_{th}(K)	s_{th}(J/kgK)	u_{th}(m/s)	$\dot{m}$(kg/m^2-s)
10	3	7.99E8	1.73E5	13490	2.1721E5	1.25E4	9.02E-4
5000	3	9.63E8	1.71E5	14280	2.2940E5	1.33E4	4.51E-1
100	3	8.97E8	1.73E5	13990	2.2456E5	1.29E4	9.02E-3
10	10	8.99E8	5.67E5	14970	2.0900E5	1.34E4	9.02E-4
100	10	9.46E8	5.77E5	15240	2.1485E5	1.34E4	9.02E-3
5000	10	9.73E8	5.82E5	15380	2.1646E5	1.34E4	4.51E-1

TABLE 9.2

PERFORMANCE FOR p_{ex} = 1 atm

P(kW)	p_o (atm)	h_{ex}(J/kg)	T_{ex}(K)	u_{ex}(m/s)	I_{sp}(s)	Th(N)	Th(lb)
10	3	7.79E8	13000	1.38E4	1410	0.124	0.0279
5000	3	9.40E8	13760	1.47E4	1500	66.4	14.9
100	3	8.74E8	13470	1.44E4	1470	1.30	0.292
10	10	6.73E8	12350	2.48E4	2530	0.224	0.0504
100	10	7.47E8	12800	2.37E4	2420	2.14	.482
5000	10	7.67E8	12930	2.40E4	2450	108.	24.3

TABLE 9.3

PERFORMANCE FOR $p_{ex} = 0$ (VACUUM)

P(kW)	p_o (atm)	u_{ex}(m/s)	I_{sp}(s)	Th(N)	Th(lb)
10	3	2.96E4	3020	0.266	0.0599
5000	3	3.24E4	3300	146.	32.5
100	3	3.13E4	3190	2.82	0.634
10	10	3.14E4	3200	0.283	0.0637
100	10	3.22E4	3280	2.90	0.652
5000	10	3.26E4	3330	147.	33.1

10. STATIONARY CORE ENGINE

10.1 INTRODUCTION

An alternative to the flowing plasma core type of rocket is one borrowed from the concept of a gas-core nuclear rocket. In that type of device a gaseous core of fissionable material is maintained in a stationary region in the center of the rocket while fissioning at high temperatures. It is surrounded by a flowing propellant gas which confines the reacting core, and is heated by thermal radiation and convective processes. The nuclear fuel burns above 100,000K, and it must be kept at least at atmospheric density to maintain criticality, so it operates at a core pressure of several hundred atmospheres.

An analogous laser-heated rocket would have a stationary plasma core, which absorbs the laser radiation and is thereby maintained at high temperature. In turn, this core re-radiates the absorbed laser energy to the surrounding propellant gas, which serves to confine the core and produce thrust, just as in the gas-core nuclear rocket. This concept may be compared with both the gas-core nuclear rocket and the flowing core laser-heated rocket.

Compared to the former, there is no criticality requirement imposed on the core. However, laser energy absorption, which is the mechanism for putting energy into the rocket, is dependent on the core density. The more dense the core, the better it absorbs, and the shorter it can be in the direction of the laser beam. But there is more freedom in the range of densities, and therefore pressures, in the core for the laser-heated case than for the gas-core case. Another difference is in the amount of core plasma which can be allowed to flow out the rocket nozzle. For nuclear rockets, one would like to have as little core material as possible entrained by the propellant gas and carried out the nozzle, since it represents a loss of energy of fission as well as of radio-active material. In the laser rocket, "detrainment" of core material is not so serious, although it does represent a loss of propulsive efficiency, since it will leave the rocket at rather high temperatures thus wasting energy. However, if we let too large a fraction of the core flow out with the propellant gas, we are back to the flowing core concept. Preventing this detainment is not so easy in the laser rocket, since the core may not be of high density relative to the propellant gas, as in the nuclear core.

Compared to the flowing-core laser-heated rocket, there are several new physical mechanisms which enter. One is the detrainment problem referred to above, which acts against the confinement of the core. The densities of the core and propellant may be nearly equal, which makes confinement difficult. Further, the heating of the propellant and its subsequent density decrease occur while it is flowing past the core, making detrainment easier as it flows. A second important mechanism is the efficient emission of radiation by the core, and its efficient absorption by the cooler propellant gas. In the flowong-core scheme, emission by the core is to be minimized as a loss of energy from the primary propellant, while in the stationary-core this emission is the main process by which energy is input to the propellant. Likewise, absorption by the propellant gas is now a primary source of propulsion rather than a necessary heat protection device, as in the flowing-core rocket. In fact, one of the main complications of the stationary-core rocket is in the control of the flowing propellant gas. This is achieved primarily by control of the flow area transverse to its direction of motion, i.e., the cross-section area of the propellant gas streamtube. The same is true, of course, in the flowing-core case; its flow properties are largely controlled by the cross-sectional area. But there is one crucial difference. In the flowing-core case, the propellant gas absorbs energy from a laser beam propagating in the axial direction, so its absorption properties depend on its axial size. Thus the control of flow and absorption depend largely on two independent geometrical parameters, the cross-section and the axial length. However, in the stationary-core rocket, the propellant gas absorbs its radiant energy mainly from emission in the transverse direction, the same direction which controls the flow. This means that flow control will be intimately connected with absorption, and the propellant gas flow area must be designed with regard for both the axial pressure, velocity and density distributions and for the gas depth for efficient absorption.

It appears, then, that the analysis of the stationary-core rocket is considerably more complex than that of the flowing-core rocket, with increased emphasis on plasma emission and subsequent absorption, and a more complicated interaction between flow and radiation.

10.2 ORDER OF MAGNITUDE ANALYSIS

The quantitative evaluation of a stationary-core rocket can be started by using some simple relations among the geometric and physical parameters which serve to indicate the physics which goes into such an analysis, as well as obtain some order-of-magnitude estimates of the parameters.

Taking a cylindrical core of radius R_c and length L, the laser power P and intensity I are related by

$$P = \pi R_c^2 I \tag{10.1}$$

The absorption of laser energy occurs with absorption coefficient k_L, a function of temperature T. The volume emission by the plasma, P_c, also depends on T. In steady state the plasma must emit the full power P, so that

$$P = \pi R_c^2 L P_c \tag{10.2}$$

Equations (10.1) and (10.2) give

$$L = I/P_c \tag{10.3}$$

The absorption and emission in the core are related by the steady state requirement that the absorption $k_L I$ equals the emission P_c:

$$k_L I = P_c \tag{10.4}$$

Equations (10.4) and (10.3) show that with these estimates, the core length L is equal to the absorption coefficient k_L.

Of the emitted radiation per unit volume P_c some portion $P_c^* < P_c$ will be absorbed by the propellant gas, depending on the depth of this gas, and its absorption coefficient k_P. If $\dot{m}_P$ is the mass flow rate of the propellant gas, the energy per unit mass added is $\pi R_c^2 P_c^*/\dot{m}_P$. If its initial enthalpy is h_i, then its heated total enthalpy is

$$H_h = h_i + u_i^2/2 + \pi R_c^2 L P_c^*/\dot{m}_P \tag{10.5}$$

This gas is then expanded at constant entropy to the chosen exhaust pressure, p_{ex}, yielding an exhaust enthalpy h_{ex}, and an exhaust velocity

$$u_{ex} = \sqrt{2 (H_h - h_{ex})} \tag{10.6}$$

and associated specific impulse $u_{ex}/g = I_{sp}$.

With these relations, estimates of the parameters of a rocket can be made. Suppose we give the power P, core temperature T_c, core pressure p_c, exhaust pressure p_{ex} and specific impulse desired, which defines u_{ex}. From T_c and the radiation properties of hydrogen we can find P_c and k_L. Then (10.4) gives I, (10.3) give L and (10.1) give R_c, so the core size is determined.

The mass flow rate of propellant $\dot{m}_P$ may now be found from u_{ex}. Equation (10.6) gives $H_h - h_{ex}$. If we assume u_h^2/s is a small contribution to this enthalpy difference, then we know the desired difference between the enthalpy of the propellant gas at the end of the heating zone, which we will take to be at constant pressure p_c, and its enthalpy at the exhaust pressure p_{ex}. These two states are connected by constant entropy. The conditions uniquely define both states, so the values of T_h, h_h, T_{ex}, h_{ex} can be found. Again assuming the velocity contribution to the total enthalpy is small, we take $h_h - h_i$ to be energy added to the gas. Now we estimate the volumetric absorption P_c^* as a fraction of the emission P_c. Then (10.5) yields the propellant mass flow as

$$\dot{m}_P = \pi R_c^2 \, L \, P_c^* / (h_h - h_i) \tag{10.7}$$

where the initial enthalpy is assumed known. The ideal thrust can also be found now as

$$Th = \dot{m}_P \, u_{ex} \tag{10.8}$$

To check the neglect of the velocity compared to the enthalpy during heating, and to estimate detainment effects, we need to define the area in which the propellant gas flows. This is in turn related to the absorption length of plasma radiation in the gas, and so depends on the detailed properties of the gas. If the radius of the outer edge of the propellant gas is R_p at any station, its velocity is

$$u_P = \dot{m}_P / \rho_P \, \pi \, (R_P^2 - R_c^2) \tag{10.9}$$

and ρ_P is known from the given gas state at the inlet, and the end of heating state, which was found above.

The detrainment occurs in the shear layer between the stationary core and the flowing propellant, where the two gases mix. If the thickness of the

mixing layer on the propellant gas side is δ, then the core gas mass flow there is

$$\dot{m}_c = 2\pi R_c \int_0^{\delta} \rho' u' \, dy \tag{10.10}$$

where ρ', u' are the density and velocity of the core gas in the mixing layer. By normalizing, this can be written

$$\dot{m}_c = 2\pi R_c \delta \rho_c u_P \int_0^1 \frac{\rho'}{\rho_c} \frac{u'}{u_P} \, d\left(\frac{y}{\delta}\right) \tag{10.11}$$

The factor in front gives the order of magnitude of the mass flow rate out of the core at any station, and the total core detrainment.

The thickness δ is determined by a balance between the diffusion of core gas into propellant gas and the convection of the propellant past the core. This can be estimated by combining the static diffusion length $\sqrt{Dt}$ with the time it takes for the propellant gas to flow past the core, $t = \int dx/u_P$. Here D is the diffusion coefficient of core gas into propellant gas. Thus at the end of the core

$$\delta = \left(D \int_0^L dx/u_P\right)^{1/2} \tag{10.12}$$

To evaluate the integral, we will use a linear increase of u_P from u_{Pi} to u_{Ph}, so

$$\delta = \left(\frac{DL}{u_{Ph} - u_{Pi}} \ln \frac{u_{Ph}}{u_{Pi}}\right)^{1/2} \tag{10.13}$$

Now the factor in front of the integral in Eq. (10.11) can be calculated as an estimate of detrainment.

10.3 NUMERICAL EXAMPLE

As an example of the use of these formulas for estimating the performance of a small stationary core engine we may take as a core:

$$P = 10 \text{ kW}, \quad p_i = p_c = 3 \text{ atm}, \quad T_c = 14,000 \text{ and } 18,000 \text{K}$$

$$p_{ex} = 1 \text{ atm}, \quad I_{sp} = 1000 \text{ s}$$

Then the core conditions are:

T_c (K)	14,000	18,000
p_c (kW/cm^3)	56.4	200
k_L (cm^{-1})	1	3
I (kW/cm^2)	56	67
R_c (cm)	.24	.22
L (cm)	1	.33
ρ_c (g/cm^3)	2.33 E-6	1.25 E-6
ρ_c^* (kW/cm^3)	29	90
$\pi R_c^2 L P_c^*$ (kW)	5.2	4.5

The emitted radiation which is assumed to be absorbed by the propellant gas, P_c^*, is that below 0.1 μm. The remaining energy is lost. This is a rough estimate based on our present knowledge of absorption by hydrogen, and ignores IR absorption.

Turning to the propellant gas, $I_{sp} = 1000$ s corresponds to $u_{ex} = 980$ E5 cm/s and a kinetic energy per unit mass of 4.8E7 J/kg. Hydrogen properties at $p_{ex} = 1$ atm then show that at $T_{ex} = 5000$ K, $h_{ex} = 0.93$ E8 J/kg at an entropy of $s_{ex} = 170$ J/kg K, which leads to $H_{ex} = 1.41$ e* J/kg. The corresponding point at $p_c = 3$ atm is at 7000K, $h_h = 1.43$ E8 J/kg, $s_h = 170$ J/kg K, $\rho_h = 5.3$ E-6 g/cm^3, which gives the state of the propellant gas after it is heated. Knowing the power to be absorbed to heat from $T_i = 300$K, $h_i = 2.10$ E8 J/kg, $P_i = 3$ atm to this state, we find the mass flow rate of propellant gas, $\dot{m}_p$, as 0.015 and 0.013 g/s for the two core temperatures.

To find the propellant gas speeds and core detrainment we must now make some assumption about absorption depths to absorb the UV radiation P_c^*. A reasonable estimate is 0.1 cm, leading to $R_P = R_c + 0.1$.

For this constant area flow of propellant gas, the value of $u_P \rho_P$ comes from Eq. (10.9), and since the density is known from the constant pressure and known temperatures T_i = 300 K, T_h = 7000 K, the velocities can be found, as can the constant factor in Eq. (10.11), using (10.13) for δ. The diffusion coefficient D is evaluated at T_h = 7000 K by scaling the value for H, H_2 diffusion in Reference 32 down to 3 atm.

T_c(K)	14,000	18,000
$\dot{m}_P$(g/s)	1.5E-2	1.3E-2
$\rho_P u_P$(g/cm^2 - s)	8.2E-2	7.7E-2
u_{Pi}(cm/s)	332	312
u_{Ph}(cm/s)	15.5E3	14.5E3
D(cm^2/s)	230	230
δ (cm)	0.23	0.14
$\dot{m}_c \sim 2\pi R_c \delta \rho_c u_{Ph}$(g/s)	1.2E-2	3.5E-3
Core Mass (g)	2.9E-7	6.3E-8
(Core mass)/$\dot{m}_c$(s)	2.4E-5	1.8E-5

The first observation from these results is that the kinetic energy in u_{Ph}, 1.1 E4 J/kg is small compared to h_h = 1.43 E8 J/kg, and so was indeed ignorable. The next observation is the tremendous acceleration of the propellant gas while being heated, although it does not reach the sonic speed, which is a_h = 9.5 E5 cm/s, but stays at very low Mach number. Finally, we see that the detrained core mass flow, by our estimate, could be comparable to the propellant mass flow. Further, it empties the core in a time of order 10^{-5} seconds. While this estimate of detrainment is quite crude, and may be on the high side since the diffusion coefficient was evaluated at T_h, still it shows that detrainment can be a big potential problem for the stationary-core concept.

This example calculation is meant to illustrate the sort of analysis necessary to define the properties of a stationary-core laser-heated rocket. Most of the uncertainty in the results comes from lack of detailed knowledge of the absorption processes in the propellant, and of

the core detrainment process. Both of these areas need further study if the stationary-core concept is to be pursued. With some more detailed models of these two processes available, parametric studies could be done at various values of T_c, p_c, P. There may well be preferred regions in which to operate such an engine, and parametric studies might uncover them.

11. CONCLUSIONS

Based on the studies of laser-heated rockets described in this report, as well as the knowledge gained in the previous study reported in Ref. 1, we can draw some conclusions about the feasibility and operation of these devices. We can also identify important areas where our knowledge is incomplete, and further research is needed to put the conclusions on a sound scientific basis.

1. The flowing core rocket starts with a laser supported combustion (LSC) wave. For a given laser power, the cross-sectional area of the rocket engine is inversely proportional to the laser intensity at which this wave operates. The temperature level of the plasma core and the mass flow rate through the engine are also determined by the LSC wave, so a knowledge of its properties are vital to the definition of the rocket. However, there is at present no theoretical or experimental information on such waves in hydrogen, and even in air they are not well-understood. The properties used here were estimates based on extrapolating a simple air theory to hydrogen. However, LSC wave properties in hydrogen represent the major uncertainty in the present study, and should be studied both experimentally and theoretically to increase confidence in the feasibility of laser-supported rockets using hydrogen.

2. Performance of the flowing-core streamtube as a rocket is good. Values of I_{sp} for expansion to 1 atm exhaust are 1500 to 2500 s while expansion to a vacuum leads to 3000 to 3300 s.

3. Only a limited number of calculations were made, using three laser powers at each of two pressures. The LSC wave properties and the core velocity distribution were not varied. To map out the region of usefulness of laser-heated rockets, more extensive parametric calculations are needed.

4. Breakdown of hydrogen to produce an electron density which is comparable to that of thermal ionization can be produced by either an electric arc discharge or by a focused laser beam. Whether this will actually initiate an LSC wave has not been determined, and probably needs to be verified by experimental investigation.

5. The radiation emission of hydrogen has been put into a form useful for fluid dynamic calculations. The black body portion of the emission depends crucially on the radial temperature profiles, and has not been included in the present one-dimensional calculations. Its inclusion would require some model for the radial-variation of temperature. It could be a significant effect, however, and should be investigated further.

6. Based on the transparent radiation emission, radiated energy loss is not a substantial fraction of the laser energy input, varying from 20% for smaller engines to 4% for larger ones. This conclusion is sensitive to the operating temperature of the plasma core, and could change if this temperature is even 1000 K higher than calculated here.

7. The energy flux radiated is sufficiently high to require some kind of active heat protection for the walls, ranging up to 75 kW/cm^2.

8. The convective energy losses calculated by assuming a hydrogen boundary layer at the edge of the plasma core, without coupling the loss to the core flow, are too high to be realistic for all but the 5000 kW laser power. A coupled calculation, not undertaken here, is needed for smaller power levels.

9. For the 5000 kW power, the convective heat losses are of the order of 30 kW/cm^2 near the throat, at 3 atm, and perhaps twice that for 10 atm, so they add significantly to the need for heat protection, though they only occur in a small region.

10. Normal injection of hydrogen into the core streamtube seems to be a useful way of reducing the convective heat losses, based on a few sample calculations. Further calculations are needed to establish this as a practical method of heat protection. Tangential injection was not studied, but should also be investigated for heat protection.

11. First estimates indicate that particle absorption does not seem a useful way to protect the walls from radiation, because of the high mass loading of particles required. This subject needs further study.

12. The length of the plasma core, up to the throat, is controlled by the inverse Bremsstrahlung absorption coefficient. Larger absorption, caused by larger pressures, leads to shorter lengths. At 3 atm, this length is 4 cm, while at 10 atm it is 0.5 cm. These short lengths at the high pressure lead to short, stubby streamtube shapes, which may be undesirable from a fluid-dynamical point of view, especially for larger

powers. This imposes a limitation on how high a pressure level can be used for operation.

13. The stationary-core rocket engine concept was studied qualitatively and semi-quantitatively. The physical processes involved in this concept are more complex than those of the flowing-core concept. Two major uncertainties were uncovered. One is a lack of knowledge of absorption lengths for high temperature hydrogen radiation in low temperature hydrogen. The other was a lack of knowledge of how the flowing propellant gas entrains core gas. Further study of these two areas would enable estimates of stationary-core rocket performance to be made with more confidence.

REFERENCES

1. Caledonia, G. E., Wu, P.K.S. and Pirri, A.N. "Radiant Energy Absorption Studies for Laser Propulsion", NASA CR-134809 (PSI TR-20), Physical Sciences Inc., Wakefield, Mass. March 1975.

2. Fowler, M.D., Smith, D. C., Brown, C.O. and Radley Jr., R.J., 'Laser Supported Absorption Waves", N921716-9, United Aircraft Research Laboratories, East Hartford, Conn., March 1974.

3. Cobine, J.D., "Gaseous Conductors", Dover Publications, New York, 1958.

4. Patch, R. W., AIAA Journal 9, 2298 (1971).

5. Hill, R.D., J. Applied Physics 46, 2910 (1975).

6. Mandelstam, S. L., Spectrochem. Acta 11, 245 (1956).

7. Tholl, H., Z. fur Naturforschung 25 a, 420 (1970).

8. Zel'dovich, Ya. B. and Raizer, Yu. P., "Physics of Shock Waves and High Temperature Hydrodynamic Phenomena", Vol. I, Academic Press, New York, 1966, p 342.

9. Ref. 8, p. 340.

10. Brown, S. C., "Basic Data of Plasma Physics, 1966", The M.I.T. Press, Cambridge, Mass., 1967.

11. Engelhardt, A.G., and Phelps, A. V., Phys. Rev. 131, 2115 (1963). This is one of the standard reference for collision cross sections. We used its values of ν_{in}, ν_i and ν_m. However the values of ϵ versus E/n_M are too high at high energies.

12. Huxley, L.G.H. and Crompton, R. W., "The Diffusion and Drift of Electrons in Gases", J. Wiley and Sons, New York, 1974. This book contains more recent values of ϵ versus E/n than Ref. 11, as well as Dn.

13. Brown, S. C., "Breakdown in Gases: Alternating and High Frequency Fields" in Encyclopedia of Physics, Vol. 22, ed. S. Flügge, Springer-Verlag, Berlin, 1956, p. 534.

14. Smith, D. C., et al., "Investigation of Gas Breakdown with 10.6 μm Wavelength Radiation", AFWL-TR-72-182, Air Force Weapons Laboratory, February 1973.

15. Lencioni, D. E., et al., "The Effect of Dust on 10.6 μm Laser Induced Air Breakdown", LTP-20, MIT Lincoln Laboratory, Lexington, MA., April 1973.

16. Schlier, R.E., et al., "Air Breakdown Studies", AFWL-TR-72-74, Air Force Weapons Laboratory, February 1973.

17. Lencioni, D. E., "Real Air Breakdown", presented at HELREG Propagation Subpanel Meeting, MITRE Corp., November 1975.

18. Triplett, J. R. and Boni, A.A., "The Interaction of Suspended Atmospheric Particles with Laser Radiation", SSS-R-71-1167, Systems, Science and Software, LaJolla, CA., June 1972.

19. Caledonia, G. E., Root, R.G., Wu, P. K.S., Kemp, N.H., and Pirri, A. N., "Plasma Studies for Laser-Heated Rocket Thruster", TR-47, Physical Sciences Inc., Wakefield, MA., March 1976.

20. Ref. 8, p. 129. The radiative transfer equation also has a time derivative term. This term is usually small. In the present application, where a steady state is assumed, it vanishes.

21. Ref. 8, p. 259.

22. Ref. 8, p. 265.

23. Ref. 1, Section 2.3.

24. Bethe, H. A. and Salpeter, E.E., "Quantum Mechanics of One- and Two-Electron Atoms", Springer-Verlag, Berlin, 1957, pp. 304-5.

25. Ref. 23, p. 265. Also given in Ref. 8, p. 297.

26. Griem, H. R., "Plasma Spectroscopy", McGraw-Hill, New York, 1964, pp. 445-448.

27. Griem, H. R., "Spectral Line Broadening by Plasmas", Academic Press, New York, 1974, p. 313.

28. Klosterman, E. L. and Byron, S.R., J. Applied Physics 45, 4751, (1974).

29. Raizer, Yu, P., JETP 31, 1148 (1970).

30. Jackson, J. P. and Nielsen, P. E., AIAA Journal 12, 1498 (1974).

31. Boni, A.A., Cohen, H.D., Meskan, D.A. and Su, F.Y., "Laser-Interaction Studies" SSS-R-74-2344, Systems, Science and Software, LaJolla, CA., August 1974.

32. Yos, J. M., "Transport Properties of Nitrogen, Hydrogen, Oxygen and Air to 30,000 K", RAD-TM-63-7, Avco Research and Advanced Development Division, Wilmington, MA., March 1963.

33. Patch, R. W., "Thermodynamic Properties and Theoretical Rocket Performance of Hydrogen to 100,000 K and 1.01325×10^8 N/m^2"; NASA SP-3069, 1971.

DISTRIBUTION LIST
FOR
FINAL REPORT

NASA Contract NAS3-19695

RECIPIENT	CYS
National Aeronautics & Space Adm. Lewis Research Center 21000 Brookpark Road Cleveland, Ohio 44135 ATTN:	
Contracting Officer, MS 500-313	1
E. A. Bourke, MS 500-205	5
Tech. Util. Office, MS 3-16	1
Tech. Rpt. Control Off., MS 5-5	1
AFSC Liaison Off., MS 501-3	2
Library, MS 60-3	2
Off. of Reliability & Quality Assurance, MS 500-211	1
N. T. Musial, MS 500-113	1
Stephen M. Cohen, Proj. Mgr., MS 500-318	5
National Aeronautics & Space Adm. Headquarters Washington, D. C. 20546 ATTN:	
Off. of Aeronautics & Space Tech. Director	1
Space Propulsion & Power/RP F. C. Schwenk/RR	1
Off. of Manned Space Flight Director Advanced Manned Mission/MT	1
Off. of Space Science Director Launch Vehicles & Propulsion/SV	1
Off. of Tech. Util. Div. Director Technology Utilization/KT	1
National Aeroanutics & Space Adm. Ames Research Center Moffett Field, CA 94035 ATTN:	
Library	1
Dr. Kenneth W. Billman	1
National Aeronautics & Space Adm. Flight Research Center P. O. Box 273 Edwards, CA 93523 ATTN: Library	1
National Aeronautics & Space Adm. George C. Marshall Space Flight Center Huntsville, Ala 35912 ATTN: Library	1
National Aeronautics & Space Adm. Goddard Space Flight Center Greenbelt, Maryland 20771 ATTN: Library	1
National Aeronautics & Space Adm. John F. Kennedy Space Center Cocoa Beach, Florida 32931 ATTN: Library	1

Distribution List (Cont'd)

RECIPIENT	CYS
National Aeronautics & Space Adm. Lyndon B. Johnson Space Center Houston, Texas 77001 ATTN: Library	1
National Aeronautics & Space Adm. Langley Research Center Langley Station Hampton, VA 23365 ATTN:	
Library	1
R. Hess	1
NASA Scientific & Technical Info. Facility P. O. Box 8757 Blat/Wash International Airport Maryland 21240 ATTN: Accessioning Dept.	10
Jet Propulsion Laboratory 4800 Oak Grove Drive Pasadena, CA 91103 ATTN:	
Library	1
G. R. Russell	1
M. J. Cork	1
G. Lewicki/180-700	1
Defense Documentation Center Cameron Station Building 5 5010 Duke Street Alexandria, VA 22314 ATTN: TISIA	1
Air Force Rocket Propulsion Lab. Edwards, CA 93523 ATTN:	
Library	1
D. A. Hart/XP	1
C. Selph/LKCG	1
F. B. Mead Jr./LKDA	1

RECIPIENT	CYS
Defense Advanced Research Projects Agency 1400 Wilson Blvd. Arlington, VA 22209 ATTN:	
Dr. Peter Clark	1
Major G. Canavan	1
ODDR&E Pentagon Washington, D. C. 20301 ATTN: Dr. Robert Greenberg	1
Commander U. S. Army Missile Command Redstone Arsenal, AL 35809 ATTN: Walter B. Jennings, Jr.	1
Director Ballistic Missile Defense Advanced Technology Center P. O. Box 1500 Huntsville, AL 35807 ATTN: ATC-OMr. W. O. Davies	1
Director U. S. Army Ballistic Research Lab. Aberdeen Proving Ground, MD 21005 ATTN:	
Dr. Robert Eichelberger	1
Office of Naval Research 495 Summer St. Boston, MA 02110 ATTN: Dr. Fred Quelle	1
Office of Naval Research 800 N. Quincy St. Arlington, VA 22217 ATTN: Dr. W. J. Condell (421)	1
Naval Missile Center Point Mugu, CA 93042 ATTN: Gary Gibbs (Code 5252)	1

Distribution List (Cont'd)

RECIPIENT	CYS
Superintendent Naval Postgraduate School Monterey, CA 93940 ATTN: Library (Code 2124)	1
Commander Naval Weapons Center China Lake, CA 93555 ATTN: Mr. E. B. Niccum Code 4011	1
Naval Research Lab. Washington, D. C. 20375 ATTN:	
Dr. P. Livingston (Code 5560)	1
Dr. J. L. Walsh (Code 5503)	1
Dr. J. T. Schriempf (Code 6410)	1
Naval Ordnance Lab. White Oak Silver Spring, MD 20910 ATTN: Dr. Leroy Harris (Code 313)	1
Air Force Weapons Lab. Kirtland AFB, NM 87117 ATTN:	
Col. Donald L. Lamberson (AR)	1
Col. John C. Scholtz (PG)	1
Col. Russell K. Parsons (LR)	1
Lt. Col. John C. Rich (AL)	1
Hq. SAMSO P. O. Box 92960 Worldway Postal Center Los Angeles, CA 90009 ATTN:	
Capt. Dorian A. DeMaio (XRTD)	1

RECIPIENT	CYS
AF Avionics Lab. (TEO) Wright Patterson AFB, OH 45433 ATTN: Mr. K. Hutchinson	1
AF Materials Lab. Wright Patterson AFB, OH 45433 ATTN:	
Maj. Paul Edler (LPJ)	1
AF Aero Propulsion Laboratory Wright Patterson AFB, OH 45433 ATTN:	
Maj. George Uhlig (AFAPL/NA)	1
RADC Griffiss AFB, NY 13441 ATTN: Mr. R. Urtz (OCSE)	1
Hq. Electronics Systems Div. (ESD) Hanscom AFB, MA 01731 ATTN: Capt. A. R. Tobin (XRE)	1
Air University Institute for Professional Develop. Maxwell AFB, AL 36112 ATTN: ACSC/EDCS	1
Aerojet Liquid Rocket Co. P. O. Box 13222 Sacramento, CA 95813 ATTN: Dr. Sandy D. Rosenberg	1
Aerospace Corp. P. O. Box 92957 Los Angeles, CA 90009 ATTN: Dr. W. R. Warren, Jr.	1

Distribution List (Cont'd)

RECIPIENT	CYS
Mr. A. Colin Stancliffe AiResearch Manuf. Co. 2525 West 190th St. Torrance, CA 90503 ATTN: Dept. 93-6	1
Astro Research Corp 1330 Cacique Box 4128 Santa Barbara, CA 93103 ATTN: R. F. Crawford, Dir. of Eng.	1
Atlantic Research Corp. Shirley Highway at Edsall Rd. Alexandria, VA 22314 ATTN: Mr. Robert Naismith	1
AVCO - Everett Res. Lab. 2385 Revere Beach Parkway Everett, MA 02149 ATTN: Dr. George Sutton Dr. Phillip Chapman	1 1
Battelle Columbus Laboratories 505 King Ave. Columbus, OH 43201 ATTN: Mr. Fred Tietzel (STOIAC)	1
Bell Aerospace Co. Buffalo, N. Y. 14240 ATTN: Dr. Wayne C. Solomon	1
Boeing Co. P. O. Box 3999 Seattle, WA 98124 ATTN: Mr. M. I. Gamble	1
ESL Inc. 495 Java Dr. Sunnyvale, CA 94086 ATTN: Arthur Einhorn	1
Electro-Optical Systems 300 N. Halstead Pasadena, CA 91107 ATTN: Dr. Andrew Jensen	1
General Electric Co. P. O. Box 8555 Philadelphia, PA 19101 ATTN: Mr. W. J. East Dr. C. E. Anderson Dr. R. R. Sigismonti Dr. Thomas W. Karras	1 1 1 1
General Research Corp. P. O. Box 3587 Santa Barbara, CA 93105 ATTN: Dr. R. Holbrook	1
Hercules, Inc. P. O. Box 210 Cumberland, MD 21502 ATTN: Dr. Ralph F. Preckel	1
Hughes Research Labs. 3011 Malibu Canyon Rd. Malibu, CA 90265 ATTN: Dr. Arthur N. Chester Dr. Viktor Evtuhov	1 1
Hughes Aircraft Co. Centinela and Teale Sts. Culver City, CA 90230 ATTN: Dr. E. Peressini (Bldg. 6, MS/E-125)	1

Distribution List (Cont'd)

RECIPIENT	CYS
Hughes Aircraft Co. P. O. Box 3310 Fullerton, CA 90230 ATTN: Dr. William Yates	1
Institute for Defense Analyses 400 Army Navy Dr. Arlington, VA 22202 ATTN: Dr. Alvin Schnitzler	1
Itek Corp. Optical Systems Div. 10 Maguire Road Lexington, MA 02173 ATTN: R. J. Wollensak	1
Johns Hopkins University Applied Physics Lab. 8621 Ga. Ave. Silver Spring, MD 20910 ATTN: Dr. Albert M. Stone	1
Lawrence Livermore Lab. P. O. Box 808 Livermore, CA 94550 ATTN: Dr. R. E. Kidder Dr. E. Teller Dr. John Emmett	1 1 1
Los Alamos Scientific Labs. P. O. Box 1663 Los Alamos, NM 87544 ATTN: Dr. Keith Boyer (MS 530)	1
Lulejian and Associates, Inc. Del Amo Financial Center Suite 500 21515 Hawthorne Blvd. Torrance, CA 90503	1
Lockheed Palo Alto Res. Lab. 3251 Hanover St. Palo Alto, CA 94304 ATTN: L. R. Lunsford Orgn. 52-24, Bldg. 201	1
Mathematical Sciences Northwest, Inc. P. O. Box 1887 Bellevue, WA 98009 ATTN: Mr. Abraham Hertzberg	1
Martin Marietta Aerospace P. O. Box 179 Denver, COL 80201 ATTN: Mr. Stewart Chapin Mail # 0485	1
Massachusetts Inst. of Technology Lincoln Lab. P. O. Box 73 Lexington, MA 02173 ATTN: Dr. S. Edelberg Dr. R. H. Rediker	1 1
McDonnel Douglas Astronautics Co. 5301 Bolsa Ave. Huntington Beach, CA 92647 ATTN: Mr. P. L. Klevatt Dept. A3-360-B3GO, M/S 14-1	1
McDonnel Douglas Res. Labs. Dept. 220, Box 516 St. Louis, MO 63166 ATTN: Dr. D. P. Ames	1

Distribution List (Cont'd)

RECIPIENT	CYS
MITRE Corp. P. O. Box 208 Bedford, MA 01730 ATTN: Mr. A. C. Cron	1
Northrop Corporation Research & Technology Center 3401 West Broadway Hawthorne, CA 90250 ATTN: Dr. M. M. Mann	1
Perkin Elmer Corp. Norwalk, Conn. 06852 ATTN: Dr. D. A. Dooley	1
Phaser Telepropulsion Inc. 1888 Century Park East Suite 1606 Los Angeles, CA 90067 ATTN: Dr. M. A. Minovitch	1
Radio Corp. of America Missile and Surface Radar Div. Morrestown, N. J. 08057 ATTN: Mr. J. J. Mayman Systems Project	1
RAND Corp. 1700 Main St. Santa Monica, CA 90406 ATTN: Dr. Claude R. Culp	1
Rasor Associates 420 Persian Drive Sunnyvale, CA 94086 ATTN: Dr. Ned S. Rasor	1
Raytheon Co. 28 Seyon St. Waltham, MA 02154 ATTN: Dr. Frank A. Horrigan (Res. Div.)	1
Raytheon Co. Bedford Laboratories Missile Systems Div. Bedford, MA 01730 ATTN: Dr. H. A. Mehlhorn Optical Systems Dept. M/S S4-55	1
Riverside Research Institute 80 West End St. New York, N. Y. 10023 ATTN: Dr. L. H. O'Neill	1
R&D Associates, Inc. P. O. Box 3580 Santa Monica, CA 90431 ATTN: Dr. R. E. LeLevier	1
Rockwell International Corp. 3370 Miraloma Ave. Anaheim, CA 92803 ATTN: Dr. J. Winocur (D/528. HA14)	1
Rockwell International Corp. Rocketdyne Div. 6633 Canoga Ave. Canoga Park, CA 91304 ATTN: Mr. Marc T. Constantine	1
Dr. Stan V. Gunn	1

Distribution List (Cont'd)

RECIPIENT	CYS
SANDIA Labs. P. O. Box 5800 Albuquerque, NM 87115 ATTN: Dr. E. H. Beckner - Org. 5200	1
W. J. Schafer Assoc., Inc. Lakeside Office Park 607 N. Avenue, Door 14 Wakefield, MA 01880 ATTN: Francis W. French	1
Standord Research Institue Menlo Park, CA 94025 ATTN: Dr. R. A. Armistead	1
Science Applications, Inc. P. O. Box 2351 LaJolla, CA 92037 ATTN: Dr. John Asmus	1
Mr. Lawrence Peckham Science Applications, Inc. 1911 N. Ft. Myer Drive, Suite 1200 Arlington, VA 22209	1
Science Applications, Inc. P. O. Box 328 Ann Arbor, MI 48103 ATTN: Dr. R. E. Meredith	1
Dr. Michael M. Monsler Science Applications, Inc. 6 Preston Court Bedford, MA 01730	1
Systems Consultants, Inc. 1050 31st St., N. W. Washington, D. C. 20007 ATTN: Dr. Robert B. Keller	1

RECIPIENT	CYS
Systems, Science and Software P. O. Box 1620 LaJolla, CA 92037 ATTN: Mr. Alan F. Klein	1
Thiokol Chemical Co. WASATCH DIV. P. O. Box 524 Brigham City, UT 84302 ATTN: Mr. James E. Hansen	1
TRW Systems Group One Space Park Bldg. 01, Rm. 1050 Redondo Beach, CA 90278 ATTN: Mr. N. F. Campbell	1
United Aircraft Research Lab. 400 Main St. East Hartford, CONN 06108 ATTN: Mr. G. H. McLafferty	1
United Aircraft Corp. Pratt and Whitney Div. Florida R&D Center West Palm Beach, FL 33402 ATTN: Dr. R. A. Schmidtke Mr. Ed Pinsley	1 1
VARIAN Associates EIMAC Div. 301 Industrial Way San Carlos, CA 94070 ATTN: Mr. Jack Quinn	1
Vought Systems Div. LTV Aerospace Corp. P. O. Box 5907 Dallas, TX 75222 ATTN: Mr. F. G. Simpson Mail Station 2-54142	1

Distribution List (Cont'd)

RECIPIENT	CYS
Westinghouse Electric Corp. Defense and Space Center Friendship International Airport Box 746 Baltimore, MD 21203 ATTN: Mr. W. F. List	1
Westinghouse Research Lab. Beulah Rd., Churchill Boro. Pittsburgh, PA 15235 ATTN: Mr. R. L. Hundstad	1